UNIVERSITY OF OKLAHOMA

GRADUATE COLLEGE

INNOVATIVE PAVEMENT DESIGN USING FIBER-REINFORCED LOW CARBON CSA CEMENT

A THESIS

SUBMITTED TO THE GRADUATE FACULTY

in partial fulfillment of the requirements for the

Degree of

MASTER OF SCIENCE

By

CADE J. HARRIS
Norman, Oklahoma
2024

INNOVATIVE PAVEMENT DESIGN USING

FIBER-REINFORCED LOW CARBON CSA CEMENT

A THESIS APPROVED FOR THE SCHOOL OF CIVIL ENGINEERING

AND ENVIRONMENTAL SCIENCE

BY THE COMMITTEE CONSISTING OF

Dr. Royce Floyd, Chair

Dr. Jeffery Volz

Dr. Shreya Vemuganti

Acknowledgements

The sentiment of 'it takes a village' was a recurring thought as I made my way through this research project. I'd like to thank a few of those in my village now.

My mentor and advisor, Dr. Floyd, has played an essential part in the trajectory of my academic career by inviting me into the realm of research my sophomore year and encouraged me through multiple research projects in my undergrad to this graduate research project. His influence has not been contained in the lab as he has been my advocate in the classroom and has made considerable efforts to give me the tools and opportunities to be successful academically, professionally, and personally.

I also thank my other committee members, Dr. Volz and Dr. Vemuganti, for their role in my academic achievements.

I would like to thank my family, my friends, and my partner for their continued support that allows me to accomplish my goals.

I would also like to thank all my Lab Mates for creating a supportive environment. I must specifically recognize Mujtaba for his efforts towards the completion of this research project, for which I am incredibly grateful.

The Fears Lab Manager, John Bullock, deserves his own acknowledgement for his devotion to not only my success, but to all the students that enter the lab. Through the good, the bad, and the ugly, John has been by my side.

Special thanks to the CTS Cement Manufacturing Corporation for the funding and donation of the materials necessary for this research.

Abstract

Motivation towards reducing the environmental impacts of concrete in the construction industry has spurred increased research on alternative cements. Calcium sulfoaluminate (CSA) cement concretes offer significant gains in sustainability while offering additional advantages in performance. Expansive Type K CSA cement concretes offer mitigation of shrinkage-related cracking and belitic CSA (BCSA) cement concretes benefit accelerated construction due to its rapid-setting behavior. Further enhancements in concrete performance can be gained with fiber reinforcement, particularly by providing post-cracking tensile strength. Additionally, the expansion of a CSA cement concrete in-tandem with the confinement offered by the fiber reinforcement has the potential to induce chemical prestressing, further enhancing performance.

This research studies a novel fiber-reinforced belitic CSA (BCSA) cement concrete that exhibits both rapid-setting and expansive behavior aiming to determine its viability for highway pavements. Fatigue tests were conducted on large-scale specimens placed on an elastic foundation with various pavement designs, including with fiber reinforcement. Standard material properties of fiber-reinforced specimens along with creep and expansion were also characterized in this research for comparison with plain specimens. An improvement in fatigue performance was seen in fiber-reinforced BCSA specimens. However, a comparison between plain and fiber-reinforced specimens showed no significant confinement of expansion. Fiber-reinforcement specimens showed a 30% gain in the modulus of elasticity and flexural tests revealed that the fiber-reinforced specimens could withstand 74% of the cracking load after cracking.

Table of Contents

List of Tables

List of Figures

List of Equations

Chapter 1: Introduction

1.1 Background

The shrinkage-compensating and rapid-setting behaviors displayed in calcium sulfoaluminate (CSA) cement concretes make the material desirable for highway pavement applications. Additionally, CSA cement concretes offer benefits in sustainability with lower carbon dioxide emissions and energy required for production.

The inclusion of shrinkage-compensating cements for pavements leads to reduction and possible elimination of shrinkage-related cracking. Cracked pavements are less durable and susceptible to internal water exposure which further propagates into structural deficiency. CSA and other shrinkage-compensating cements address shrinkage-related cracking by not reducing the experienced shrinkage but rather by introducing an early expansive period to offset the later shrinkage. By mitigating shrinkage-related cracking, the dimensional limitations in pavements that are dictated by shrinkage-related cracking may be increased.

When confined, the expansion exhibited by the concrete made with shrinkage-compensating cement can induce a state of chemical prestress. This leads to improved performance, notably towards elements expecting tensile stresses as the prestress can mitigate the anticipated tensile stress by inducing compressive stress.

Rapid-setting cement concretes offer time benefits for applications where high early strengths are required. This makes rapid-setting behavior desirable for accelerated construction to decrease wait times for the hardening of concrete elements. Conducting repairs also benefits from rapid-setting cement concretes as it leads to minimal disruption and a fast return to traffic.

Concrete behavior can further be enhanced by the inclusion of steel fiber-reinforcement. This offers post-cracking tensile strength and improved fatigue performance. Similar to traditional rebar, steel fibers can add confinement to elements, which can contribute to the chemical prestressing seen in confined shrinkage-compensating cement concretes.

1.2 Research Question

The shrinkage-compensating and rapid-setting behaviors exhibited by concretes made with CSA cements make the material an apt candidate for highway pavements. The material allows for accelerated construction and repair and can reduce shrinkage-related cracking.

This research assessed the applicability of a novel rapid setting and expansive CSA cement through comparison with another industry-standard expansive CSA cement and ordinary portland cement (OPC). This novel CSA cement is an expansive belitic CSA (Expansive BCSA) that has significantly demonstrated both shrinkage-compensating and rapid-setting behavior. The other CSA cement used in this study is a 25% replacement of OPC with Komponent®, a commercially available Type K cement more known for its shrinkage-compensating behavior. Fatigue performance and expansive behavior were determined to be the major factors in determining applicability of these materials. The change in performance by the inclusion of steel fiber-reinforcement was also investigated in this research.

1.3 Research Objectives

This research characterized the fatigue behavior of pavement specimens made with various cements with consideration of the effect of fiber reinforcement. Relevant material properties were also evaluated: elastic modulus, modulus of rupture, restrained and unrestrained expansion, and creep.

This research is a companion project to a recently completed project at the University of Oklahoma: Mechanical Performance of Post-Tensioned Residential Foundation Slabs Using Expansive BCSA Cements (Starks 2023). Material properties of concretes made with the

Expansive BCSA and 25% Komponent® without steel fiber reinforcement were characterized. The material properties of specimens with steel fiber-reinforcement that are investigated in this project are compared to findings from the completed project. The methods used by Starks (2023) were replicated for steel fiber-reinforced specimens.

The objectives for this project were as follows:

- Characterize material properties of 25% Komponent® and Expansive BCSA cement concretes with steel fiber reinforcement.
- Gather comparable fatigue data between concretes made with Expansive BCSA, 25% Komponent®, and OPC under different pavement designs.
- Assess the performance of concrete made with expansive BCSA in relation to those made with 25% Komponent® and OPC to determine the viability of applying expansive BCSA cement concretes for applications requiring rapid-setting and shrinkage-compensating behavior, particularly highway pavements.

The hypothesis of this study is, for a given induced stress, expansive BCSA specimens will be on par with, or outperform, 25% Komponent® specimens due to the expansive BCSA's increased strength found in Starks (2023). It is expected for the presence of steel fibers to offer minor enhancement to the fatigue behavior before cracking and will provide post-cracking tensile strength.

Chapter 2: Literature Review

2.1 CSA Cement Concretes

2.1.1 Chemical Composition & Production

Portland cement is distinguished into four primary oxides: alite (C_3S), belite (C_2S), aluminate (C_3A), and ferrite (C_4AF). CSA cements contain higher concentrations of alumina sulfate in the form of Ye'elimite ($C_4A_3\hat{S}$), gypsum ($C\hat{S}H_2$), and anhydrite ($C\hat{S}$) with no alite or aluminate. The larger sulfate content in CSA results in increased production of ettringite ($C_6A\hat{S}_3H_{32}$) and demands a higher water-cementitious materials ratio (*w/cm*) for hydration. (Sorensen 2018). This higher *w/cm* enhances workability and since the water is consumed rapidly, there is minimal excess water that is associated with porosity and shrinkage (Murray 2019). The increased quantity of belite in BSCA cements contributes to later strength gain due to additional production of calcium silicate hydrate (CSH) after setting (Murray 2019).

CSA cement offers great advantages for sustainability. Energy demand for production of CSA cement is 60% relative to portland cement (Sorensen 2018). This results from a combination of a lower temperature required in the kiln for the clinker phases of CSA cement, use of recycled materials such as aluminum or fly ash, and less energy required to grind the clinker. The chemical sintering process itself also produces less carbon emissions for CSA cements due to its lower limestone content (Bescher 2012). CSA cements demonstrate rapid-setting and shrinkage-compensating behaviors which can be adjusted based on chemical composition. ACI 223: Standard Practice for the Use of Shrinkage-Compensating Concrete, requires shrinkage-compensating concretes to undergo wet curing for at least 7 days after placing to ensure full development of the expansive qualities of the concrete.

2.1.2 *Expansive & Rapid-Setting Behavior*

The total amount of drying shrinkage has been found to be inversely proportional to the duration of the wet cure for CSA cements. Acarturk (2023) found that shrinkage is significantly reduced when wet cured for 1 day but recommended maximizing the wet cure duration to minimize shrinkage. Ideker (2013) found that wet curing shrinkage-compensating cements after 3 days did not result in any additional reduction of drying shrinkage. These studies indicate that the wet cure duration of 7 days as required in ACI 223 is a conservative duration for mitigating cracking due to drying shrinkage.

Applications of Type K cement concretes have had success using a wet cure of 7 days to reduce shrinkage cracking (Ramseyer 2009). Starks (2023) found that the expansive BCSA cement, like 25% Komponent® cement, requires a wet curing period to display expansive behavior. Unrestrained expansion (ASTM C157: Length Change of Hardened Hydraulic-Cement Mortar and Concrete) and restrained expansion (ASTM C878: Restrained Expansion of Shrinkage-Compensating Concrete) specimens were cast for each CSA cement. A set of C157 and C878 specimens were subjected to an indefinite wet-curing period. A companion set of C157 specimens with a 7-day wet curing period was added to consider field expectations for wet curing. The data collected showed that the Expansive BCSA specimens had a net-expansion while 25% Komponent® specimens was only shrinkage-compensating. This is due to the Expansive BCSA specimens undergoing three times the expansion and only a third of the shrinkage experienced by the 25% Komponent® specimens (Starks 2023).

It has been proposed that due to its expansive quality, a single BSCA slab with rapid-setting and shrinkage-compensating behavior could replace four regular-sized portland cement slabs (McNerney 2021). The increase in joint spacing has cost benefits alongside a reduction in joint maintenance without compromising performance. Seattle-Tacoma (SEA-TAC) International Airport has used BCSA cement for overnight concrete slab replacement for the past 25 years as its rapid-setting behavior allows for minimal disruption. A quadruple sized BCSA test slab (37.5 ft. by 40 ft.) was cast at the airport and did not show any shrinkage cracking at one year (McNerney 2021).

The use of retarders for improved workability with CSA cement concretes has been investigated by Roswurm J. (2018). Citric acid proved to be an effective retarder with a superplasticizing effect but showed a positive correlation with overall shrinkage. Another retarder used by Roswurm J., Delvo©, displayed no superplasticizing effect and no impact on shrinkage at 28 days.

Slump loss of BCSA cement concrete under various ambient temperatures was explored by Starks (2023). Temperature proved to have a significant impact on working time as higher temperature would result in a faster loss in workability. However, working time is better correlated with internal temperature which had more control on working time than retardation. Additionally, Starks (2023) found that including ice for excessive temperatures (90°F) shows an improvement in working time. Dosage of a high-range water reducer was also investigated by Starks (2023) which found that the dosage improved workability and working time but displayed more aggressive setting.

2.2 *Hardened Properties*

2.2.1 CSA Cements

In 1995 SEA-TAC conducted a repaving in under 4 hours using rapid-setting CSA cement with a 20-year design life, which was determined to be 1,150,000 MD-11 aircraft movements (Bescher 2012). Static flexural tests and fatigue tests revealed that the pavement, with only the strength at four hours, would be able to handle 60 times the design life. Bescher (2012) speculates that the improved fatigue behavior of CSA cement could be from improved strength, mineralogical composition, fineness, porosity, and pore size distribution. Bescher (2012) did find that CSA cement had a lower pore volume and a finer pore size distribution using mercury intrusion porosimetry.

Bowser (2020) investigation into development length of prestressing strands in precast, prestressed CSA cement concrete involved evaluating early age compressive strengths to determine adequacy of an early prestress release. The compressive strength of the CSA cement concrete used in Bowser's research reached 4000 psi within 2 hours, approximately half of the 28 overall strength. In comparison, the PC cement concrete did not reach the minimum strength required for prestress release until 24 hours.

Experimental Type K cement concrete bridge decks were cast with the support of the Wisconsin Department of Transportation to determine the efficacy of Type K cement to mitigate shrinkage-related cracking (Battaglia 2012). While successful as the decks made with Type K cement having little to no cracking, the decks did have higher chloride permeability than Type 1 cement and did undergo scaling. This behavior, along with increased cost of Type K cement, resulted in discouragement of further utilizing the material.

Sorensen (2018) notes that "rapid precipitation of ettringite in CSA cement pastes forms a dense microstructure with low porosity and permeability" and suggests more research in the chloride ion penetration of CSA cements as there is a lack of consensus with published research. The sulfate resistance of BCSA cement was explored by Dillard (2022) which determined that BCSA cement had more resistance to sulfuric acid than portland cement. This can be attributed to its lower C_3A (tricalcium aluminate) content.

2.2.2 *Fiber Reinforcement for Expansion*

Kevern (2016) found that fiber-reinforcement does enhance the fatigue performance of portland cement concrete, particularly at lower stress ratios. Polypropylene fibers outperformed steel fibers for the increase of fatigue performance, as determined by the greater number of cycles before failure. However, polypropylene fibers did not offer any significant post-cracking support. Pre-cracked fatigue testing showed that tensile strength along with fiber dosage and length contributed to fatigue performance. These parameters are more prevalent when analyzing post-cracking performance. It was also determined that fiber-reinforcement can reduce the required thickness of pavements when anticipating low stress and high-volume loading (Kevern 2016).

The inclusion of steel fiber reinforcement has also been shown to affect expansion behavior of concretes. Gennings (2018) found that introducing fibers decreased the overall expansion of concretes made with shrinkage-compensating cements which induces a state of chemical prestressing into the concrete. This behavior is desirable for concrete elements that experience tensile forces generated through flexural action such as pavements. While this is achievable through traditional methods of reinforcing concrete with rebar, fibers reduce manual labor and the overall amount of steel required for chemical prestressing.

Chapter 3: Research Methods

This project expanded on mix designs developed by Starks (2023) by adjusting for fiber-reinforcement with 100 pounds of steel fibers per cubic yard (0.75% by volume). This was achieved by a proportional replacement of materials.

The initial testing in this project was to characterize material properties of Expansive BCSA cement and 25% Komponent® cement concrete containing steel fiber reinforcement. Testing procedures replicated many processes used by Starks (2023) to allow for analysis between concretes that have fiber reinforcement with those that do not. Afterwards, the large-scale testing involved inducing cyclic loading onto precast slabs resting in a soil containment box on realistic base and subgrade materials.

3.1 ***Material Properties***

3.1.1 *Overview*

Table 2 provides detailed information for testing ages and variant wet-curing conditions (if applicable) for the standard material properties tested between this project and the companion project of Starks (2023). The scope of this project considers the portion of Table 2 that includes steel fiber reinforcement.

Table 1: Material Properties Testing Ages or Wet-Curing Conditions

Test	**Number of Specimens per Testing Age or Condition**	**Cement**			
		Expansive BCSA (Starks 2023)	**Type K (Starks 2023)**	**Expansive BCSA (with Fibers)**	**Type K (with Fibers)**
Compression Cylinders (ASTM C39)	3	(6h, 1d, 7d, 28d)	(3d, 7d, 14d, 28d)	(6h, 1d, 7d, 28d)	(3d, 7d, 14d, 28d)
Modulus of Elasticity (ASTM C469)	3	(6h, 1d, 7d, 28d)	(3d, 7d, 14d, 28d)	(6h, 1d, 7d, 28d)	(3d, 7d, 14d, 28d)
Modulus of Rupture (ASTM C78)	2	(6h, 1d, 7d, 28d)	(3d, 7d, 14d, 28d)	(6h, 1d, 7d, 28d)	(3d, 7d, 14d, 28d)
Unrestrained Expansion (ASTM C157)	3	*(Indefinite & 7d Wet Cured)	*(Indefinite & 7d Wet Cured)	*(Indefinite & 7d Wet Cured)	*(Indefinite & 7d Wet Cured)
Restrained Expansion (ASTM C878)	3	*(Indefinite Wet Cured)	*(Indefinite Wet Cured)	*(Indefinite Wet Cured)	*(Indefinite Wet Cured)
Creep Columns (Influenced by ASTM C512)	3	*(7d Wet Cured)	*(7d Wet Cured)	*(7d Wet Cured)	*(7d Wet Cured)
Shrinkage Companions for Creep Columns	2	*(7d Wet Cured)	*(7d Wet Cured)	*(7d Wet Cured)	*(7d Wet Cured)

* Description relates to wet-curing condition(s) only

Companion ASTM C39 compressive strength cylinders (4 in. by 8 in.) were cast with all conducted tests. The wet curing schedule used in Starks (2023), outlined in Table 2, was observed for both Expansive BCSA and 25% Komponent® specimens. Note that both concretes were wet cured for seven days after demolding as recommended by ACI 223: Standard Practice for the Use of Shrinkage-Compensating Concrete.

Table 2: Wet-Curing Schedule

Cement	Age to Begin Wet-Cure	Age to End Wet-Cure
Expansive BCSA	6 hours	7 days
Type K	3 days	10 days

3.1.2 *Hardened Strength Properties*

Modulus of elasticity (ASTM C469) was measured by loading end-ground 4 in. by 8 in. cylinders to 40% of the compressive strength of companion cylinders tested at the same age. The time series data including stress and axial deformation was recorded with the inclusion of a linear variable differential transformer (LVDT) attached to the cylinders using a compressometer. Each cylinder was loaded three times, but only the data from the second and third loading was used for calculation of the modulus of elasticity. Figure 1 presents the loading apparatus and compressometer used for the modulus of elasticity tests.

Figure 1: Modulus of Elasticity Compressometer

Modulus of rupture was determined using ASTM C78 with some modifications. Specimens (of 6 in. by 6 in. by 20 in.) were tested with third-point loading on an 18 in. span as shown in Figure 2. Due to the post-cracking tensile strength provided by the inclusion of steel fibers, failure does not result in complete separation at the initial crack caused by the third-point loading. After cracking, the specimens were loaded further to propagate the crack until it reached the full depth of the specimen. The post-cracking cross-section was then determined by measuring the average dimensions of both sides of the cracking interface to be used in the modulus of rupture formula in ASTM C78. For 28-day testing, a modified ASTM C1609 test was utilized to capture deflection. An LVDT was placed at half-depth and midspan of the specimen. Placement of the LVDT can be seen in Figure 3.

Figure 2: Modulus of Rupture, Third Point Loading

Figure 3: LVDT Placement for 28 Day Modulus of Rupture Testing

3.1.3 *Expansion and Shrinkage Properties*

Unrestrained expansion (ASTM C157: Length Change of Hardened Hydraulic-Cement Mortar and Concrete) and restrained expansion (ASTM C878: Restrained Expansion of Shrinkage-Compensating Concrete) specimens were cast for both CSA cement concretes with fibers. Indefinite wet curing was imposed on a set of three ASTM C878 specimens and three ASTM C157 specimens. In addition, another set of ASTM C157 specimens was only wet cured for the designated wet curing procedure: 7 days after the demolding of specimens. All curing was completed by submerging the specimens in water tanks placed in a temperature and humidity controlled environmental chamber. The water tanks used for these specimens are shown in Figure 4. A plastic board was used to cover tanks to minimize water evaporation.

Figure 4: Water Tanks Storing C157 and C878 Specimens

Expansive BSCA specimens were first measured at demolding age of 6 hours followed by 9 and 12 hours after casting. Specimens with 25% Komponent® were first measured at the demolding age of 3 days. Daily measurements were taken on all specimens for the first seven days of the wet cure. Weekly measurements were then taken until readings reasonably stabilized, at which time measurements were switched to a monthly basis. Figure 5 shows the length comparators used for the C878 and C157 specimens length measurements. The first reading at the time of demolding provided the baseline for comparison to all future readings. This was used to produce an engineering strain tracked throughout the testing period.

Figure 5: Length Comparators

3.1.4 *Creep and Shrinkage Behavior*

Concrete creep was measured according to a modified version of ASTM C512 Standard Test Method for Creep of Concrete in Compression. A stack of three 6 in. x 12 in. cylinder specimens was loaded in a load frame designed to maintain a near constant load with the use of stiff springs. Each cylinder specimen contained a Vibrating Wire Strain Gauge (VWSG) located in the center of the cylinder. The load was limited to 60% of the compressive strength of companion ASTM C39 cylinders tested at the age of loading (6 hours for Expansive BCSA and 3 days for 25% Komponent® specimens). Two additional 6 in. x 12 in. companion shrinkage cylinders containing VWSGs cast and placed in the same environment as the creep specimens, but were not loaded. The ends of these companion shrinkage cylinders were covered to have a matching exposed surface area as the creep cylinders loaded in the frame.

Following the methodology used by Starks (2023), the creep cylinders were loaded at the beginning of wet curing. This was achievable by assembling a watertight PVC pipe with a drainage valve inside the load frame before placing the stack of cylinders. This method created an expected challenge of centering the stack of cylinders when lowered inside the PVC pipe. A machined aluminum ring connected at the base of the frame aided in centering the first cylinder lowered into the PVC pipe. The next two cylinders did experience slight shifting when being lowered. This sacrifice in precise placement led to a reliable method to wet cure specimens inside the frame. Once the specimens were in place within the PVC pipe, the pipe was filled with water and the specimens were loaded to the target stress level. The water was drained after the wet-cure period and the PVC pipe was disassembled (Figure 6). Measurements of the internal VWSGs were taken at an initial sample rate of 5-minute intervals for the first week after loading which was then extended to 30-minute intervals.

Figure 6: Creep Cylinders Stacked in Loading Frame

3.2 ***Large-Scale Fatigue Testing***

To simulate realistic pavement conditions, fatigue testing of large-scale pavement sections was conducted inside a steel soil containment box (Figure 6) with the specimens resting directly on a compacted subgrade and base rather than freely spanning between supports. The soil containment box was centered beneath an MTS actuator attached to a steel load frame. This actuator utilized in this research has the capability to load up to 22,000 lb with frequencies up to 10 Hz (cycles per second). The actuator and loading frame are depicted in Figure 7. The interface between specimens and the actuator was selected to simulate a design wheel for load distribution.

Figure 7: Soil Containment Box

Figure 8: MTS Actuator and Load Frame

3.2.1 *Soil Containment Box Preparation*

The soil containment box allowed for comparable pavement conditions with the inclusion of a subgrade and a subbase beneath concrete specimens. Dry sand was utilized for the subgrade to minimize changes in soil behavior between tests. This sand was spread in a thin layer outside in the sun until it reached a maximum moisture content less than the saturated surface dry condition as confirmed by a modified rapid moisture content ASTM D4643. Oklahoma Department of Transportation (ODOT Type A) aggregate was selected for the subbase following the gradation guidelines from Table 703:1 in the ODOT 2019 Standard Specifications for Highway Construction. The methods of ASTM D1557: Standard Test Methods for Laboratory Compaction Characteristics of Soil Using Modified Effort (modified proctor test) were utilized to determine the optimal moisture content of the aggregate used for compaction in the soil containment box. A modified rapid moisture content, ASTM D4643, taken from aggregate at the time of compaction showed that the aggregate was within 98% of maximum density as required for the compaction in the Oklahoma Department of Transportation 2019 Standard Specifications.

A geosynthetic was added to be a barrier between the subgrade and subbase to minimize blending between layers. Additionally, a moisture barrier was placed on top of the subbase to maintain soil conditions across the tests. A thin layer of dry sand (≈1 in.) was then added on top of the moisture barrier to ensure a level contact interface with the specimens. Figures 1 – 12 show the specific steps listed in Table 3 during the soil containment box preparation. Figure 13 is a cross-section showing the layers in the soil containment box.

Table 3: Soil Containment Box Preparation Procedure

Step	Action
1	Fill with dry subgrade (16 in.) and screed for levelness
2	Fill with moist subbase (8 in.) and compact
3	Cover subbase with moisture barrier
4	Fill with approximately 1 in. of dry sand and screed for levelness

Figure 9: Step 1: Leveled Sand Subgrade in the Soil Containment Box

Figure 10: Step 2: Compacted Aggregate Subbase in the Soil Containment Box

Figure 11: Step 3: Moisture Barrier Placed in the Soil Containment Box

Figure 12: Step 4: Leveled Sand Top Layer Placed in Soil Containment Box

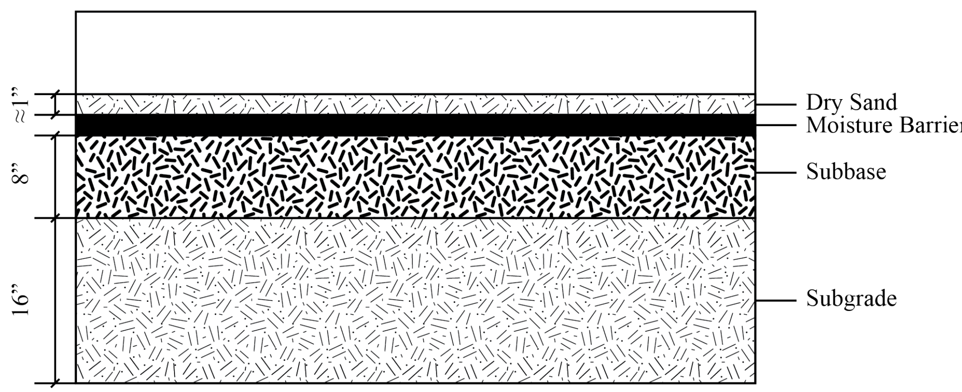

Figure 13: Section Diagram of Soil Containment Box

3.2.2 *Testing Matrix and Pavement Design*

The original testing matrix (Table 3) called for 18 total specimens with 2 specimens for each type of pavement design. Unfortunately, due to the research schedule and issues with obtaining required cementitious materials, large-scale 25% Komponent® specimens were not included in the testing. This resulted in a total of 12 specimens tested. Specimen designation was comprised of cement type, pavement design type, and count with abbreviations as noted in Table

3. For example, the first Expansive BCSA specimen with fiber-reinforced pavement design is designated as CSF1. The dimensions of the specimens were selected to be 62 in. in length, 24 in. in width, and 8 in. in thickness. Specimens were cast in pairs using wooden formwork and a single batch of concrete. Figure 14 depicts a set of slabs in the formwork used for the large-scale specimens immediately after casting.

Table 3: Large Scale Testing Matrix

Cement	Pavement Design		
Expansive BCSA (CS)	Plain (P)	Fiber-Reinforced (F)	Continuously Reinforced (CR)
25% Komponent® (K)	Plain (P)	Fiber-Reinforced (F)	Continuously Reinforced (CR)
OPC	Plain (P)	Fiber-Reinforced (F)	Continuously Reinforced (CR)

Figure 14: Example Large-Scale Slabs in Formwork

To allow for wet-curing of Expansive BCSA specimens, the slabs were placed on a plastic lining (Figure 15), covered in wet burlap, and then had the plastic lining folded over itself to create a moist environment. During the seven-day wet-curing period, the water would be reapplied to the wet burlap to avoid moisture loss.

Figure 15: Expansive BCSA Slabs Laid Upon Plastic Lining for Wet-Curing

OPC specimens followed a different protocol for curing conditions as these specimens were covered in wet-burlap and plastic lining for seven days while in the forms, as depicted in Figure 16. A set of modulus of rupture specimens were cast alongside the OPC specimens with fibers. For all OPC specimens, compressive strength was only tested for 7-day, 28-day, and day of fatigue testing.

Figure 16: Curing Conditions of OPC Specimens

The thickness of the pavement specimens (8 in.) was chosen by examining ODOT drawings of pavements and examining the stresses that could be applied with the available MTS equipment. It was determined that the addition of fibers should have a minimal effect compared to the addition of continuous reinforcement, so no specimens were tested with combined fiber reinforcement and continuous reinforcement.

Cast-in-place specimens would provide the most accurate representation of actual pavement behavior; however, pre-cast specimens would allow a substantially higher number of specimens to be tested compared to cast-in-place specimens in the same timeframe. Pre-cast specimens would not experience confinement from the subgrade in the soil containment box, potentially reducing the effects of chemical prestressing. This indicates that results from this testing procedure should underestimate the performance of cast-in-place pavements in the field.

The spacing and sizing of reinforcement for the continuously reinforced specimens was designed with consideration of the Continuously Reinforced Concrete Pavement Manual: Guidelines for Design, Construction, Maintenance, and Rehabilitation from the Federal Highway

Administration (Roesler 2016). Figure 17 provides the reinforcing details in the continuously reinforced specimens. Figure 18 shows the reinforcement within the formwork immediately before casting.

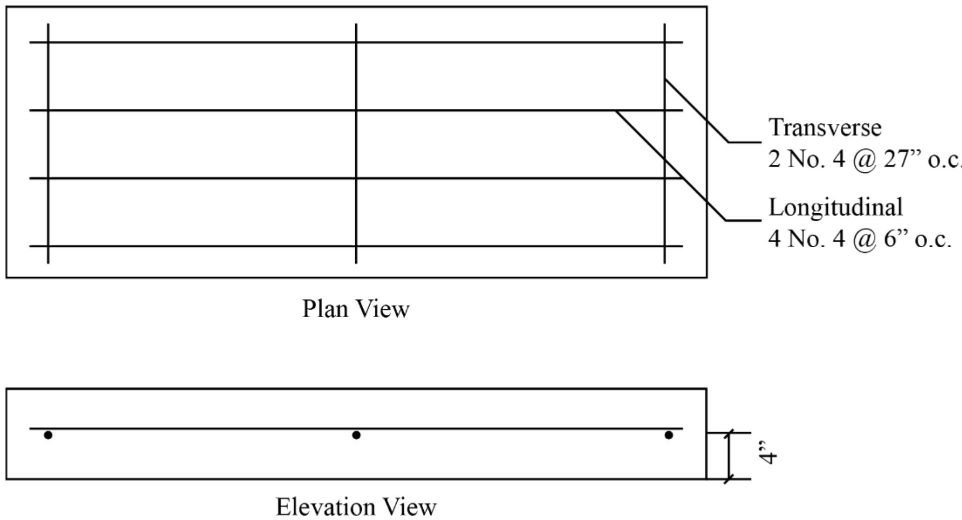

Figure 17: Reinforcing Details for Continuously Reinforced Specimens

Figure 18: Reinforcement for Continuously Reinforced Specimens in Formwork

3.2.3 *Stress Analysis and Testing Setup*

Specimens were analyzed as infinite beams on a continuous elastic foundation with a point load applied at midspan to determine induced stresses from the applied load. Winkler springs were considered as an appropriate approximation of the elastic foundation behavior. For the initial stress analysis, ranges for the modulus of subgrade reaction of the subbase and subgrade were sourced from the Supplement to the AASHTO Guide for Design of Pavement Structures. Part II - Rigid Pavement Design & Rigid Pavement Joint Design. A harmonic average for these ranges of values was then used for stress evaluation. Due to the range in values, there is approximately a ±7% range in stress ratios induced in the specimens depending on the selected subgrade properties. Data from this initial stress analysis can be found in Appendix II.

This initial stress analysis also verified that that load required to induce the desired stress ratios was within the capability of the available testing equipment. The thickness of specimens was controlled by the limitations of the actuator with the goal to only use 50% of the actuator's capacity (≈10 kips).

The load plate (Figure 19) that transfers the load from actuator to the specimen measures 20 in. by 10 in. A bearing pad was placed between the load plate and the specimen surface for improved load distribution.

Figure 19: Load Plate for Large-Scale Testing

The actuator has a built-in LVDT to provide displacement data. As this LVDT would also capture the deformation of the bearing pad beneath the load plate (Figure 19), two LVDTs were added to the slab at midspan to capture relative displacement of specimens without interference from the bearing pad. Additionally, LVDTs were added at both ends of specimens, giving a displacement profile along the length of specimens. Displacement data from the LVDTs allows for back-calculation of the modulus of subgrade reaction to determine the stress during testing.

Foil strain gages were utilized to measure tension strains on the pavement specimens. As placing these foil strain gauges directly on the tension face would place the gauges in direct contact with the subbase, the gauges were rather applied to the sides of the specimens near the tension face (Figure 20). Due to the limited quantity of available foil strain gauges, three Expansive BCSA slabs (one of each pavement design) had an additional gauge applied to the compression face at midspan.

Figure 20: Placement of Foil Strain Gauges on Slab Specimen

The application of foil strain gauges was completed as follows:

1) Slightly grind a portion of the concrete surface with minimal voids using a diamond wheel on an angle grinder
2) Clean surface with rubbing alcohol to remove dust particles
3) Apply epoxy to surface and scrap to fill voids and remove excess epoxy
4) After the epoxy has set, apply strain gauge with fast-setting adhesive

The application method was examined by attaching foil strain gauges to a concrete cylinder that was tested under the same procedure as a modulus of elasticity specimen. The strain measured by the gauge was compared to the strain calculated from the deflection measured using the LVDT in the compressometer. Graphing the strain over time revealed that the behavior matched between the foil strain gauge and the LVDT; however, the magnitude of the strain indicated by the foil strain gauge was roughly a third of the strain calculated with the LVDT. While not accurate in actual strain of specimens, the foil strain gauges can provide information on changes in behavior, particularly as an indicator of when the specimen is cracked. It is expected that the foil strain gauge near the tension face will measure less strain post-cracking as stress is redistributed. The placement of all LVDTs and foil strain gauges are depicted in Figure 21.

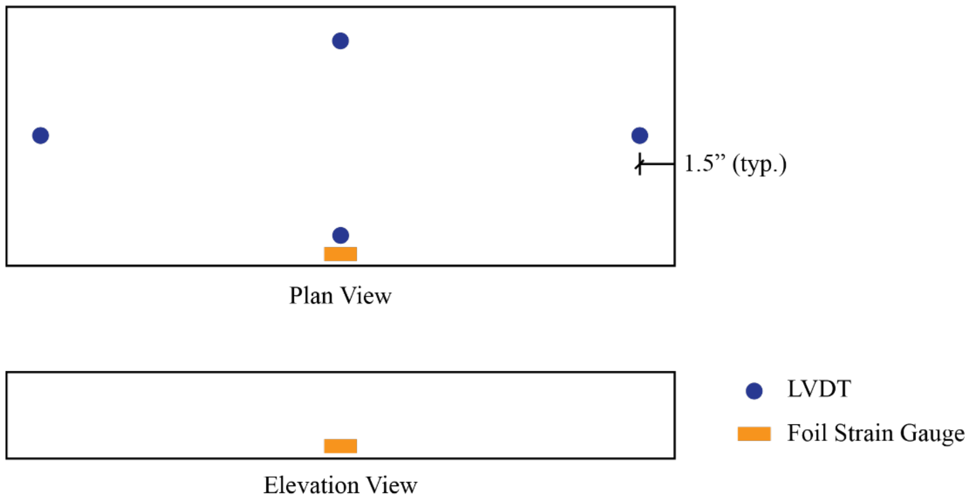

Figure 21: LVDT and Foil Strain Gauge Placement on Large-Scale Specimens

The selection of a stress ratio and loading rate of the cyclical loading was based on fatigue data for concretes made with the same cements without fiber-reinforcement gathered in another current research project being conducted at the University of Oklahoma. This other research involves flexural fatigue for unreinforced 6 in. x 6 in. by 21 in. and 8 in. by 8 in. by 30 in. specimens. A stress ratio of 0.85 and a loading rate of 1 Hz were chosen to be used on all large-scale specimens with the objective of having a meaningful number of cycles without overextended testing durations.

During testing of the first specimens, the LVDT outputs revealed that the specimen’s deformed shape displayed behavior more similar to axial loading on the plan area rather than bending as the displacement at midspan did not significantly vary from the ends. It was also observed that the specimen displayed a diagonal rotation. Load-deflection curves also revealed that each cycle induced permanent deformation in the soil. Back-calculation of reaction of subgrade modulus revealed that the stiffness of the compacted subbase and subgrade was significantly higher than anticipated. The first specimen was then incrementally subjected to larger loads to investigate the system behavior. During this investigation, the limits of the actuator were reached without showing signs of cracking.

The difference between the soil's calculated and actual reaction of subgrade modulus may be related to the compaction procedure, actual vs. theoretical soil behavior, and possible interaction from the steel and strong floor below the subbase and subgrade. To induce cracking, the configuration of the support conditions was adjusted. Elastomeric bearing pads supported on the subgrade were added beneath the ends of the specimen. Stress analysis of the specimen was taken as a simple-span beam with a partial uniformly distributed load applied at midspan to match the dimensions of the bearing pad in contact with the specimen. A stress ratio of 0.85 was then used under this configuration. Under this configuration, the specimen did crack after a few minutes under the fatigue loading.

A new testing procedure was then developed detailed in Table 4 intended to be used on the remaining specimens. The stress ratio presented is based on the initial estimated reaction of subgrade modulus.

Table 4: Adjusted Large-Scale Testing Procedure

Step	Stress Ratio*	Cycles	Configuration
1	1	5000	Elastic Foundation
2	1.5	5000	Elastic Foundation
3	2	50000	Elastic Foundation
4	0.85	Until Failure	Simple Span

*Stress Ratio based on initial modulus of subgrade reaction

Chapter 4: Results & Discussion

Results from the experimental testing outlined in Chapter 3 along with an analysis of those results are encompassed in this chapter. Data collected by Starks (2023) is combined with data collected within the scope of this project when appropriate for comparison and is noted explicitly as such.

4.1 *Hardened Strength Properties*

4.1.1 Compressive Strength

Figure 22 and Figure 23 show the average compressive strengths of all companion cylinders tested for concretes made with the two CSA cements and including steel fibers.

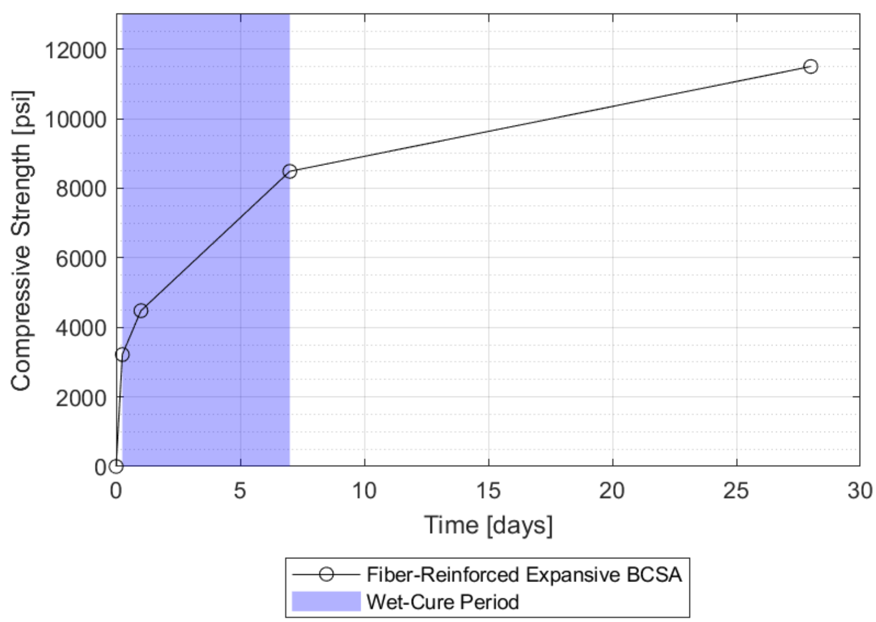

Figure 22: Compressive Strength of Fiber-Reinforced Expansive BCSA Concrete

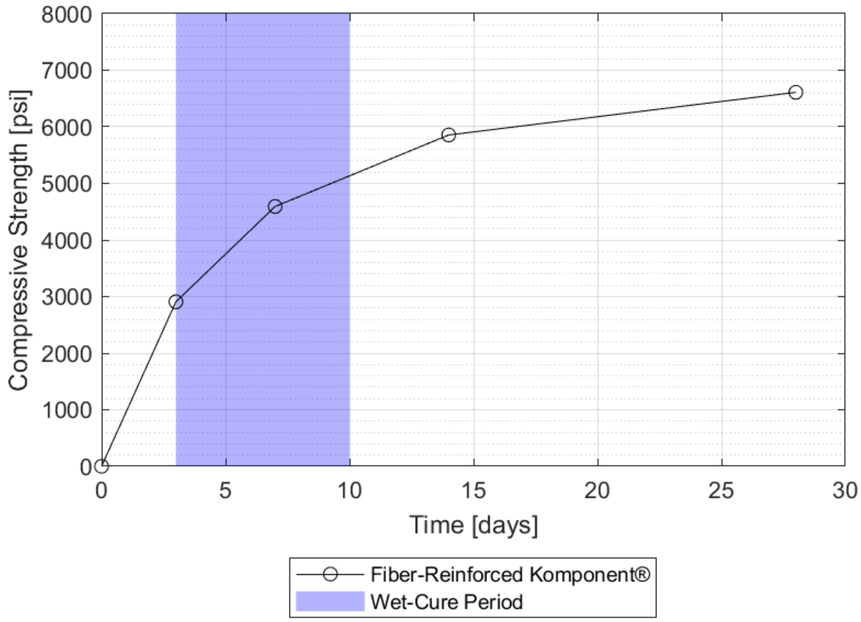

Figure 23: Compressive Strength of Fiber-Reinforced 25% Komponent® Concrete

The Expansive BCSA concrete displayed higher early strengths compared to 25% Komponent® concrete. At six hours, the strength of Expansive BCSA is comparable to the strength of 25% Komponent® at three days. For applications requiring high early strengths, using Expansive BCSA instead of 25% Komponent® would be beneficial. Additionally, the strength of Expansive BCSA specimens at the end of its wet cure is higher than the maximum strength achieved by 25% Komponent® specimens.

Figure 24 and Figure 25 show both plain and fiber-reinforced CSA cement concrete compressive strengths with plain concrete data from Starks (2023).

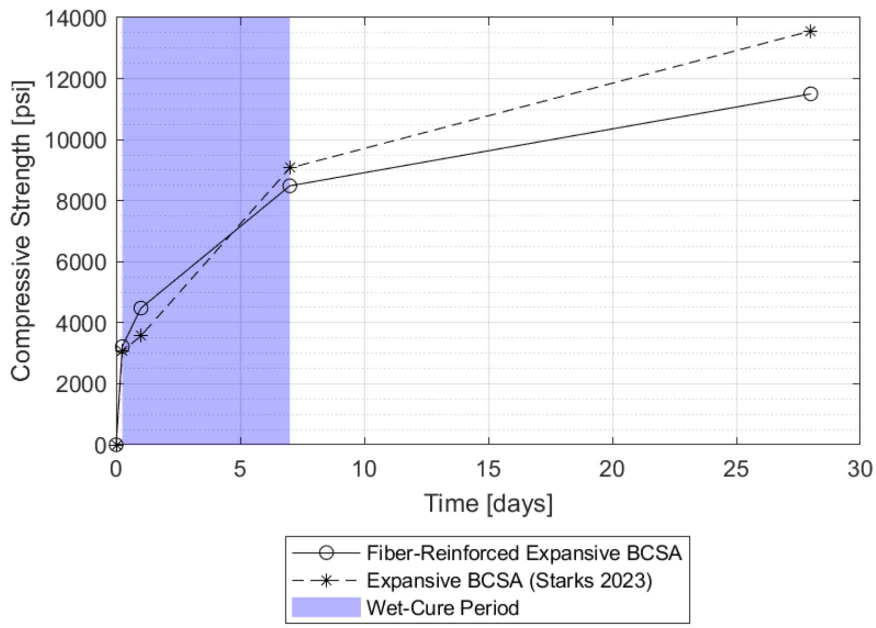

Figure 24: Compressive Strength of Expansive BCSA Concrete with and without Fibers

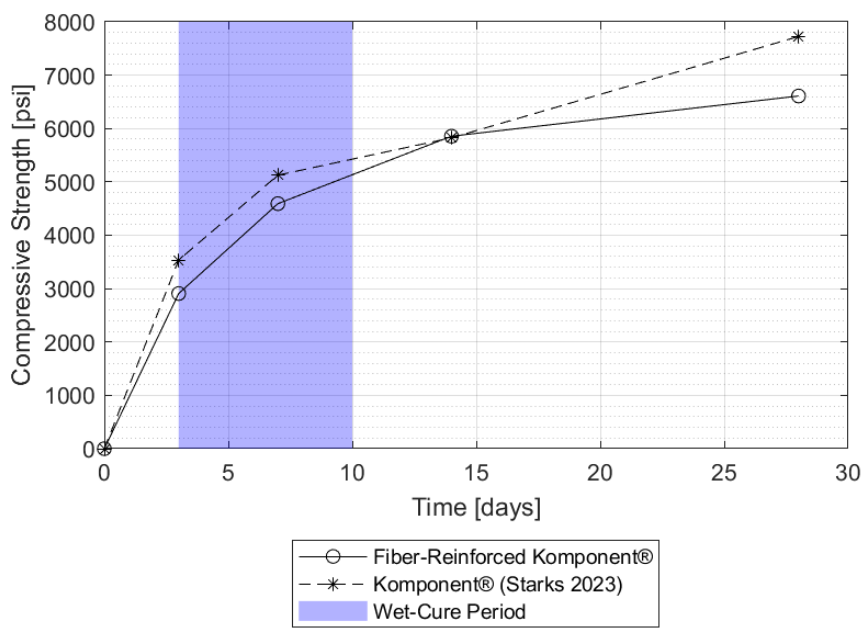

Figure 25: Compressive Strength of 25% Komponent® Concrete with and without Fibers

Specimens containing steel fiber reinforcement displayed a slight decrease in overall compressive strength compared to specimens without fibers. There is potential that the proportional replacement of mix design constituents to introduce steel fibers that reduced cement content per cubic yard may have also reduced compressive strength. However, external factors such as environmental conditions of different months of the year and the difference in operators between tests of the different mix designs can reasonably contribute to the differential in compressive strengths.

Figure 26 and Figure 27 show the development of compressive strengths for both fiber-reinforced and plain specimens as a percentage of the compressive strength at 28 days. Compressive strength development is similar between specimens with fiber reinforcement and those without. This is expected as the introduction of steel fibers should not influence the chemistry of concrete hardening. As for comparing concretes made with the two CSA cements, due to the differing chemical composition of the two CSA cements, comparing relative ages may be more beneficial to insights on the two concretes relative behavior. The wet cure of the Expansive BCSA concrete began at around 30% of overall compressive strength and ended around 70% of its overall compressive strength. The wet cure of the 25% Komponent® concrete began around 45% of the overall compressive strength and ended at around 75% of its overall compressive strength. As the initiation of the wet cure period considered the strength at the age of demolding and that Expansive BCSA specimens have higher final strengths than 25% Komponent® specimens, it is expected for Expansive BCSA to begin the wet cure period with a lower overall strength development. However, both CSA cement concretes did have similar compressive strength development (70-75%) at the end of the wet cure period requiring that the Expansive BCSA concrete develop more of its overall compressive strength during the wet cure period. Additionally, both CSA cement concretes developed roughly 25-30% of the compressive strength after wet curing.

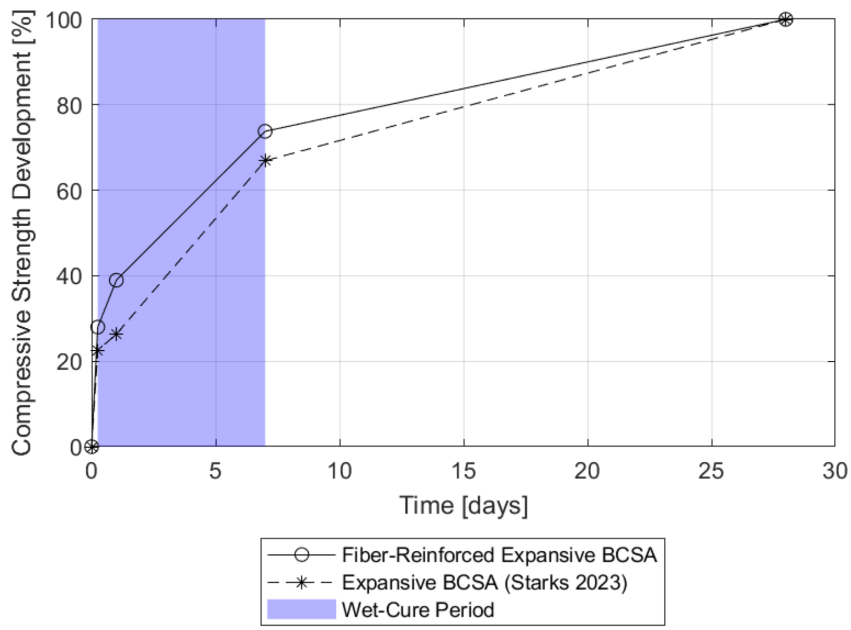

Figure 26: Compressive Strength Development of Expansive BCSA Concrete

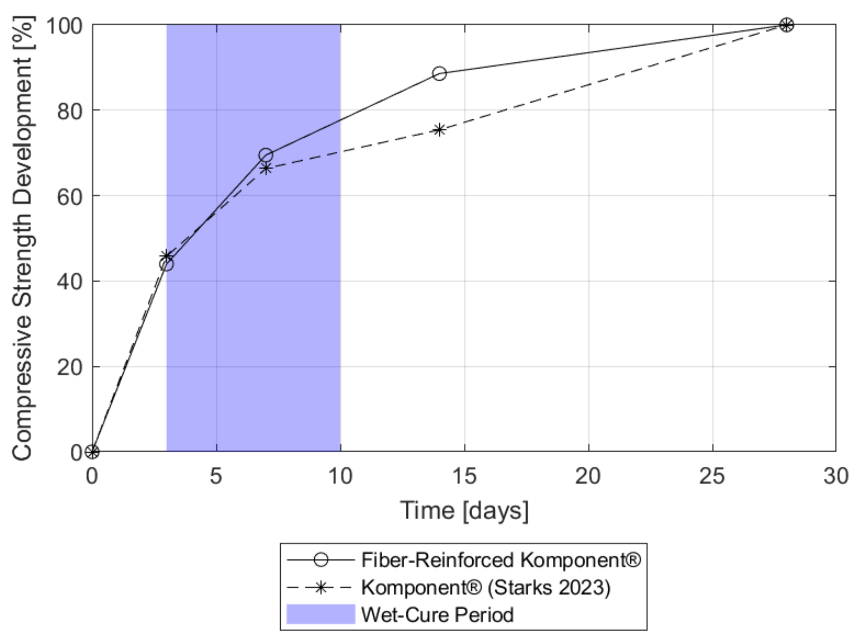

Figure 27: Compressive Strength Development of 25% Komponent® Concrete

4.1.2 Modulus of Elasticity

Figure 28 and Figure 29 show the measured modulus of elasticity for fiber-reinforced specimens and specimens without fiber-reinforcement collected from Starks (2023).

Unfortunately, the modulus of elasticity for fiber-reinforced 25% Komponent® specimens at the age of 10 days was not recorded.

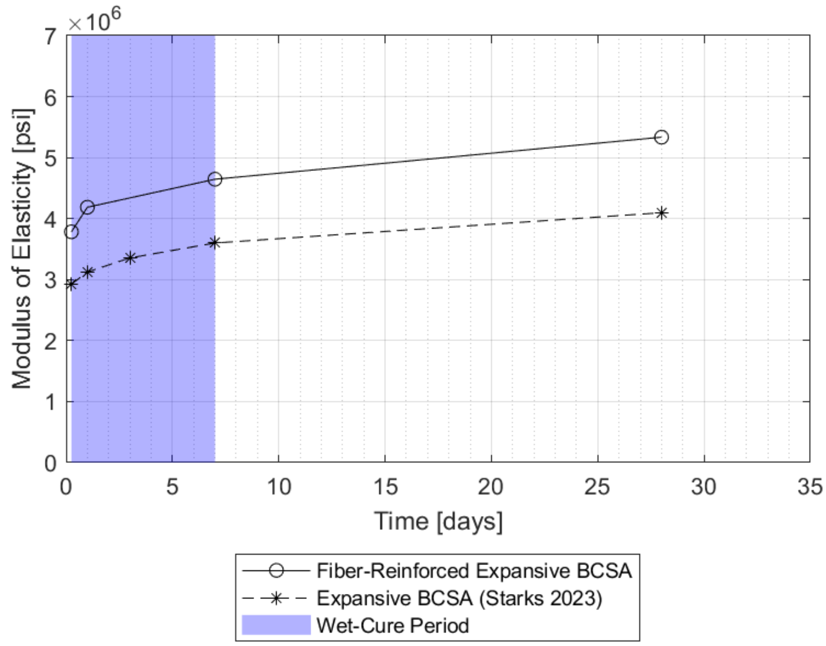

Figure 28: Modulus of Elasticity of Expansive BCSA Concrete

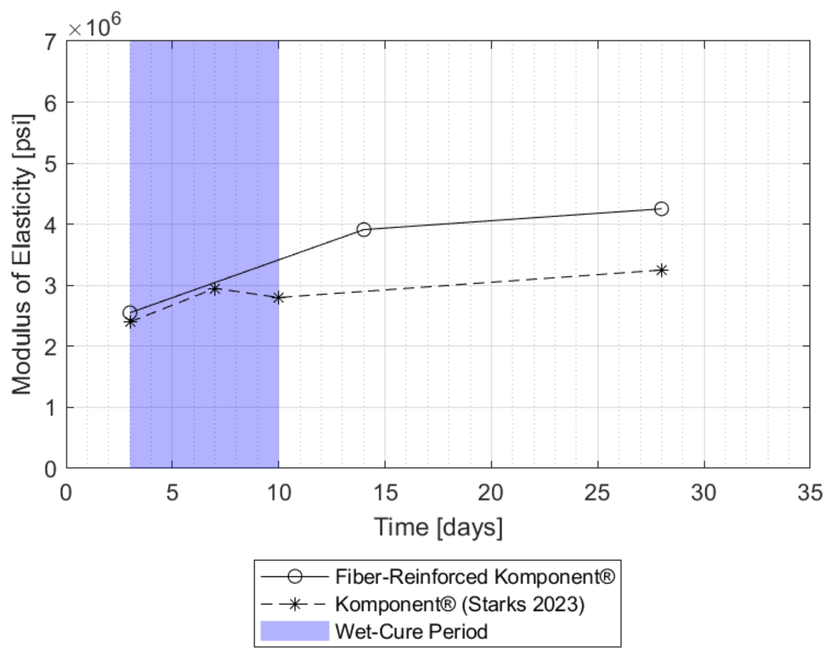

Figure 29: Modulus of Elasticity of 25% Komponent® Concrete

Despite having a decrease in compressive strength, fiber-reinforced specimens exhibited an approximately 30% increase in the modulus of elasticity compared to plain concrete for both CSA cements. Correlation between the modulus of elasticity with the compressive strength and the square root of compressive strength is shown in Figures 30 through 33.

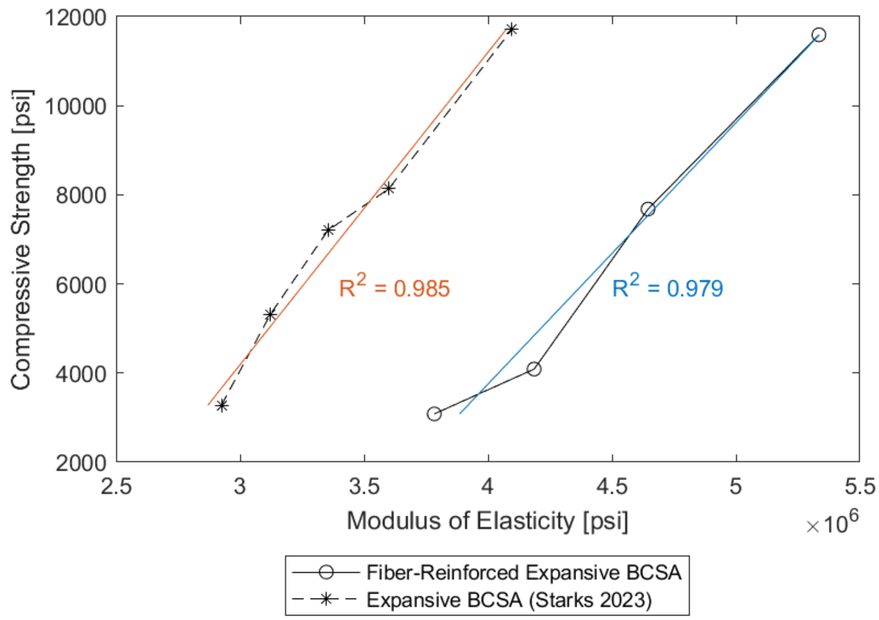

Figure 30: Modulus of Elasticity vs. Compressive Strength for Expansive BCSA Concrete

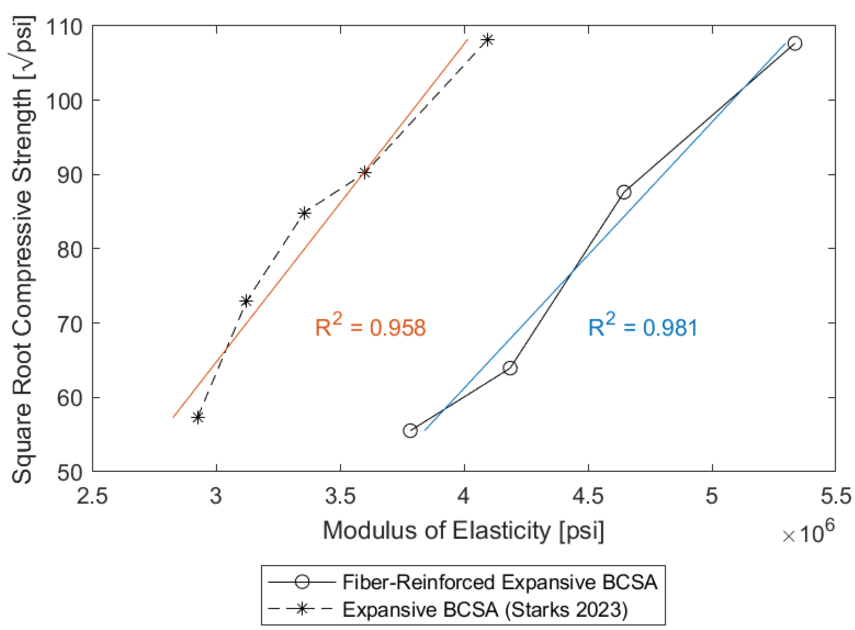

Figure 31: Modulus of Elasticity vs. Square Root of Compressive Strength for Expansive BCSA Concrete

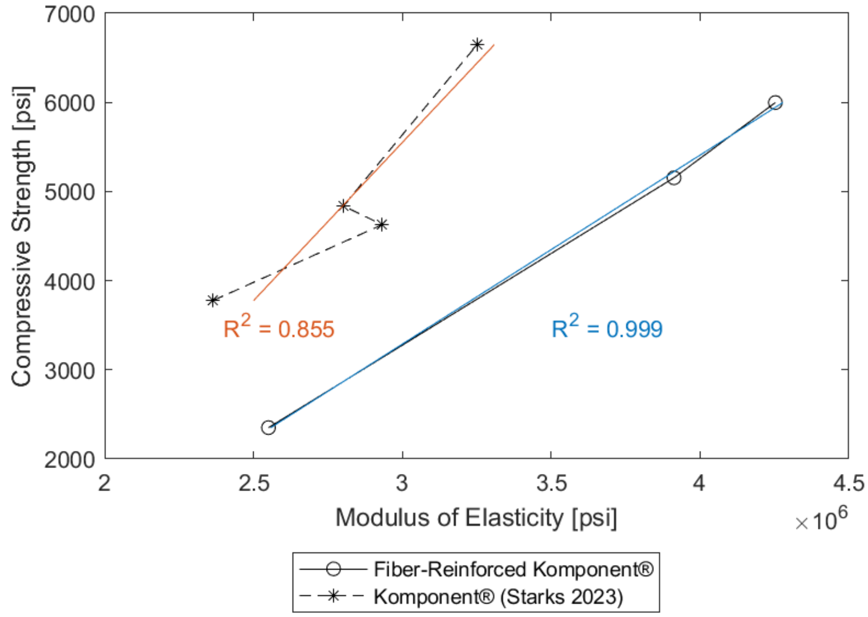

Figure 32: Modulus of Elasticity vs. Compressive Strength for 25% Komponent® Concrete

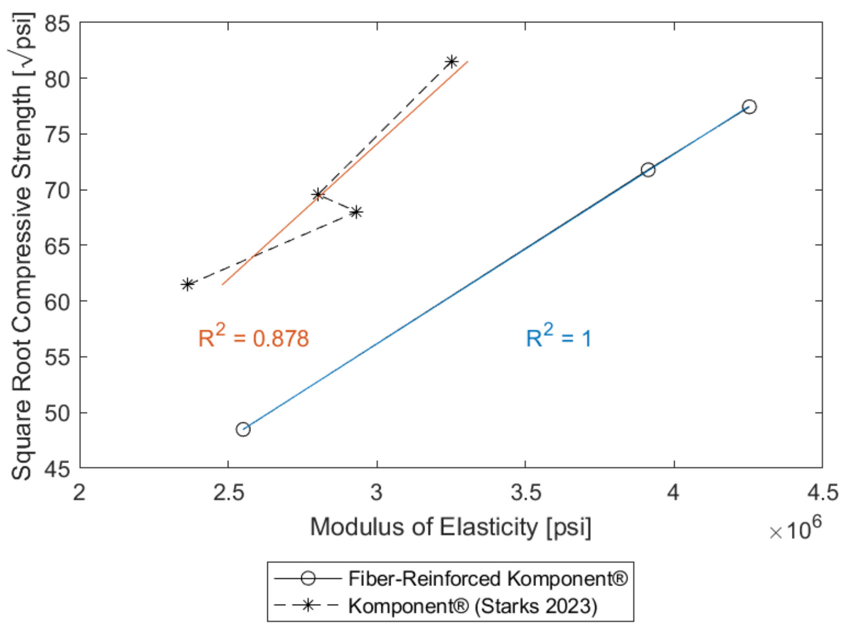

Figure 33: Modulus of Elasticity vs. Square Root of Compressive Strength for 25% Komponent® Concrete

A linear regression reveals that fiber-reinforced concretes made with both CSA cements had a stronger correlation to the square root of compressive strength for the specimens tested, which is similar to typical behavior found in concretes made with OPC. While this is expected for the 25% Komponent® specimens as it is a partial replacement of OPC, the correlation found in fiber-reinforced Expansive BCSA with the square root of compressive strengths conflicts with the behavior observed in Starks (2023) which found a stronger correlation to the unaltered compressive strengths of plain specimens.

ACI 318-19 19.2.2.1a provides an empirical equation for estimating the modulus of elasticity based on compressive strength and unit weight as shown in (Eq. 1). Figure 34 and 35 show this estimated value using the unit weights from Starks (2023) of 143.4 pcf and 148 pcf for Expansive BCSA and 25% Komponent® specimens without fibers, respectively.

$$E = 33{w_c}^{1.5}\sqrt{f_c'} \tag{1}$$

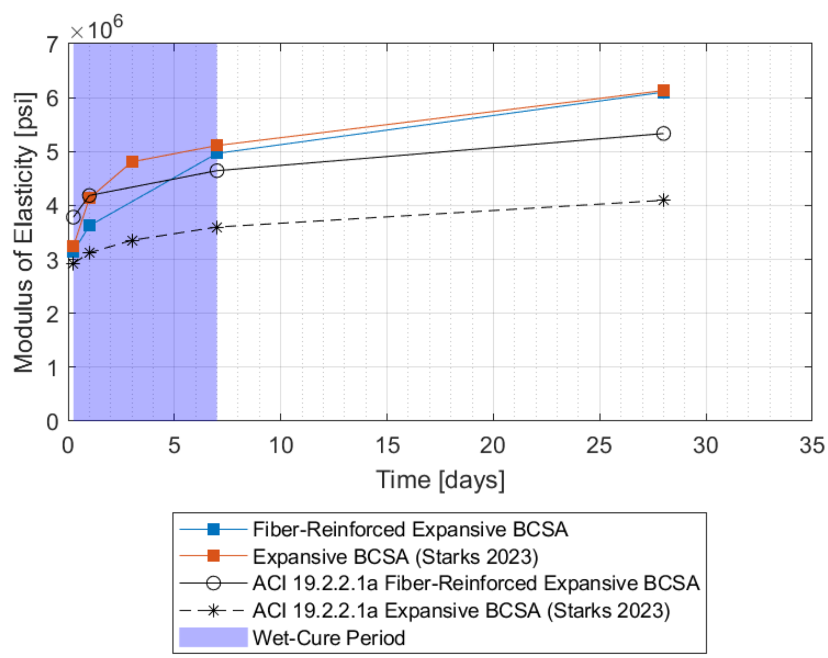

Figure 34: Modulus of Elasticity of Expansive BCSA Concrete with ACI Predictions

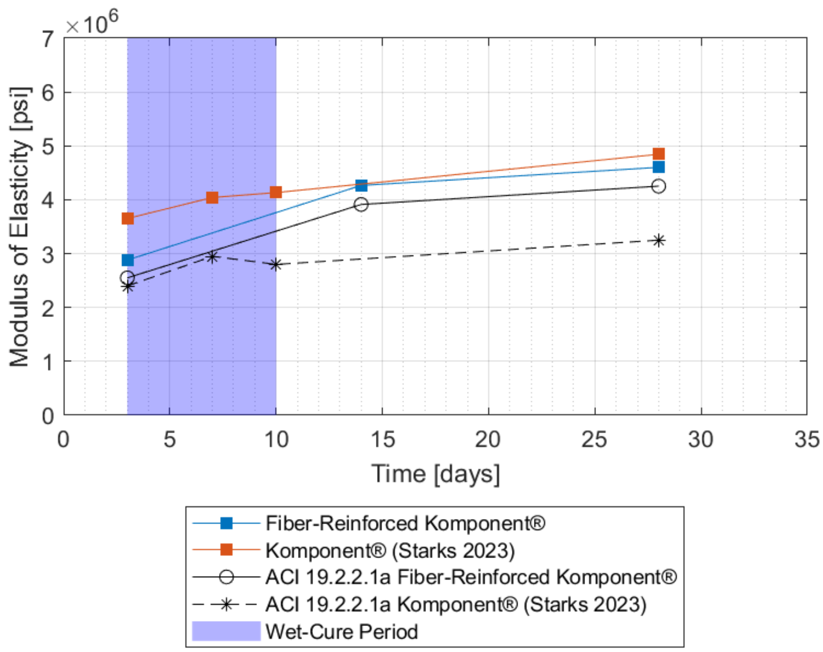

Figure 35: Modulus of Elasticity of 25% Komponent® Concrete with ACI Predictions

The ACI 318-19 19.2.2.1a equation overestimates the modulus of elasticity for both CSA cements for both fiber-reinforced and plain concrete specimens. At 28 days, the ACI prediction overestimates the modulus of elasticity for Expansive BCSA concretes by ≈14% for fiber-reinforced specimens and ≈50% for plain specimens. Values for the 25% Komponent® concretes are overestimated by ≈8% for fiber-reinforced specimens and ≈49% for plain specimens. As noted in Starks (2023), the expansive quality of both CSA cement concretes may decrease overall stiffness. This may be due to the matrix density being lowered due to the expansion, making ACI 19.2.2.1a inaccurate in estimating the modulus of elasticity. While this equation still overestimates the modulus of elasticity for the fiber-reinforced specimens, it is not as severe as plain specimens. This could potentially be attributed to a decrease in expansion caused by confinement by the steel fibers, reducing the expansion's effect on the concrete's stiffness. The increased stiffness provided by the steel fiber reinforcement may also be responsible for fiber-reinforced Expansive BCSA specimens being more correlated with the square root of compressive strength rather than unaltered compressive strength as found with plain Expansive BCSA specimens by Starks (2023). In addition, the commentary in ACI 318-19 recognizes that larger differences between calculated and measured modulus of elasticity are observed for higher strength concretes (>8000 psi). While ACI 318-19 19.2.2.1a provides closer estimations of Expansive BCSA specimens with fiber-reinforcement, it is suggested that an alternative equation be used for design purposes that considers higher compressive strength and expansive cement concretes.

4.1.3 Modulus of Rupture

Figure 36 and 37 shows the measured modulus of rupture for fiber-reinforced specimens alongside the results for plain concrete specimens from Starks (2023).

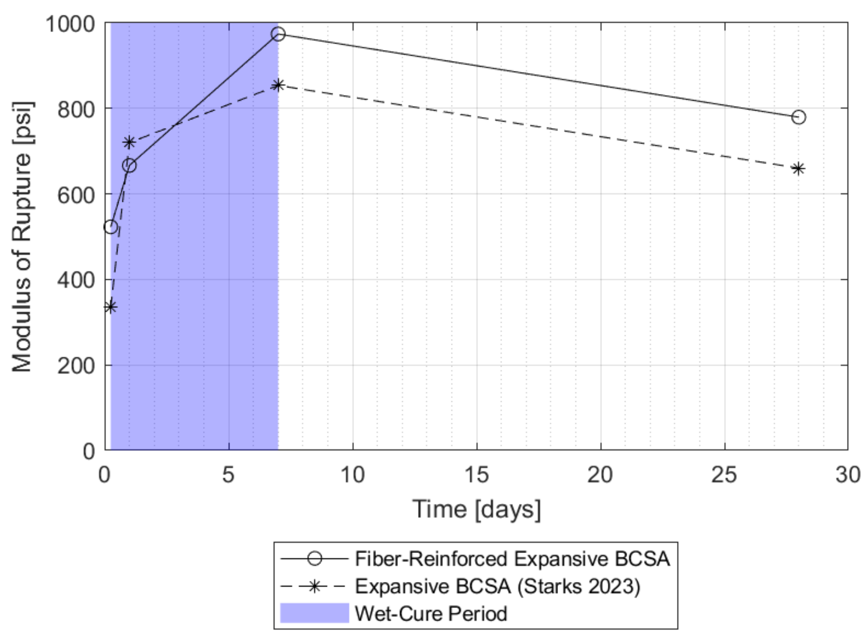

Figure 36: Modulus of Rupture of Expansive BCSA Concrete

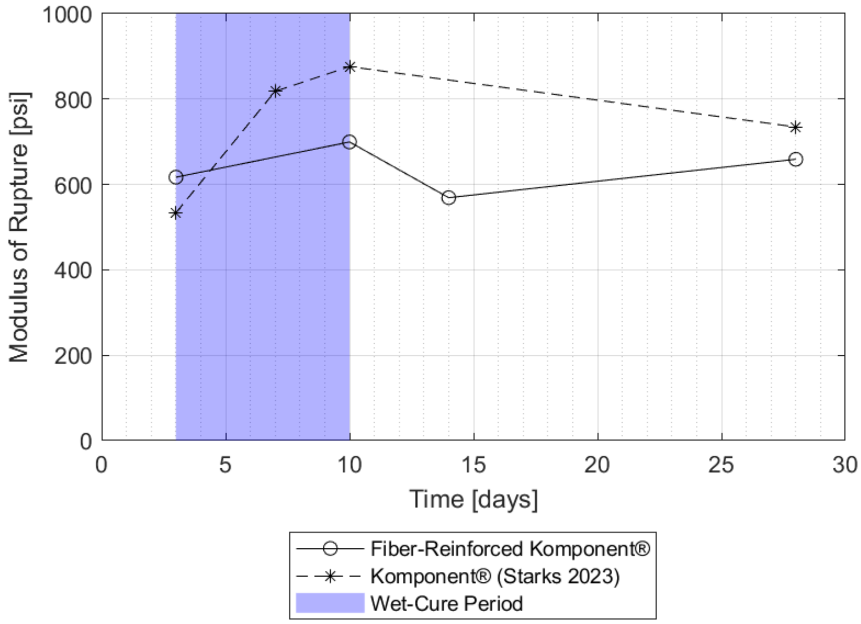

Figure 37: Modulus of Rupture of 25% Komponent® Concrete

The Expansive BCSA specimens displayed slight improvement with the inclusion of fiber reinforcement, while the 25% Komponent® specimens exhibited conflicting behavior as the measured modulus of rupture decreased with the inclusion of fiber reinforcement. Major changes in the modulus of rupture are not expected with the inclusion of steel fibers before cracking. Fiber reinforcement's more notable influence is the post-cracking tensile strength caused by the discontinuous steel reinforcement bridging over cracks within the specimen as depicted in Figure 38 and Figure 39. As there is similar behavior seen in a concurrent research project with recent concretes made with this cement, there is a possible issue with the supply of Komponent® cement that was used for the specimens including steel fibers.

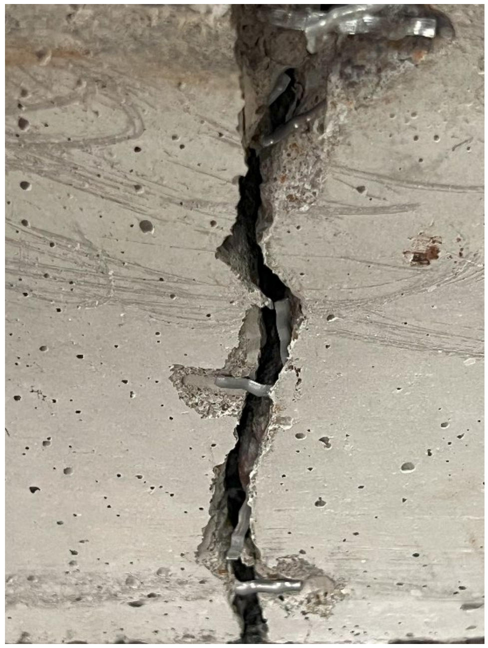

Figure 38: Fiber-Reinforcement Bridging Cracking Interface, Example 1

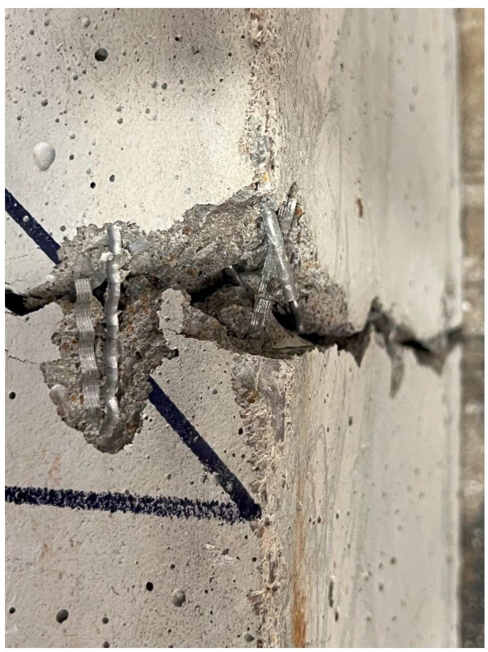

Figure 39: Fiber-Reinforcement Bridging Cracking Interface, Example 2

Similar to the findings of Starks (2023), peak modulus of rupture was observed at the end of the wet cure period for both CSA cement concretes. This is in agreement with the consensus that flexural strength decreases when a specimen has been at least partially dried as tensile stress develops during the drying process. Due to this behavior, a linear regression of modulus of rupture data is problematic. A comparison to the modulus of rupture calculated using the prediction from ACI 318-19 19.2.3.1 (Eq. 2) is shown in Figure 40 and Figure 41. The modification factor (λ) in Eq. 2 accounts for lightweight concrete adjustments and is taken as 1.0 for both concretes due to both CSA cement concretes having a density greater than 135 pcf.

$$f_r = 7.5\lambda\sqrt{f_c'} \tag{2}$$

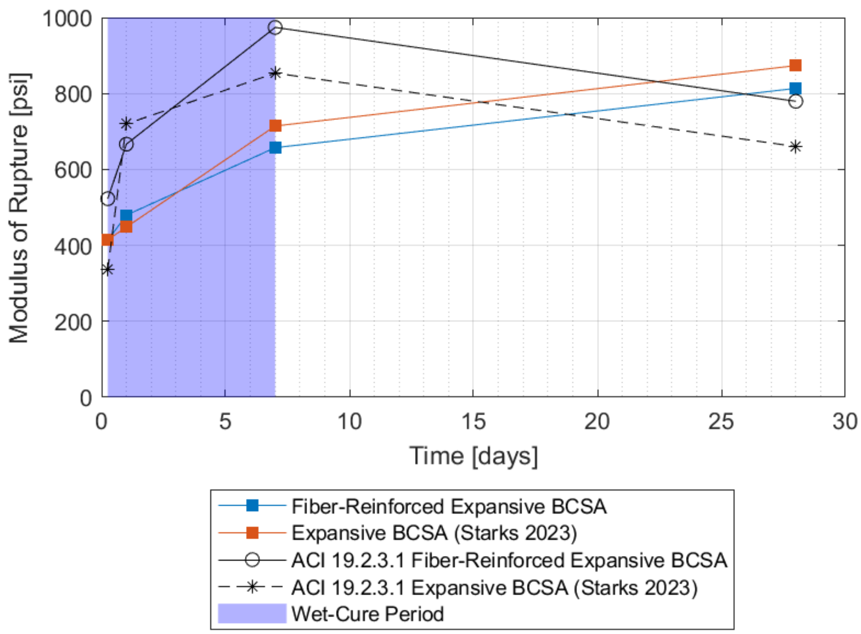

Figure 40: Modulus of Rupture of Expansive BCSA Concrete with ACI Predictions

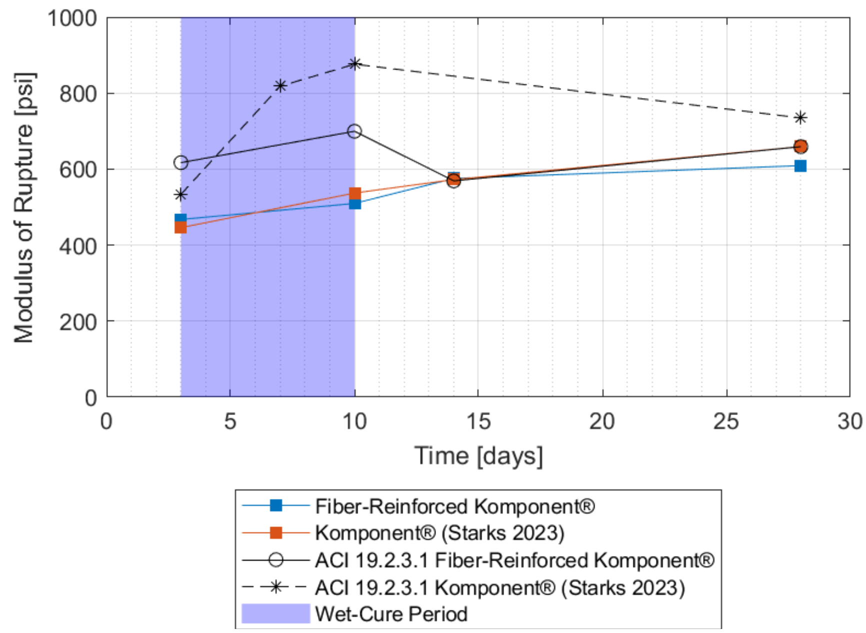

Figure 41: Modulus of Rupture of 25% Komponent® Concrete with ACI Predictions

The ACI 318-19 19.2.3.1 equation tended to underpredict the modulus of rupture for both fiber-reinforced and plain Expansive BCSA specimens at early ages and began to overpredict at 28 days due to the modulus of rupture decreasing due to drying. The results for the 25% Komponent® specimens displayed a similar relationship with the ACI 318-19 19.2.3.1 equation, which underpredicted the modulus of rupture for all ages, especially at earlier ages. As early age material characteristics are necessary for accelerated construction involving rapid-setting cement concretes, it is not recommended to utilize the ACI 318-19 19.2.3.1 equation for these types of cement. The utilization of a wet cure further separates the behavior of modulus of rupture from estimated calculations.

Load-deflection curves were generated using the LVDT data collected for the 28-day fiber-reinforced Expansive BCSA and OPC specimens, as shown in Figures 42 through 44. Unfortunately, the LVDT did not collect any data during the testing of the first Expansive BCSA MOR specimen.

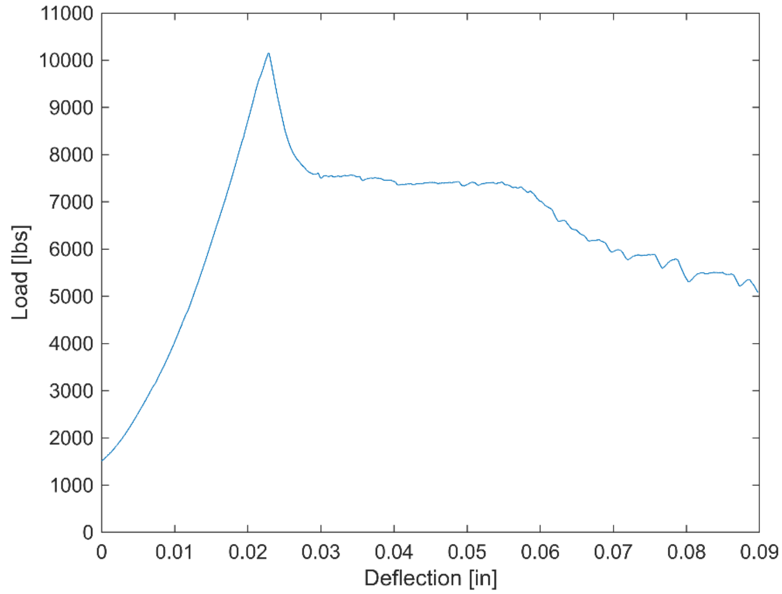

Figure 42: Load-Deflection Curve for Expansive BCSA 28-Day Modulus of Rupture Test, Specimen 2

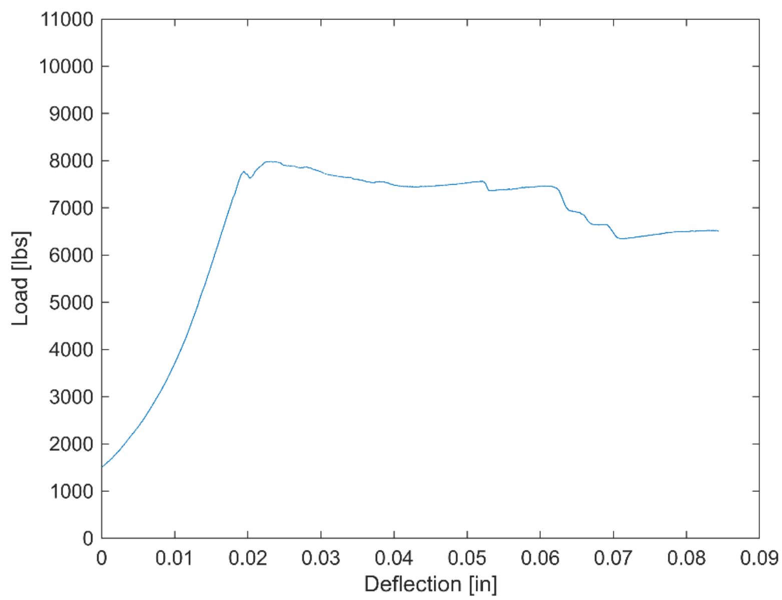

Figure 43: Load-Deflection Curve for 25% Komponent® Concrete 28-Day Modulus of Rupture Test, Specimen 1

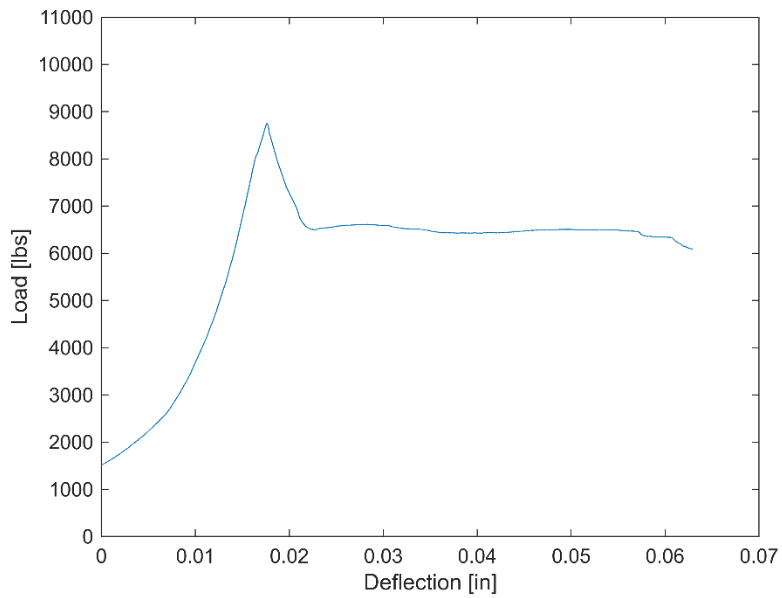

Figure 44: Load-Deflection Curve for 25% Komponent® Concrete 28-Day Modulus of Rupture Test, Specimen 2

The peak of the load-deflection curve marks the point of initial cracking. The deflections of all specimens featured a plateau after the initial crack due to the post-cracking tensile strength of the fiber-reinforcement. By comparing this load held during the plateau period to the max load for each specimen, a relative strength was calculated. For the Expansive BCSA specimen, the strength held after cracking as a percentage of maximum load was 74%. This percentage for the two 25% Komponent® specimens were 93% and 79% for an average of 85.5%.

Certain limitations of the testing procedure may restrict some of the conclusions that can be drawn from this information such as the small deflections at the beginning of the test. Particularly, the testing mechanism relies on hydraulics to apply the load which can apply a steady load rate as long as the speed of the hydraulic itself is greater than the rate of deflection. When the rate of deflection becomes too fast for the hydraulics, the testing apparatus cannot apply the same load rate, and the testing mechanism becomes more deflection-based as the hydraulic system attempts to keep up with the deflection of the specimen. Due to this limitation, the specimens' measured strength post-cracking results from the large deflection alleviating some of the applied stress by the hydraulics. This is representative of the actual strength of the specimen, but a more sudden failure would be observed if the hydraulic was able to maintain the maximum load achieved. This loading situation would be more similar to dead loads in design.

While structural elements that would crack due to a persistent load would not benefit from reduced post-cracking strength, members such as pavements that are designed to withstand traveling loads could benefit from post-cracking strength if the load that induced the crack only occurred once. Design of pavements could utilize the post-cracking strength as a limit in design instead of strength at failure as an additional factor of safety as overloading the pavement would be less detrimental.

4.2 *Expansive Properties*

4.2.1 Expansive BCSA

Figures 45 through 47 show the measured strain for fiber-reinforced Expansive BCSA specimens for various restraint and wet-curing conditions.

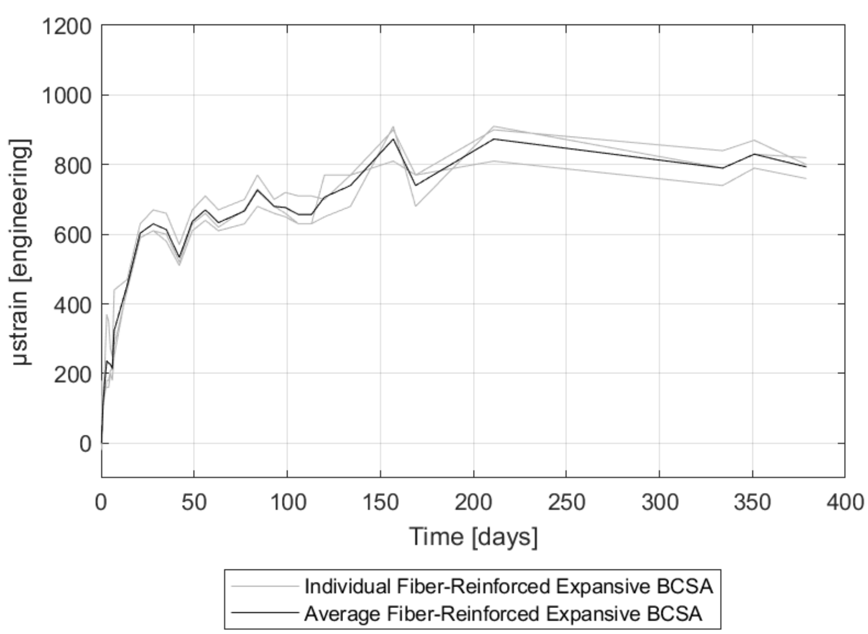

Figure 45: Expansion of Fiber-Reinforced Expansive BCSA Concrete,

ASTM C878 Restrained, Indefinite Wet Cure

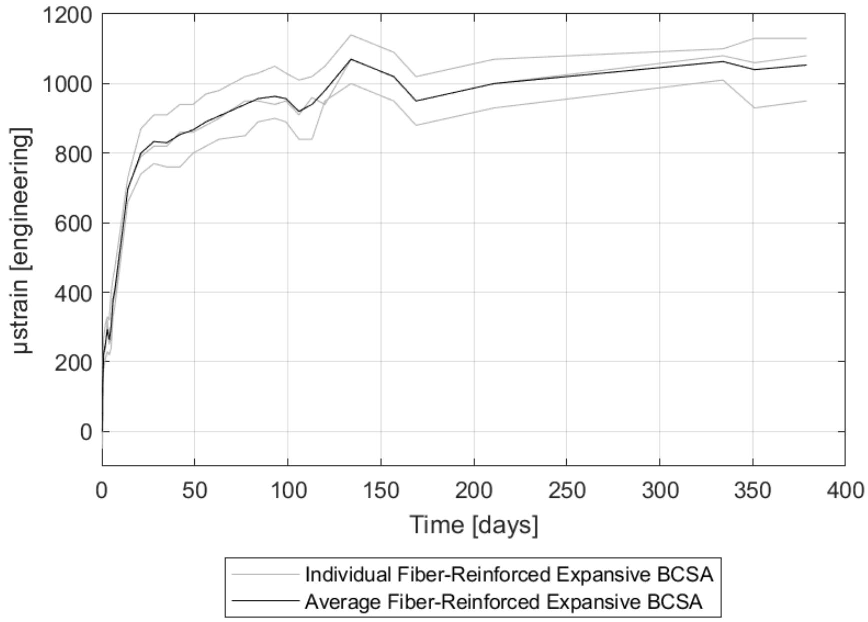

Figure 46: Expansion of Fiber-Reinforced Expansive BCSA Concrete,
ASTM C157 Unrestrained, Indefinite Wet Cure

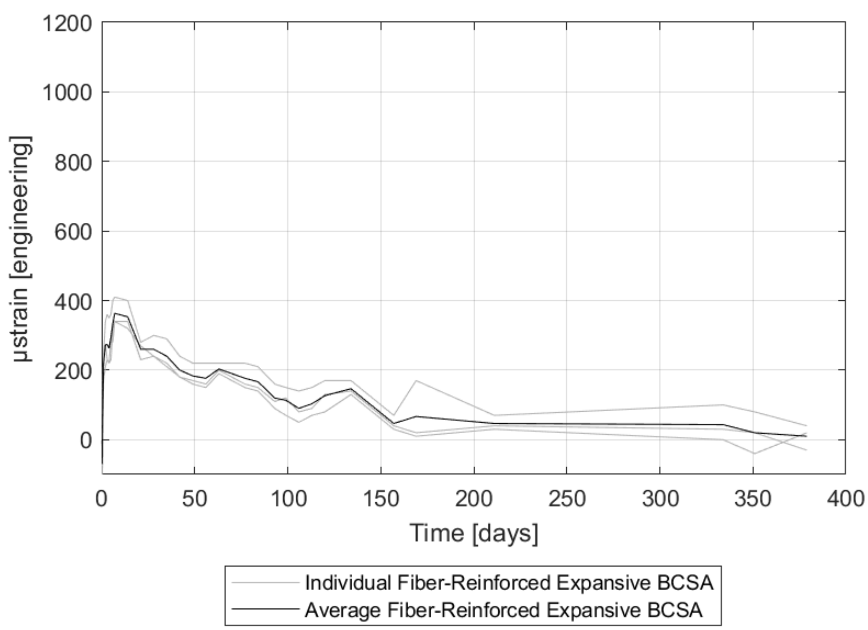

Figure 47: Expansion of Fiber-Reinforced Expansive BCSA Concrete,
ASTM C157 Unrestrained, 7-Day Wet Cure

A summary of Figures 45 through 47 is provided in Table 5 based on the average strain between conditions.

Table 5: Summary of Expansion of Fiber-Reinforced Expansive BCSA Concrete at 1 Year

Specimen	Curing Condition	Max Expansion (μstrain)	Max Shrinkage (μstrain)	Notes
Restrained Expansion	Indefinite	873	-	Net Expansion
Unrestrained Expansion	Indefinite	1070	-	Net Expansion
Restrained Expansion	7-Day	363	350	Net Shrinkage

The indefinite wet-cured Expansive BCSA specimens displayed a net expansion after 1 year. With a 7-day wet cure, the expansion of the Expansive BCSA specimens was able to completely offset the drying shrinkage experienced between when the specimens were removed from the water tanks and 1 year of age. These specimens experienced a change of approximately 350 μstrain caused by shrinkage. As expected, for indefinite wet cured specimens, restrained ASTM C878 specimens realized a reduced maximum expansion compared to unrestrained ASTM C157 specimens due to the confinement of the internal steel rod and steel end plates. The indefinitely wet-cured specimens exhibited continued expansion after the first seven days of the wet-cure which indicates that the seven day wet-cured specimens had expansive potential beyond the recommended duration of standard ACI practices for wet-curing expansive cement concretes. Depending on the utilization of the Expansive BCSA, the wet-cure period could be extended in more expansion is desired. Further insights can be made through comparison between fiber-reinforced and plain specimens from Starks (2023) as depicted in Figures 48 through 50. These plots use the minimum and maximum individual specimens to act as a margin of error.

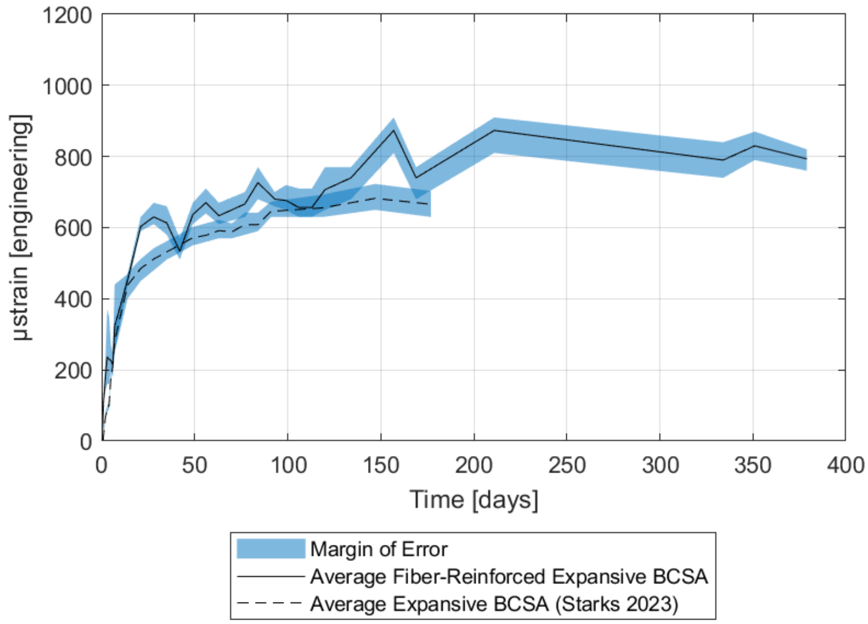

Figure 48: Expansion of Fiber-Reinforced and Plain Expansive BCSA Concrete, ASTM C878 Restrained, Indefinite Wet Cure

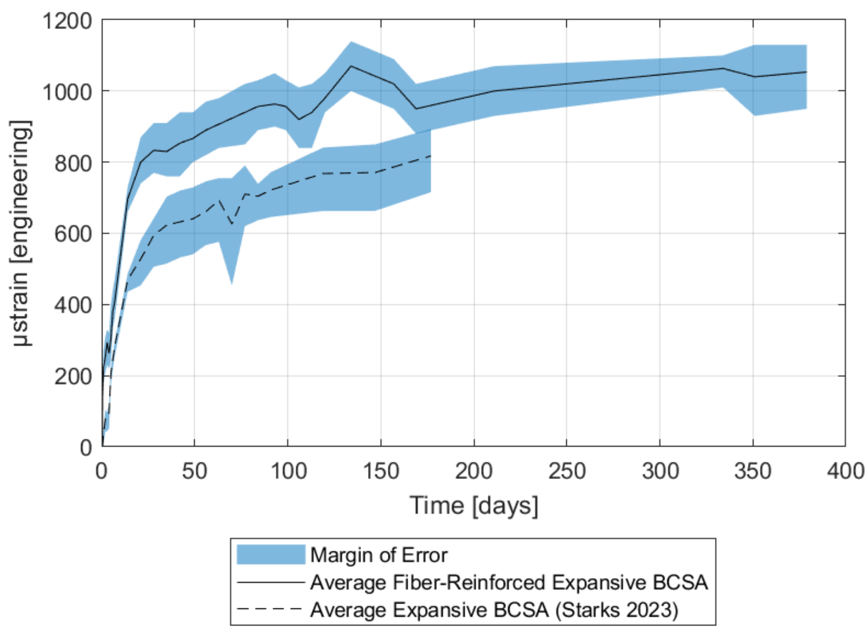

Figure 49: Expansion of Fiber-Reinforced and Plain Expansive BCSA Concrete, ASTM C157 Unrestrained, Indefinite Wet Cure

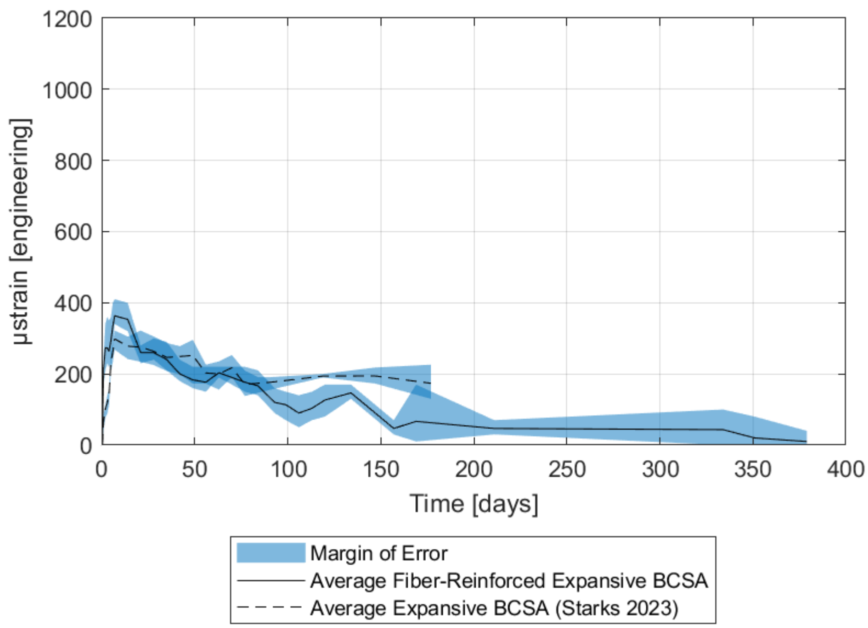

Figure 50: Expansion of Fiber-Reinforced and Plain Expansive BCSA Concrete, ASTM C157 Unrestrained, 7-Day Wet Cure

The margins of error for restrained specimens with an indefinite wet cure and unrestrained specimens with a seven-day wet cure overlap considerably between fiber-reinforced and plain specimens, indicating minimal difference in behavior due to the addition of steel fibers. However, the fiber-reinforced unrestrained indefinite wet cure specimens displayed a higher expansion than specimens without fibers in Starks (2023). This behavior is counterintuitive and could be caused by certain external factors such as the environment at the time of year of casting and the measurements being sensitive to the individual conducting the test. Due to the overall similar behavior between fiber-reinforced and plain specimens, there is no indication of chemical prestressing through reinforcement provided by the presence of steel fiber reinforcement at the dosage of fibers used in the original mix design.

4.2.2 Double Fiber-Reinforced Expansive BCSA

Due to the overall similar behavior between fiber-reinforced and plain specimens, an additional set of ASTM C157 unrestrained specimens with double the fiber-reinforcement (1.5%

fibers by volume) of all the other fiber-reinforced specimens was cast and tested under indefinite and seven-day wet curing conditions. A comparison of compressive strength for the double fiber-reinforced Expansive BCSA specimens is provided in Figure 51. These specimens exhibited higher compressive strengths than the original fiber-reinforced specimens, resulting in the compressive strengths to be more similar to those that are without fiber reinforcement. It is expected that adding additional fibers would further increase compressive strength. However, there was a significant loss in workability for the double fiber-reinforced specimens. Even with the reduced workability with a slump of 2.5 in., the double fiber-reinforced concrete was within the slump requirement of 2 ±1 in. for a Class A concrete in the Oklahoma Department of Transportation 2019 Standard Specifications for Highway Construction. Unlike all other specimens, the double fiber-reinforced specimens required a vibratory table during placement rather than rodding. This change in method of consolidating the concrete could also contribute to difference in compressive strengths compared to the original fiber-reinforced specimens.

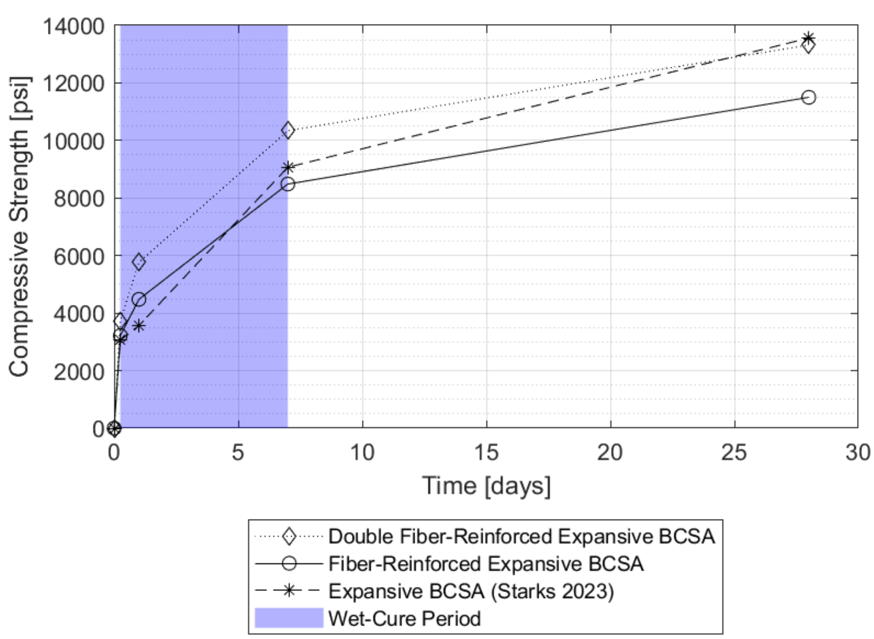

Figure 51: Compressive Strengths of Double-Fiber Reinforced Expansive BCSA Concrete

Figure 52 and Figure 53 show the expansion data for the double fiber-reinforced specimens. Similar to the other unrestrained specimens subjected to a seven-day wet cure, The double fiber-reinforced specimens subjected to a seven-day wet cure reached a near net zero strain after 207 days, an earlier age than the original fiber-reinforced specimens.

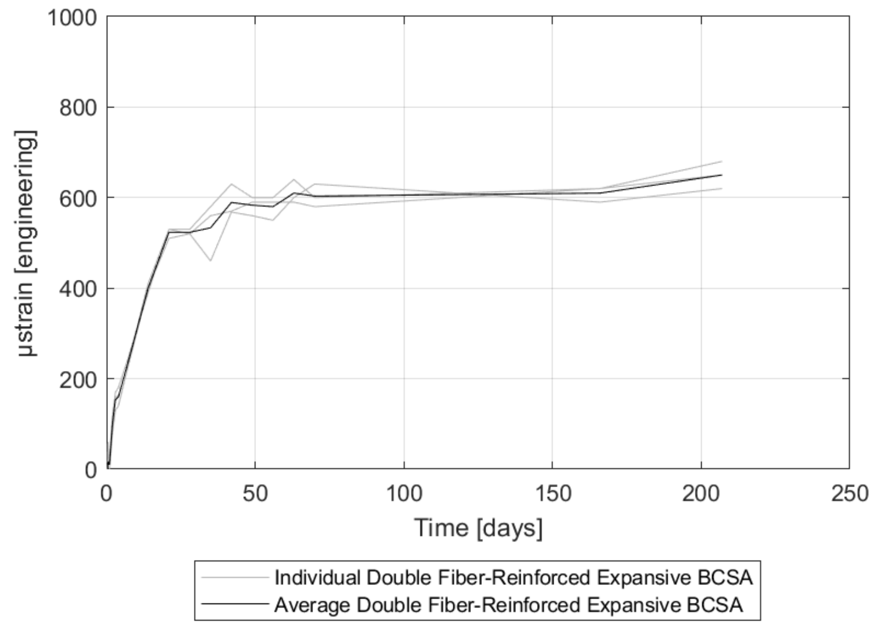

Figure 52: Expansion of Double Fiber-Reinforced Expansive BCSA, ASTM C157 Unrestrained, Indefinite Wet Cure

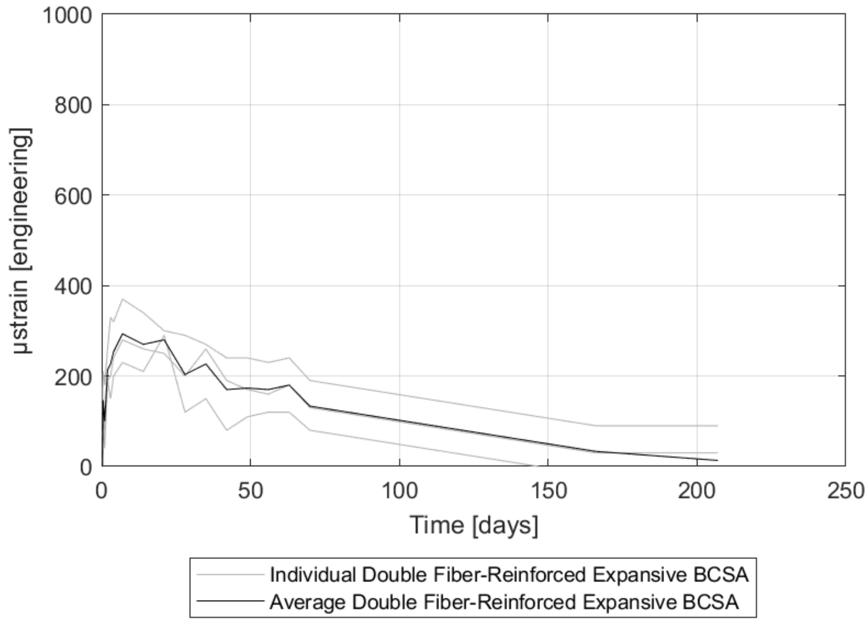

Figure 53: Expansion of Double Fiber-Reinforced Expansive BCSA, ASTM C157 Unrestrained, 7-Day Wet Cure

Figure 54 and 55 compare the expansion for the double fiber-reinforced specimens with results from the single fiber-reinforced specimens.

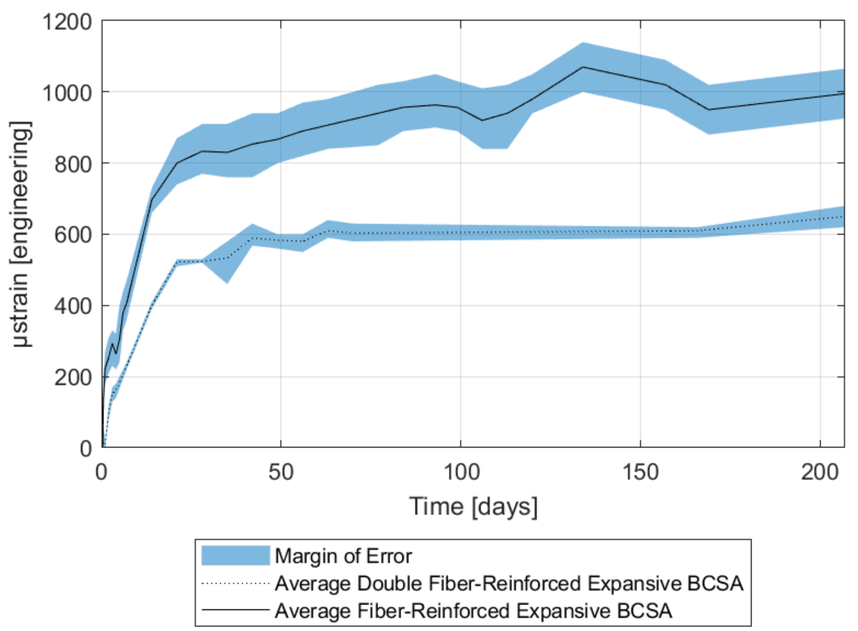

Figure 54: Expansion of Various Fiber-Reinforcement of Expansive BCSA, ASTM C157 Unrestrained, Indefinite Wet Cure

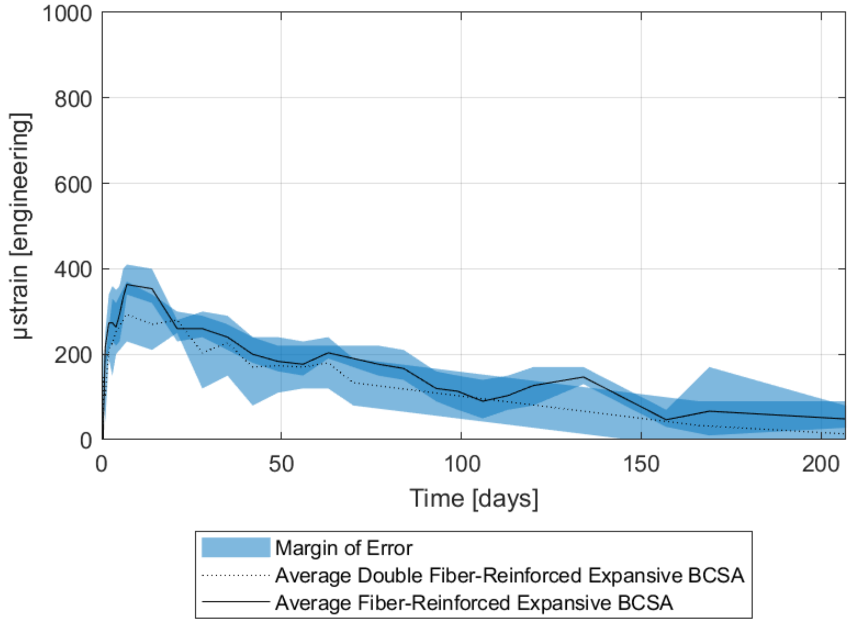

Figure 55: Expansion of Various Fiber-Reinforcement of Expansive BCSA, ASTM C157 Unrestrained, 7-Day Wet Cure

Although double the dosage of steel fibers was included in the concrete, there is considerable overlap in the margin of error for the double fiber-reinforced and original fiber-reinforced Expansive BCSA unrestrained specimens with a wet cure of seven days. However, there is a significant deference between double fiber-reinforced and original fiber-reinforced specimens when subjected to an indefinite wet cure, indicating that there is confinement provided by the higher dosage of steel fibers. The average strain for the unrestrained double fiber-reinforced specimens is more similar to the restrained single fiber-reinforced specimens. Using the modulus of elasticity calculated for original fiber-reinforced specimens at 28 days and the difference in strain at the same age for double fiber-reinforced specimens to original fiber reinforced specimens, a theoretical prestress can be calculated using Eq. 3. While a theoretical calculated prestress, this could greatly improve flexural resistance.

$$\sigma = E_c \Delta\varepsilon \quad (3)$$

$$\sigma = (5.335 * 10^6\ psi) * \ (833 - 523)\ \mu strain$$

$$\sigma = 1654\ psi$$

4.2.3 25% Komponent®

Figures 56 through 58 show the measured strain for fiber-reinforced 25% Komponent® specimens for various restraint and wet-curing conditions.

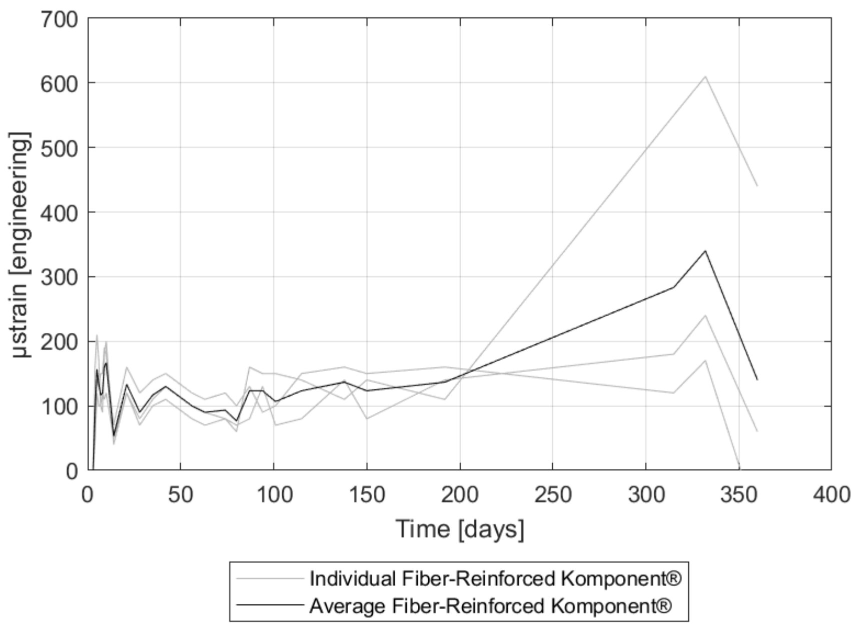

Figure 56: Expansion of Fiber-Reinforced 25% Komponent® Concrete, ASTM C878 Restrained, Indefinite Wet Cure

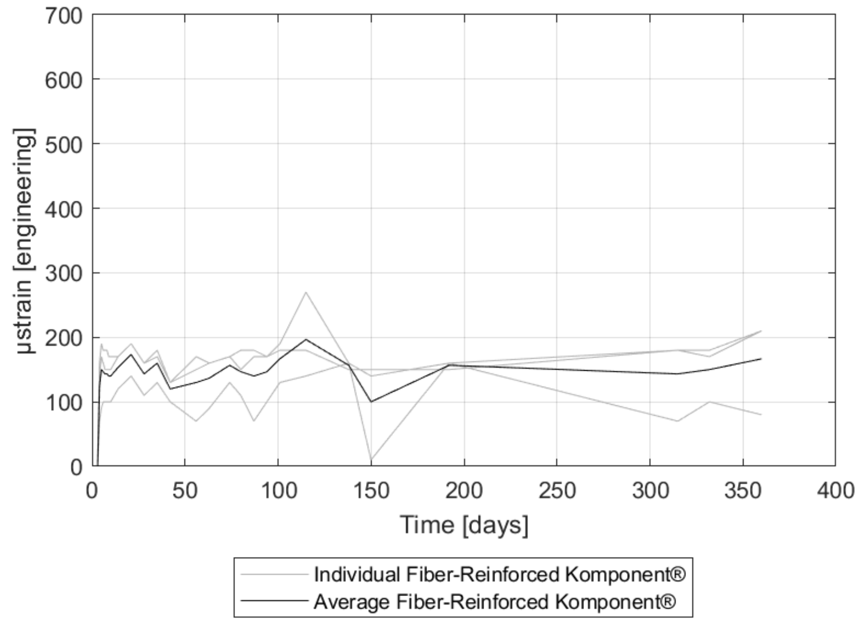

Figure 57: Expansion of Fiber-Reinforced 25% Komponent® Concrete, ASTM C157 Unrestrained, Indefinite Wet Cure

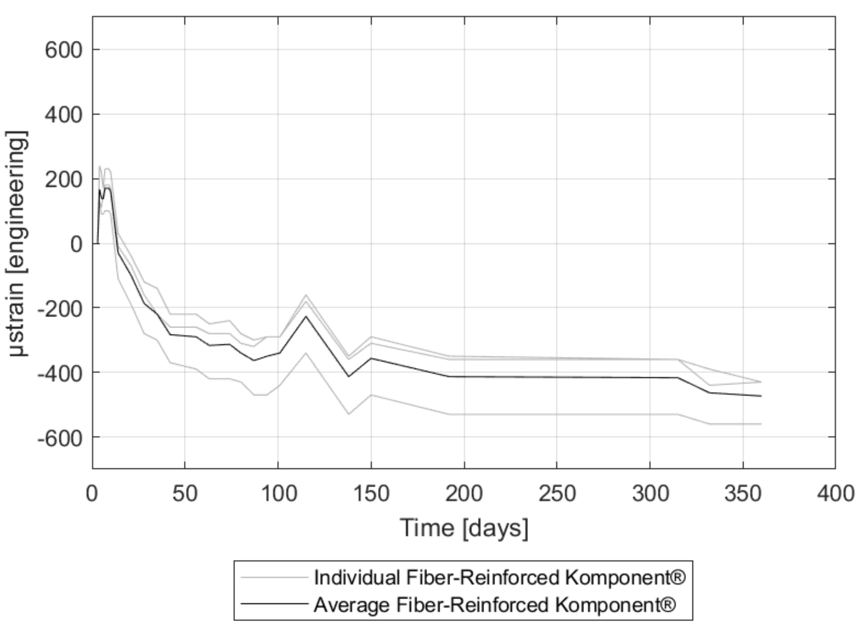

Figure 58: Expansion of Fiber-Reinforced 25% Komponent® Concrete, ASTM C157 Unrestrained, 7-Day Wet Cure

A summary of Figures 56 through 58 are provided in Table 6 based on the average strain between conditions. The measurements of the ASTM C878 restrained indefinitely wet-cured 25% Komponent® specimens exhibited volatility and is not included in the expansion analysis for the concrete. As the operator of the comparator when taking measurements can have a significant effect on the results, it was intended for the same operator to conduct all measurements. However, for the later age measurements, a second operator conducted measurements which could have contributed to the volatility of the ASTM C878 specimens.

Table 6: Summary of Expansion of Fiber-Reinforced 25% Komponent® Concrete at 1 Year

Specimen	Curing Condition	Max Expansion (µstrain)	Max Shrinkage (µstrain)	Notes
Restrained Expansion	Indefinite	167	-	Net Expansion
Unrestrained Expansion	Indefinite	197	-	Net Expansion
Restrained Expansion	7-Day	170	643	Net Shrinkage

The indefinitely wet-cured 25% Komponent® specimens displayed a net expansion at 1 year. The 25% Komponent® concrete specimens subjected to a 7-day wet cure experienced 643 µstrain in drying shrinkage, a third of which was offset by the initial expansion. There is negligible difference between the strain at the initial expansion for the indefinitely wet-cured restrained ASTM C878 and unrestrained ASTM C157 specimens, indicating that the magnitude of the expansion was not significant enough to engage the confinement provided by the internal steel rod and steel end plates. Additionally, all 25% Komponent® concrete specimens shared a similar maximum expansion, suggesting that the initial expansive period is contained within the first seven days of wet curing. Figures 59 through 61 show the strain measured for the fiber-reinforced specimens alongside the strain measured for plain specimens by Starks (2023).

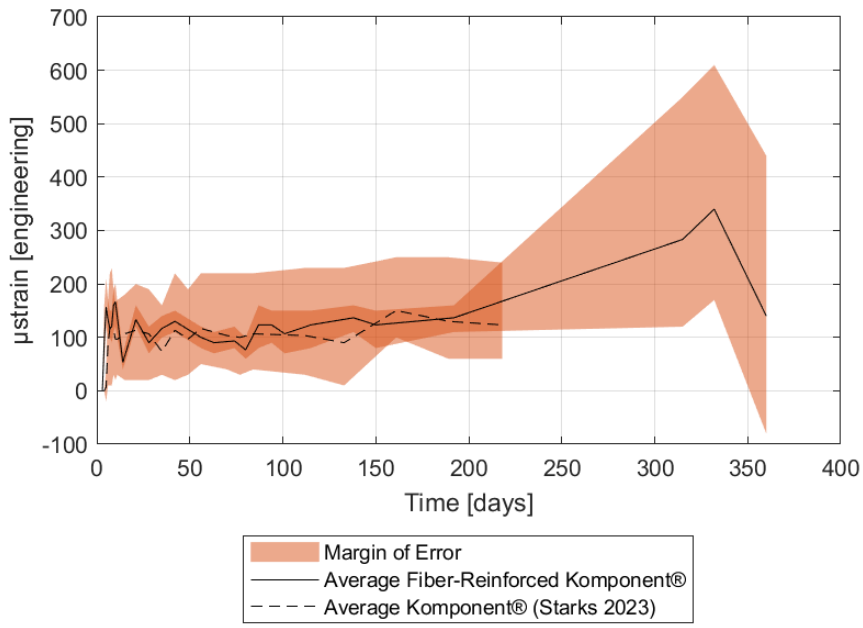

Figure 59: Expansion of Fiber-Reinforced and Plain Expansive BCSA Concrete, ASTM C878 Restrained, Indefinite Wet Cure

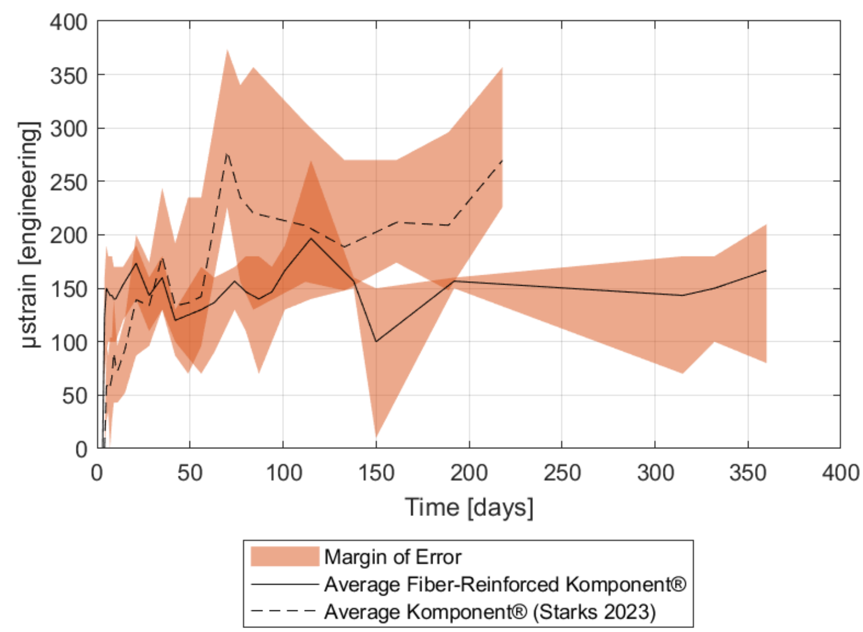

Figure 60: Expansion of Fiber-Reinforced and Plain Expansive BCSA Concrete, ASTM C157 Unrestrained, Indefinite Wet Cure

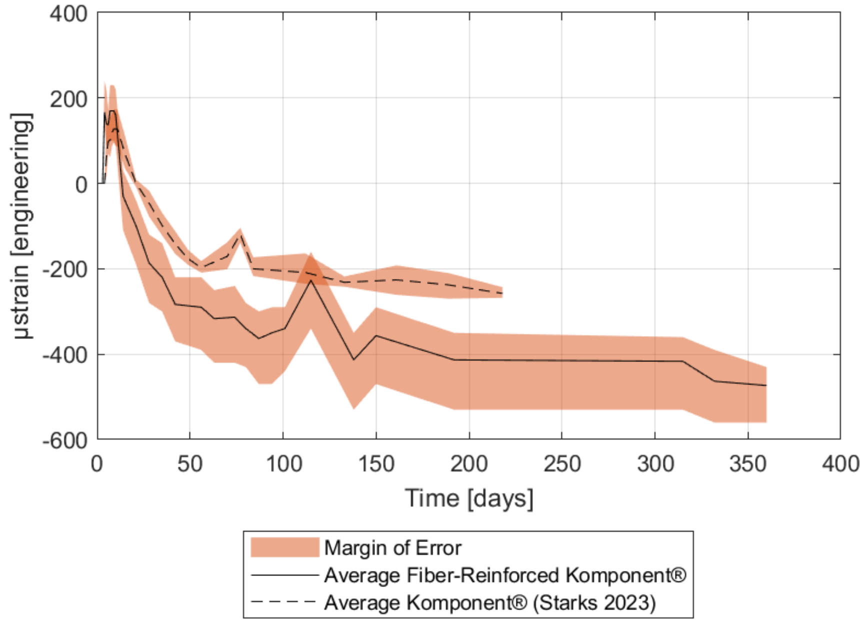

Figure 61: Expansion of Fiber-Reinforced and Plain Expansive BCSA Concrete, ASTM C157 Unrestrained, 7-Day Wet Cure

Similar to Expansive BCSA specimens, strain measurements between the indefinitely wet-cured fiber-reinforced and plain 25% Komponent® specimens shared considerable overlap indicating negligible effect by the inclusion of steel fibers in the concrete. However, for the seven day wet-cured 25% Komponent® specimens, more shrinkage was observed for the fiber-reinforced specimens. As mentioned prior, strain measurements is highly influenced by external factors such as environmental conditions at the time of measurement along with heightened sensitivity to the individual collecting the measurement. The concerns with the supply of Komponent® cement used in the fiber-reinforced specimens raised by results from the modulus of rupture testing might be related to the unexpected expansive behavior.

4.3 *Creep and Shrinkage Behavior*

4.3.1 Expansive BCSA

Figure 62 plots the raw results for the three creep cylinders in the creep column and the two companion shrinkage cylinders for the fiber-reinforced Expansive BCSA concrete specimens. The initial sample rate was taken at 5-minute intervals for the first week after casting and then extended to 30-minute intervals. The compressive strength at the time of loading was 3630 psi. The load applied to reach 60% of compressive strength was 61.5 kips.

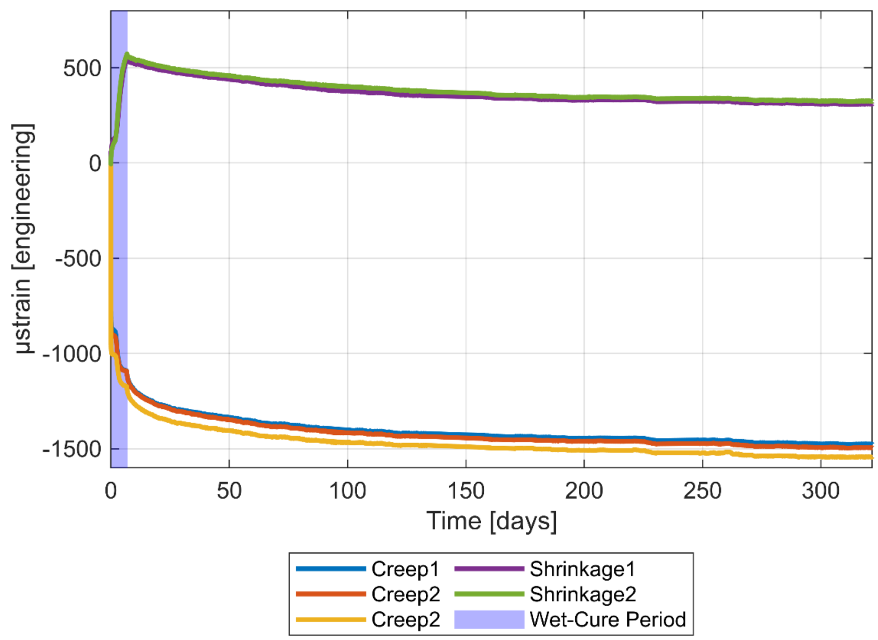

Figure 62: Raw Creep and Shrinkage Specimens of Fiber-Reinforced Expansive BCSA Concrete

Adjustments for elastic strain behavior developed during the loading of the creep cylinder is shown in Figure 63. Additionally, initial shrinkage is modified to begin at the time of loading to distinguish behavior post-loading.

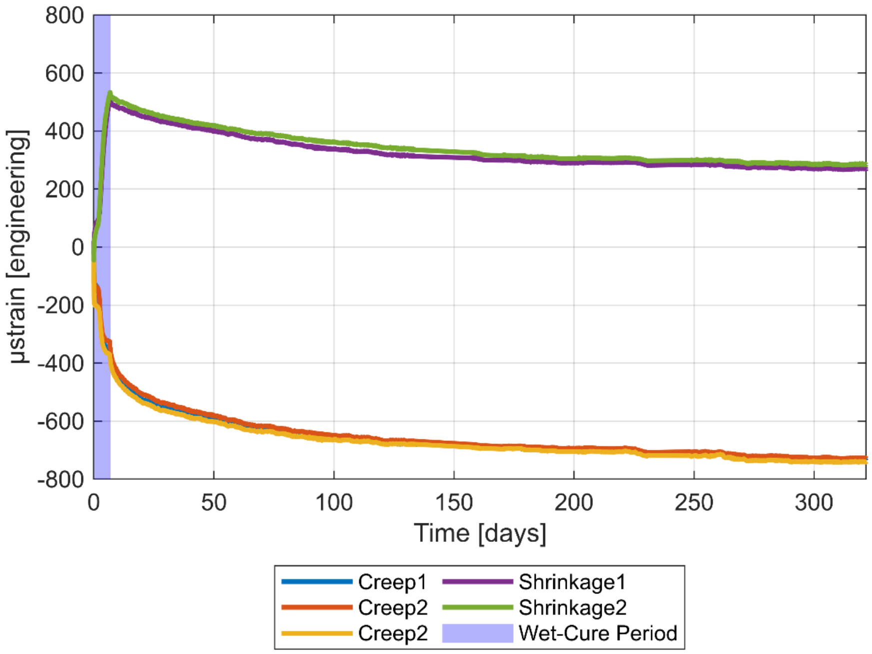

Figure 63: Adjusted Creep and Shrinkage Specimens of Fiber-Reinforced Expansive BCSA Concrete

Several commonalities are observed between the fiber-reinforced Expansive BCSA specimens and Starks' plain specimens. Of note is the rapid rate of creep and expansion displayed in the early ages of specimens. Figure 64 plots the first four weeks of measurements with averages of specimens. True creep (difference between shrinkage companion cylinders and creep cylinders) is also plotted. Figure 65 plots these averages for the entire duration of testing.

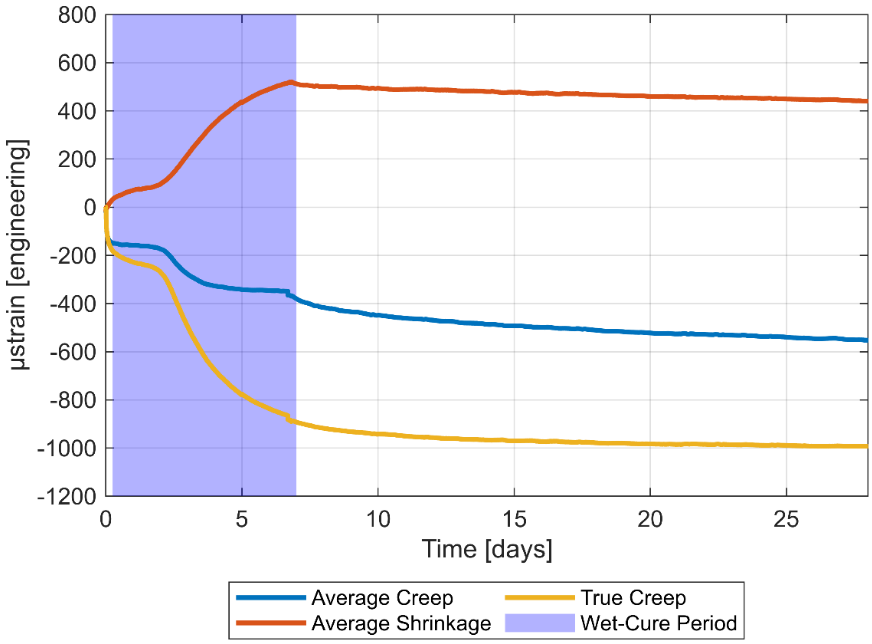

Figure 64: 28-Day Adjusted Creep and Shrinkage Specimens of Fiber-Reinforced Expansive BCSA Concrete

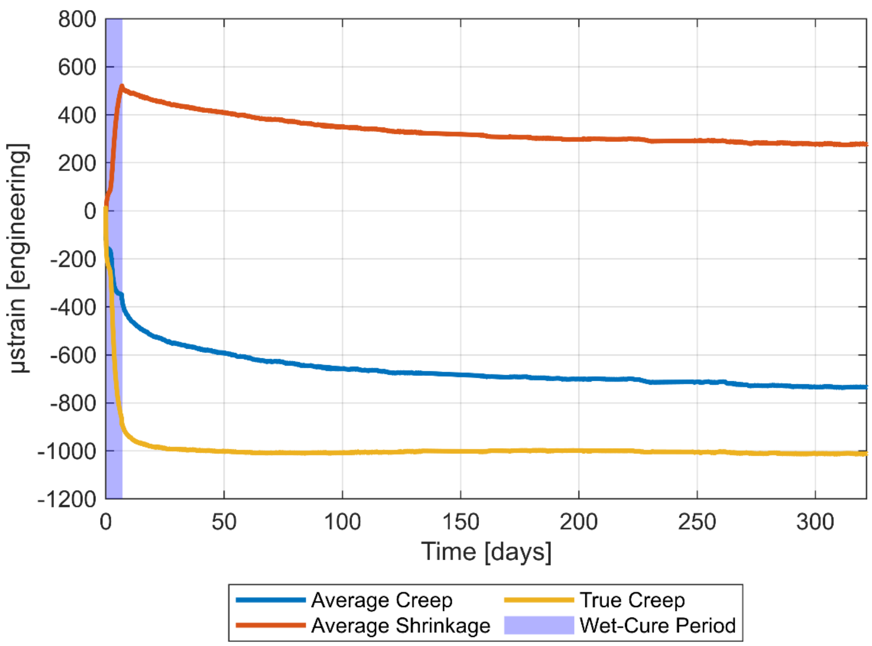

Figure 65: Average Adjusted Creep and Shrinkage Specimens of Fiber-Reinforced Expansive BCSA Concrete

Fiber-reinforced Expansive BCSA concrete developed 200 µstrain of true creep in the first 12 hours of loading or 20% of ultimate creep strain. In contrast, Starks' plain specimens exhibited a significantly higher creep strain of 500 µstrain (60% of their ultimate creep strain) during that time period. The initial loading of plain specimens, as noted by Starks, was delayed due to specimens not exhibiting enough strength until 12 hours after casting. While shrinkage adjustments were accounted for, overall behavior could be affected by delayed loading. This, alongside general variability such as environmental conditions, could contribute to other discrepancies between strain data for fiber-reinforced and plain Expansive BCSA specimens.

Another key difference in behavior between fiber-reinforced and plain Expansive BCSA specimens was the nearly double expansion observed in the fiber-reinforced companion shrinkage specimens. This expansion is also in disagreement with the ASTM C157 and C878 specimens made with the same mix design. This could also relate to the reduced immediate creep observed in fiber-reinforced specimens. As the true creep is the difference between strains in the creep cylinders and shrinkage cylinders, the higher measured expansion produces in a larger calculated true creep. This results in an overall true creep of 1000 µstrain observed in fiber-reinforced specimens, roughly 200 µstrain more than the plain specimens. This difference is reduced when comparing the creep cylinder strains, roughly 50 µstrain.

A significant behavior change was displayed by the fiber-reinforced Expansive BCSA specimens around the second day after casting in which creep and expansion rates increased after initially plateauing after the first day. This delay in expansion could also contribute to less immediate creep as the confined expansion generates additional sustained compressive stresses within the creep cylinders. However, both plain and fiber-reinforced specimens developed approximately 90% of their ultimate creep strain during the wet-cure period.

Another similarity is the overall relative mitigation of creep by expansive behavior. Both fiber-reinforced and plain specimen creep data reveal that 1/3 of true creep is offset by the expansive behavior when comparing the strain in the shrinkage cylinders to the calculated true creep at the end of testing.

4.3.2 25% Komponent®

Unfortunately, complications arose during the loading of fiber-reinforced 25% Komponent® creep cylinders. Similar to Starks' Expansive BCSA specimens mentioned previously, the 25% Komponent® specimens did not have enough strength at the intended time of loading. Instead of extending the period before loading, the specimens were loaded at a reduced load and loaded again to a higher magnitude after two weeks. When analyzing the raw data from these specimens, all three VWSGs within the creep cylinders failed early in the testing procedure. The VWSGs contained in the companion shrinkage cylinders did not exhibit this failure. While the shrinkage readings from the fiber-reinforced specimens were slightly less than the recorded plain specimens, no insights can be definitely stated as the difference in expansion is not consistent with data collected from the ASTM C157 specimens.

Table 7: Average Max Shrinkage of 25% Komponent® Companion Shrinkage Cylinders

Specimen	Max Expansion (μstrain)
Plain	344
Fiber-Reinforced	275

4.4 *Large-Scale Testing*

4.4.1 Initial Loading Protocol

Specimen CSP2 was the first specimen to be tested under the original protocol outlined in Chapter 3. The initial tests revealed that the expected reaction of subgrade modulus and deformed shape were inaccurate. LVDT data display the global tilt that the specimen experienced during the cyclic loading (Figure 66 shown for sample). It was anticipated that the fatigue loading would result in the deflection measured by the midspan LVDTs (North and South) to be similar and the deflection measured by the end LVDTs (West and East) to also be similar.

Instead, one midspan LVDT and one end LVDT would often have larger displacements than the other two, indicating a tilting effect. Additionally, the direction of the tilting was variable across testing.

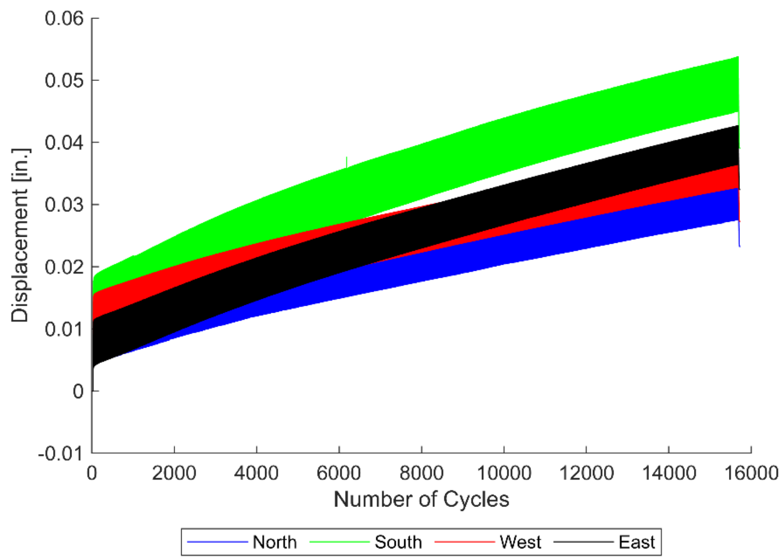

Figure 66: Example CSP2 - Individual LVDT Displacement

The delta used to back-calculate the modulus of subgrade reaction, plotted in Figure 67, is taken as the difference between the average of displacements measured by the end and midspan LVDTs. The spread of the plot is a function of the cyclical loading as load is continuously applied and removed. However, due to the global tilting of the specimen, this average is a false representation of the specimen's actual deformed shape, resulting in inaccurate stress ratio calculations as the actual stress distribution may show more resemblance to a uniformly loaded member on an elastic foundation. The load-deflection curve (Figure 69) generated by data collected by the MTS actuator and its internal LVDT can provide further insight into specimen behavior as a significant drift in deflection can be observed. This reveals that energy is being directed towards permanent deformation in the elastic foundation rather the generating bending stress in the specimen.

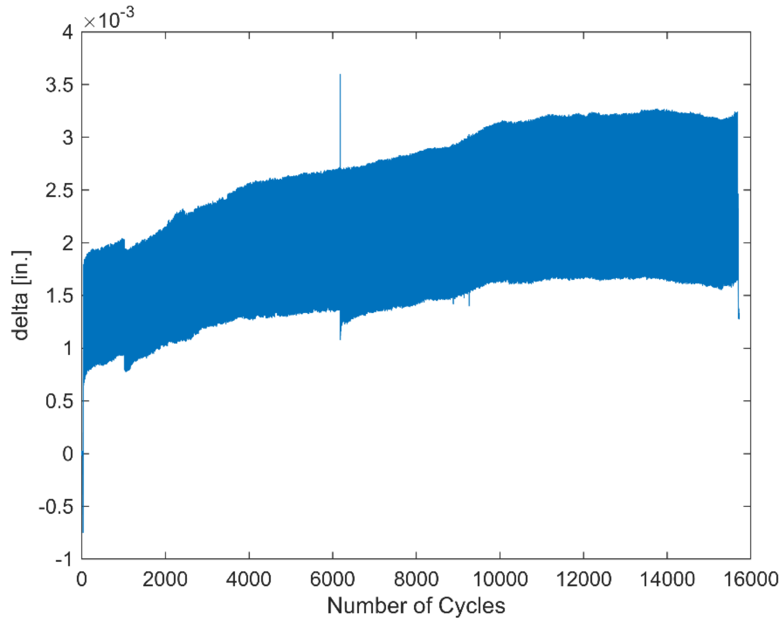

Figure 67: Example CSP2 – Difference Between Averaged End and Midspan LVDTs

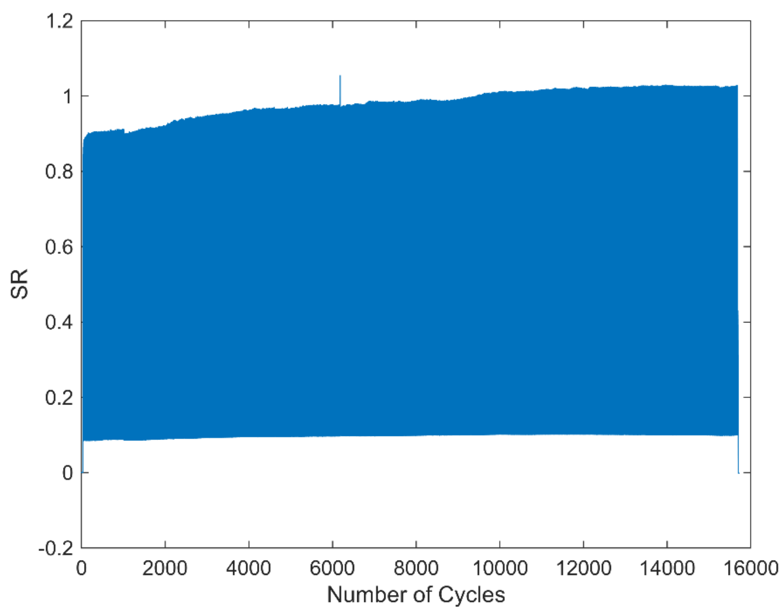

Figure 68: Example CSP2 - Elastic Foundation Stress Ratio

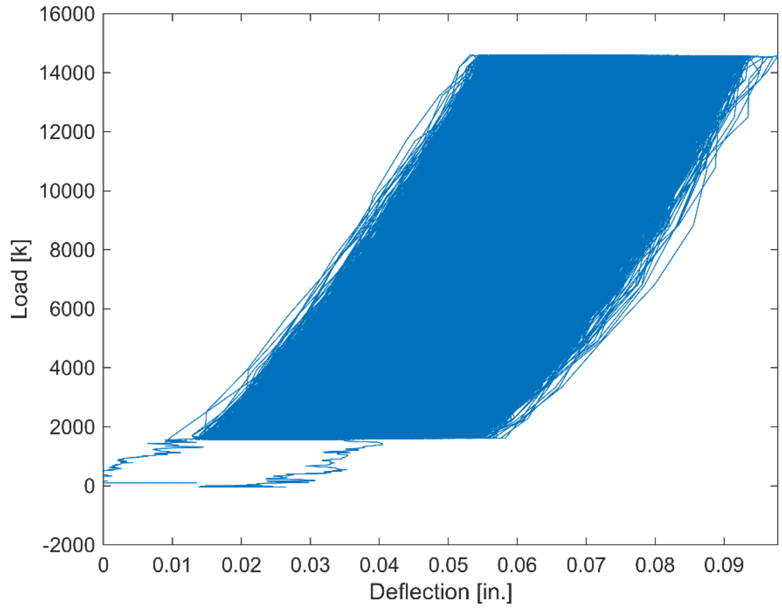

Figure 69: Example CSP2 - Load-Deflection Curve

The specimen CSP2 was further investigated under various loadings including a considerable range of loads with a total of over 100,000 cycles with no indication of cracking. As the load limits of the MTS were reached, the support conditions were adjusted to have the specimen be simply supported across bearing pads resting on the elastic foundation. LVDT data from the simply supported testing configuration reveal similar tilting behavior to the elastic foundation configuration (Figure 70). As expected with an unreinforced specimen, cracking resulted in a sudden failure with a large displacement.

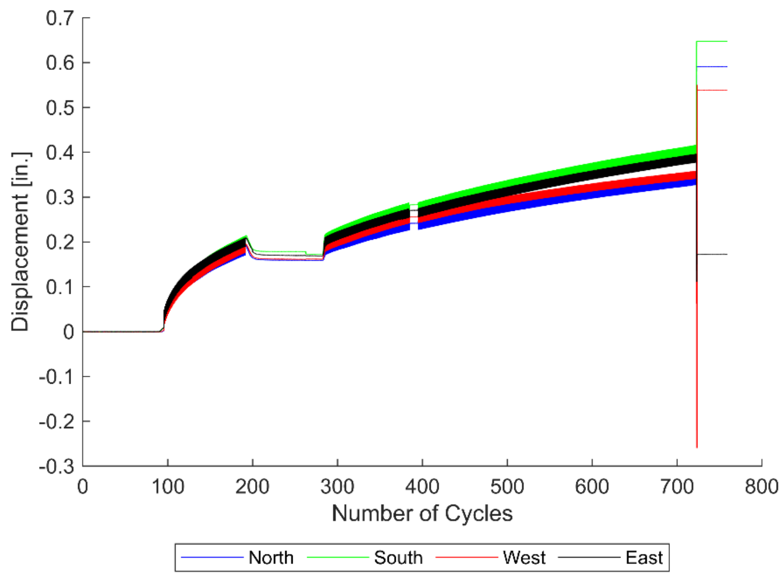

Figure 70: Example CSP2 (Simple Span) - Individual LVDT Displacement

The results of specimen CSP2 informed the modified testing protocol that all future specimens were subjected to. Due to the highly variable loading that specimen CSP2 experienced, testing results from this specimen were not included in further analysis. Unfortunately, it was also found that the foil strain gauges often provided unreliable information. Although the initial desire was for the foil strain gauges to provide information about crack development, the data collected were not useful for this purpose and no strain gauge data are included in the specimen analysis.

4.4.2 Modified Loading Protocol

The modified loading protocol selected based on the behaviors seen in the initial testing of specimen CSP2 was conducted on the eleven remaining specimens. Additionally, all slab specimens displayed the tilting behavior described for specimen CSP2 and no cracking was observed for all tests on the slab specimens when under the elastic foundation configuration. This section evaluates the behavior of specimens paired by matching cement and reinforcement type to avoid redundancy then comparing specimens across reinforcement type. Relevant plots, such as the calculated elastic foundation stress ratio and the load deflection curve generated by data collected by the MTS actuator and its internal LVDT are included for the eleven remaining specimens. Unfortunately, while it was the intention to load specimens based on a stress ratio calculated based on properties of each specimen type, the majority specimens were subjected to loading based on strengths calculated for CSP1 due to a miscommunication. Specimens that received their intended loading are noted as such.

4.4.3 Plain Expansive BCSA

Specimen CSP1 was subjected to the loading detailed in Table 8. Figures 71 through 74 plot testing results.

Table 8: CSP1 Loading Protocol

Step	Load (k)	Cycles	Configuration
1	8	5000	Elastic Foundation
2	12	5000	Elastic Foundation
3	15.5	50000	Elastic Foundation
4	12.5	Until Failure	Simple Span

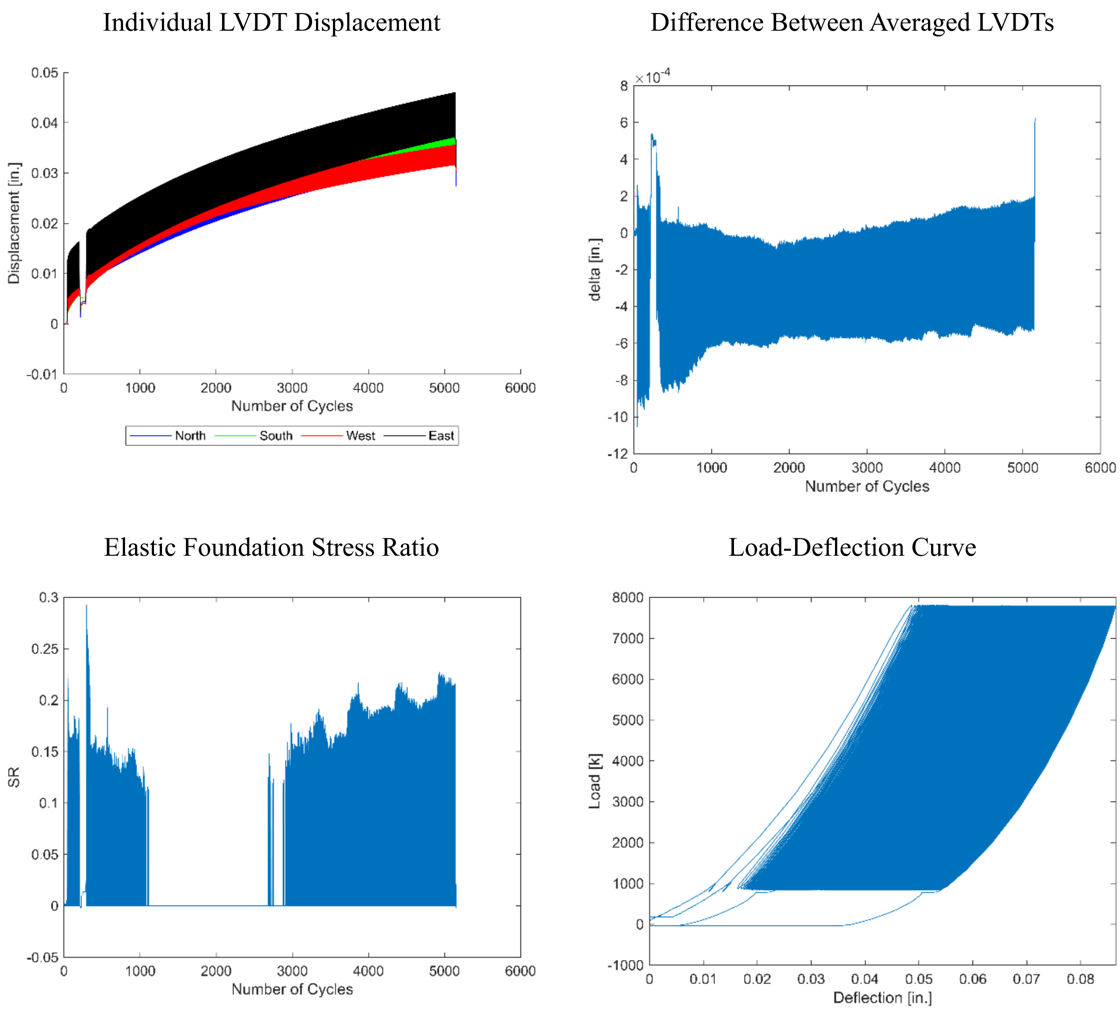

Figure 71: CSP1 Results - Step 1 (Elastic Foundation)

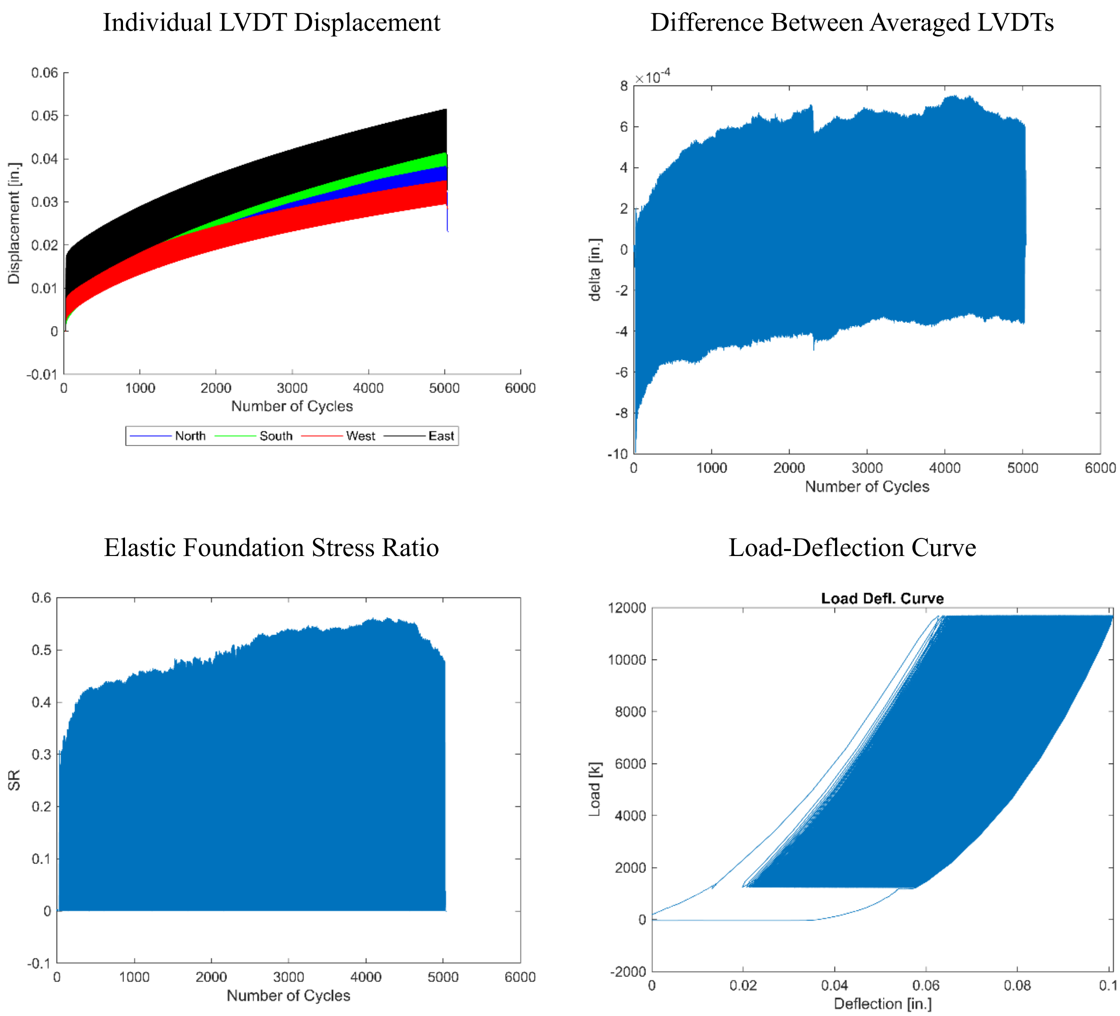

Figure 72: CSP1 Results - Step 2 (Elastic Foundation)

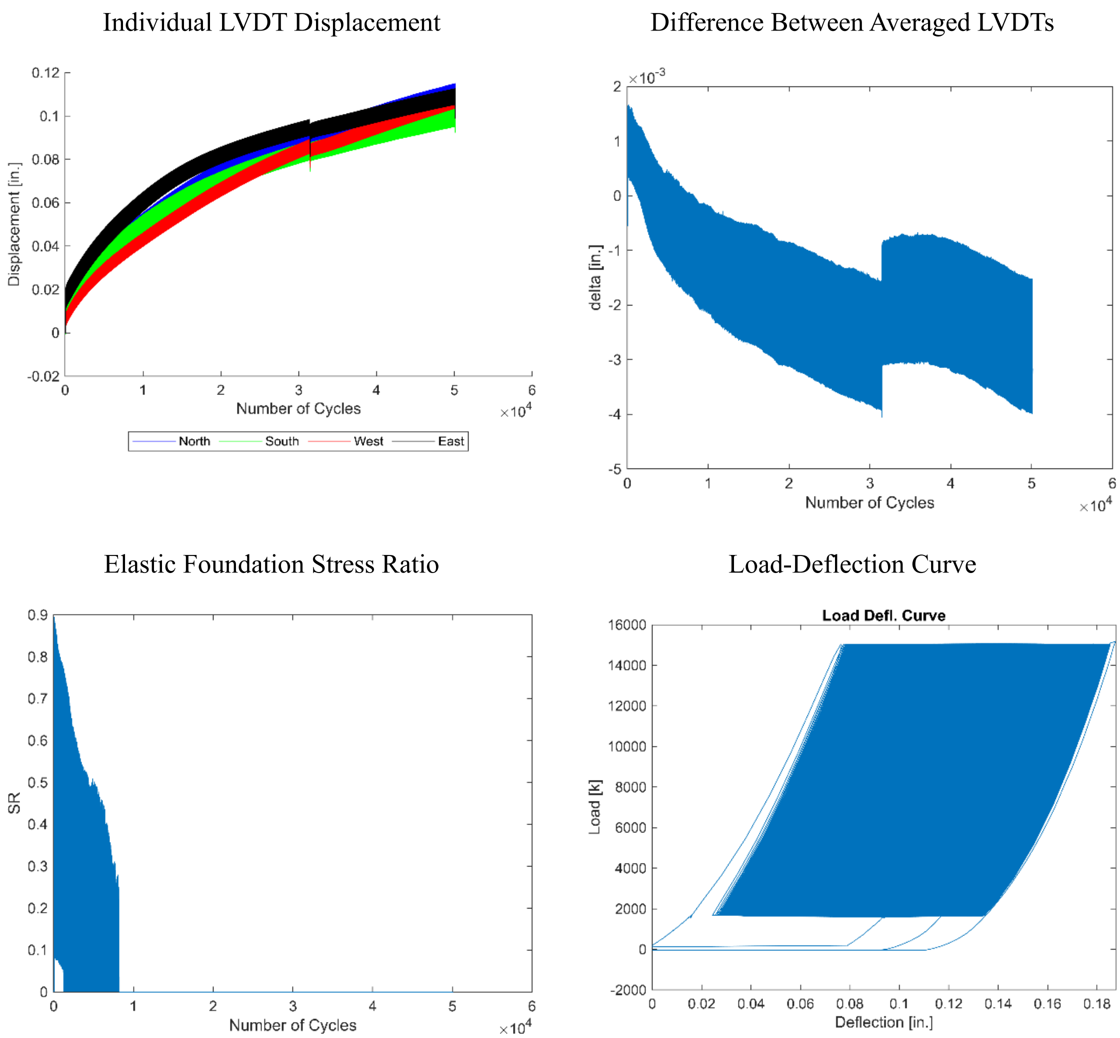

Figure 73: CSP1 Results - Step 3 (Elastic Foundation)

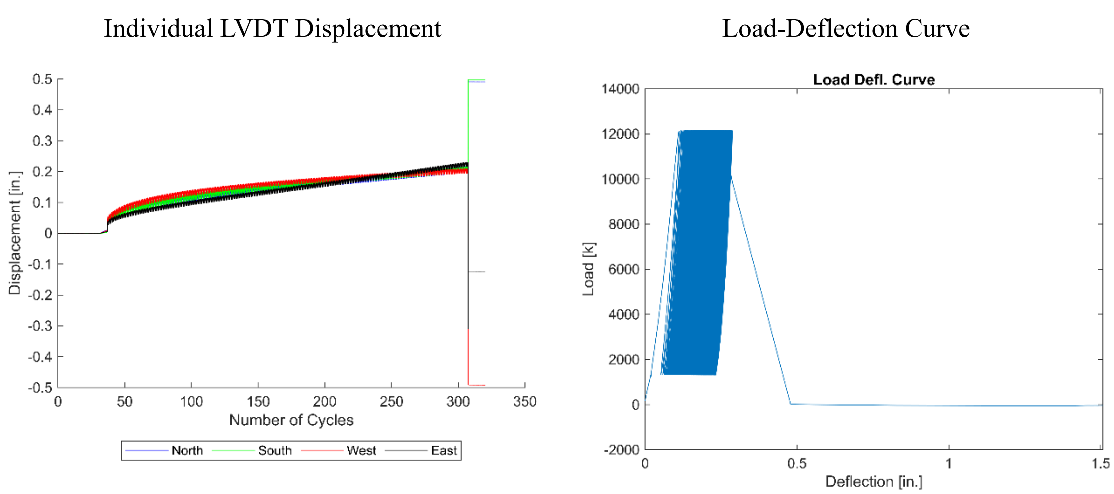

Figure 74: CSP1 Results - Step 4 (Simple Span)

Specimen CSP1 displayed a negative delta in loading Steps 1 and 3 during the cyclic loading, meaning the tilting effect was substantially controlled the deformed shape during these steps. As the stress ratio calculation expects a positive delta (i.e. midspan displacing more than the ends), the stress ratio is zeroed in regions with a negative delta. Cracking occurred during loading Step 4 at the 270th induced cycle, resulting in a sudden displacement. All steps indicated global tilting and support settlement.

4.4.4 Fiber-Reinforced Expansive BCSA

Specimens CSF1 and CSF2 were subjected to the loading detailed in Table 9 and Table 10. Figures 75 through 82 plot testing results. CSF2 was subjected to its original intended load increments based on the measured modulus of rupture of fiber-reinforced specimens.

Table 9: CSF1 Loading Protocol

Step	Load (k)	Cycles	Configuration
1	8	5000	Elastic Foundation
2	12	5000	Elastic Foundation
3	15.5	50000	Elastic Foundation
4	12.5	Until Failure	Simple Span

Table 10: CSF2 Loading Protocol

Step	Load (k)	Cycles	Configuration
1	8.75	5000	Elastic Foundation
2	13	5000	Elastic Foundation
3	17.25	50000	Elastic Foundation
4	15	Until Failure	Simple Span

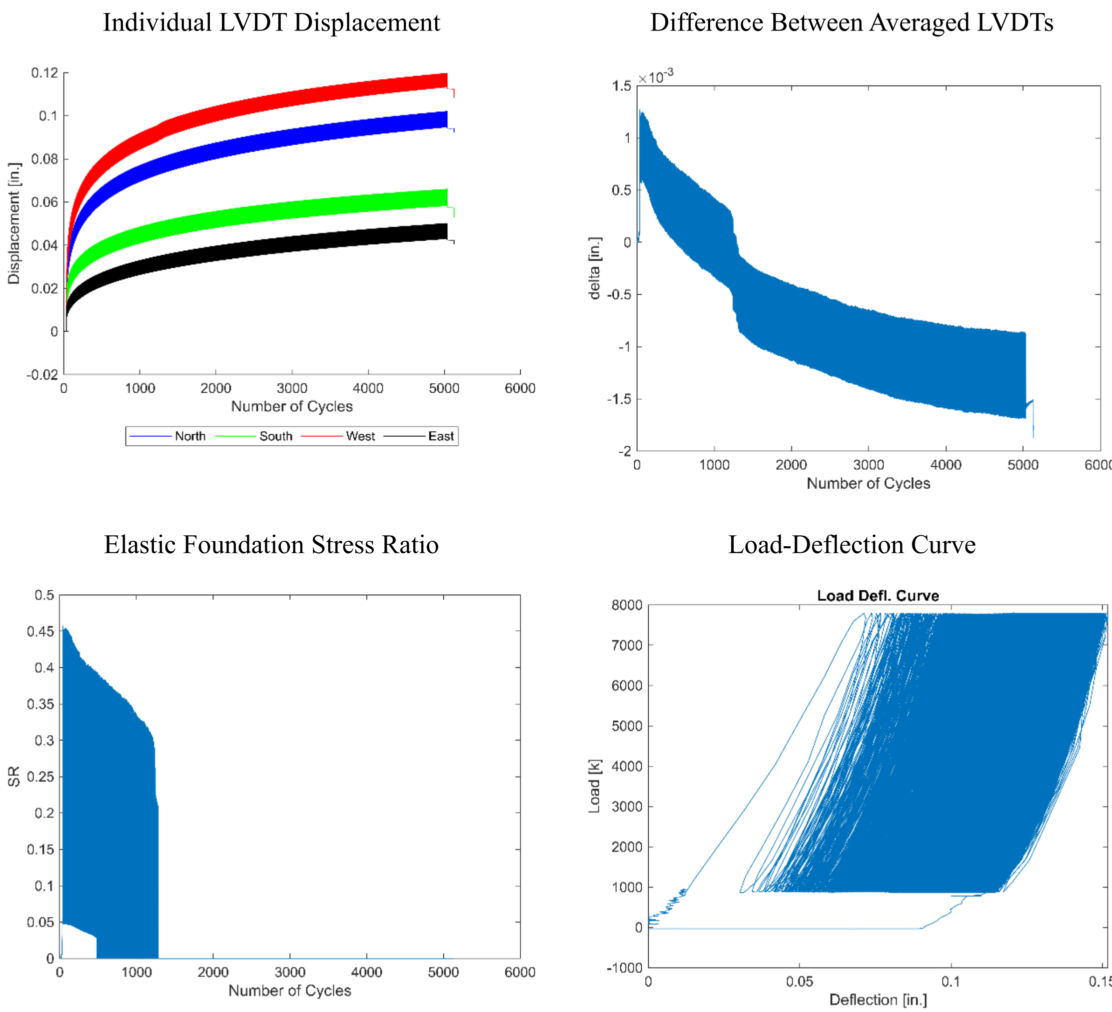

Figure 75: CSF1 Results - Step 1 (Elastic Foundation

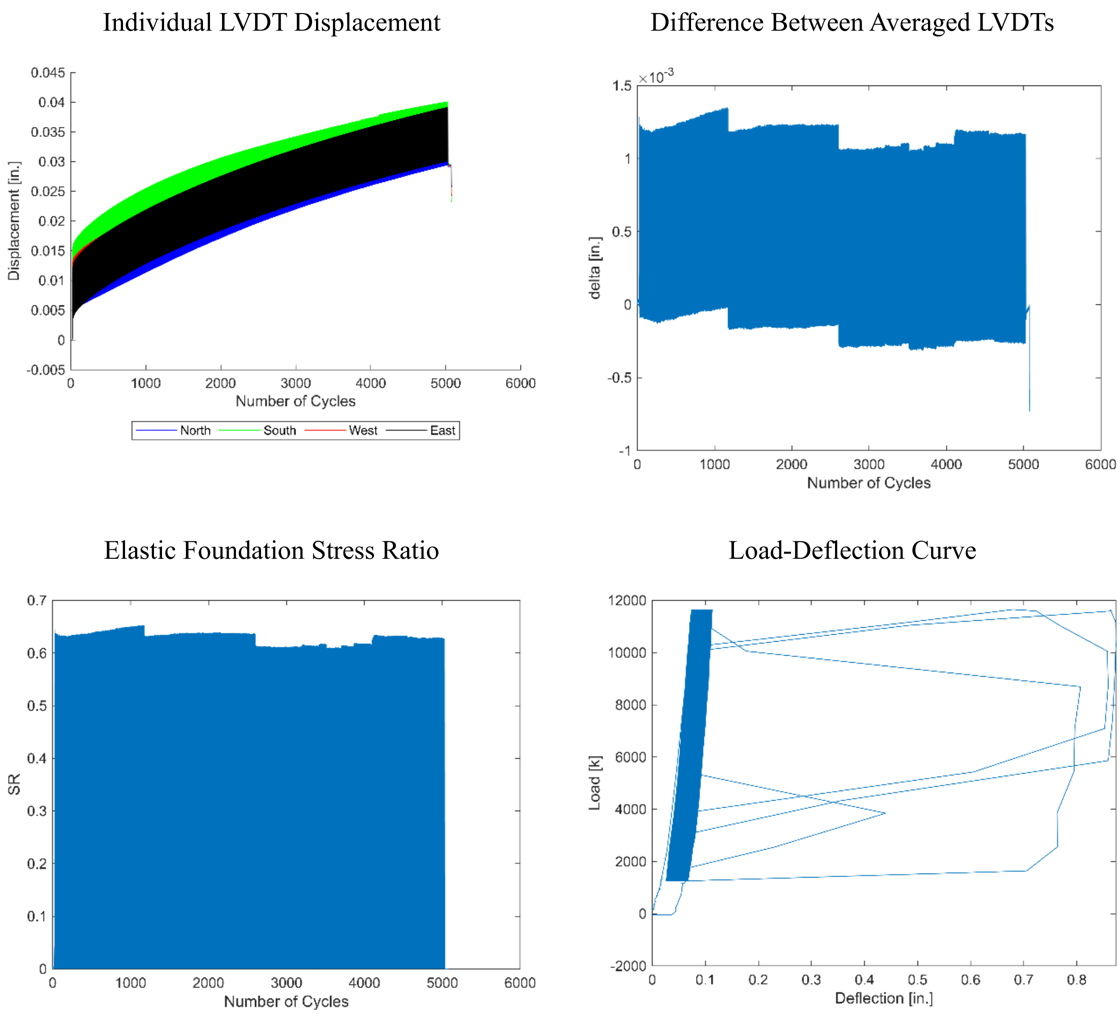

Figure 76: CSF1 Results - Step 2 (Elastic Foundation)

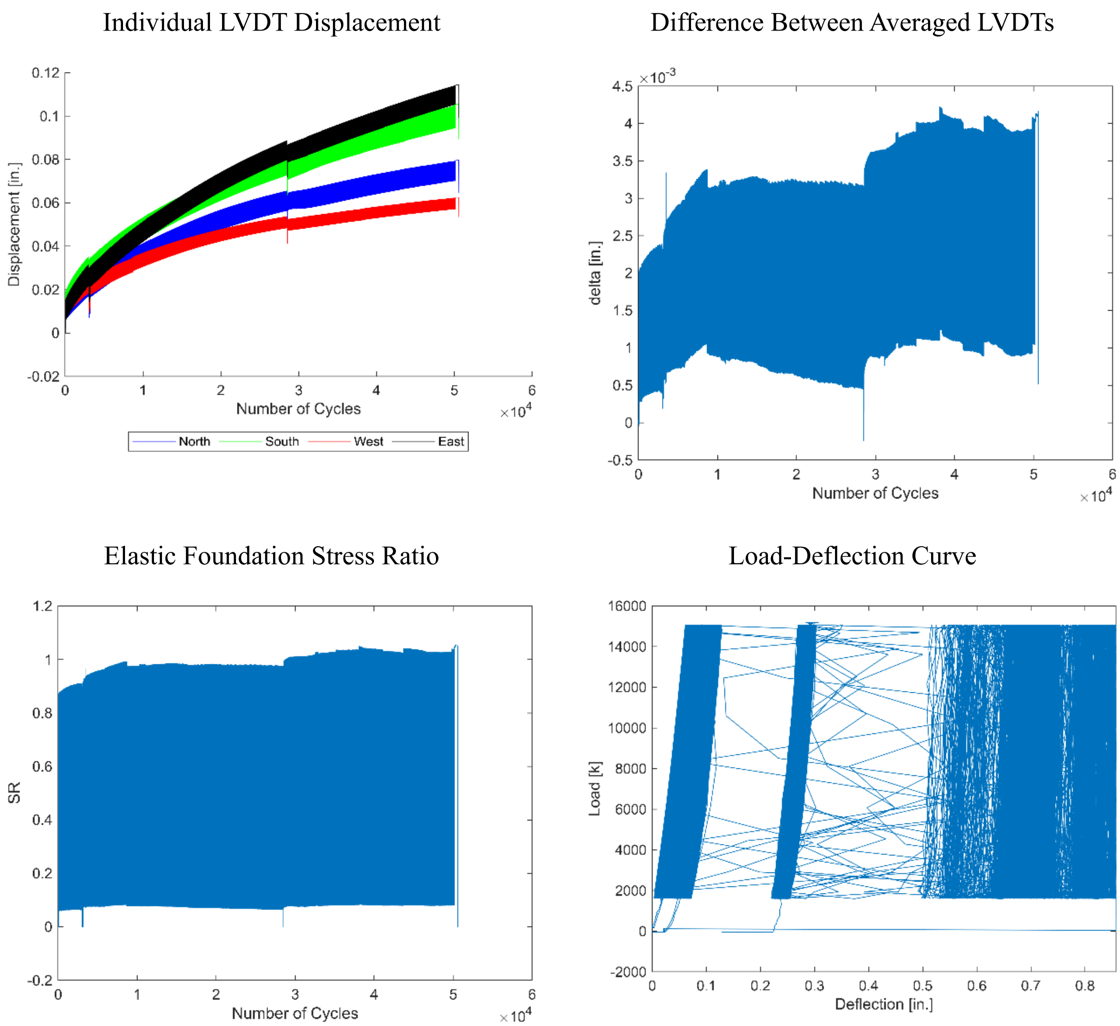

Figure 77: CSF1 Results - Step 3 (Elastic Foundation)

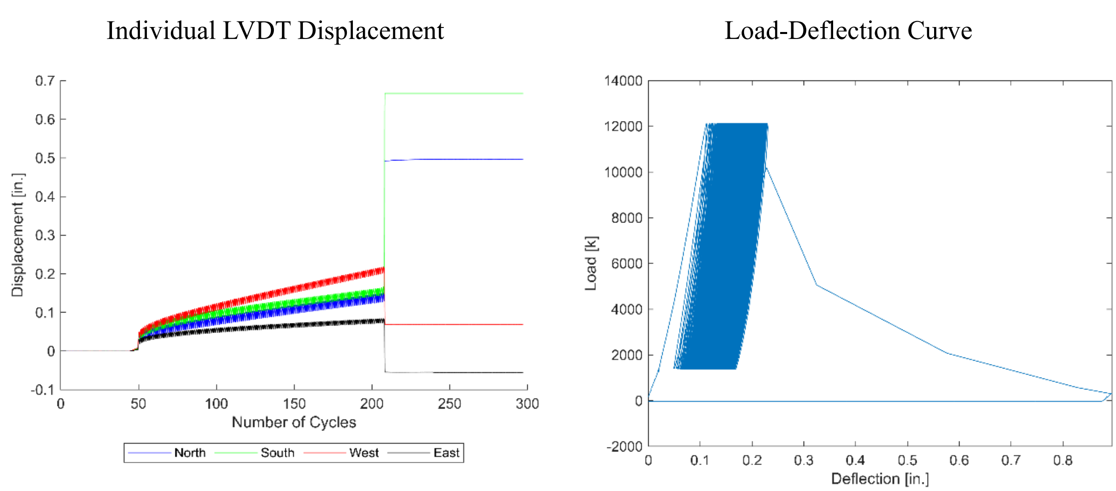

Figure 78: CSF1 Results - Step 4 (Simple Span)

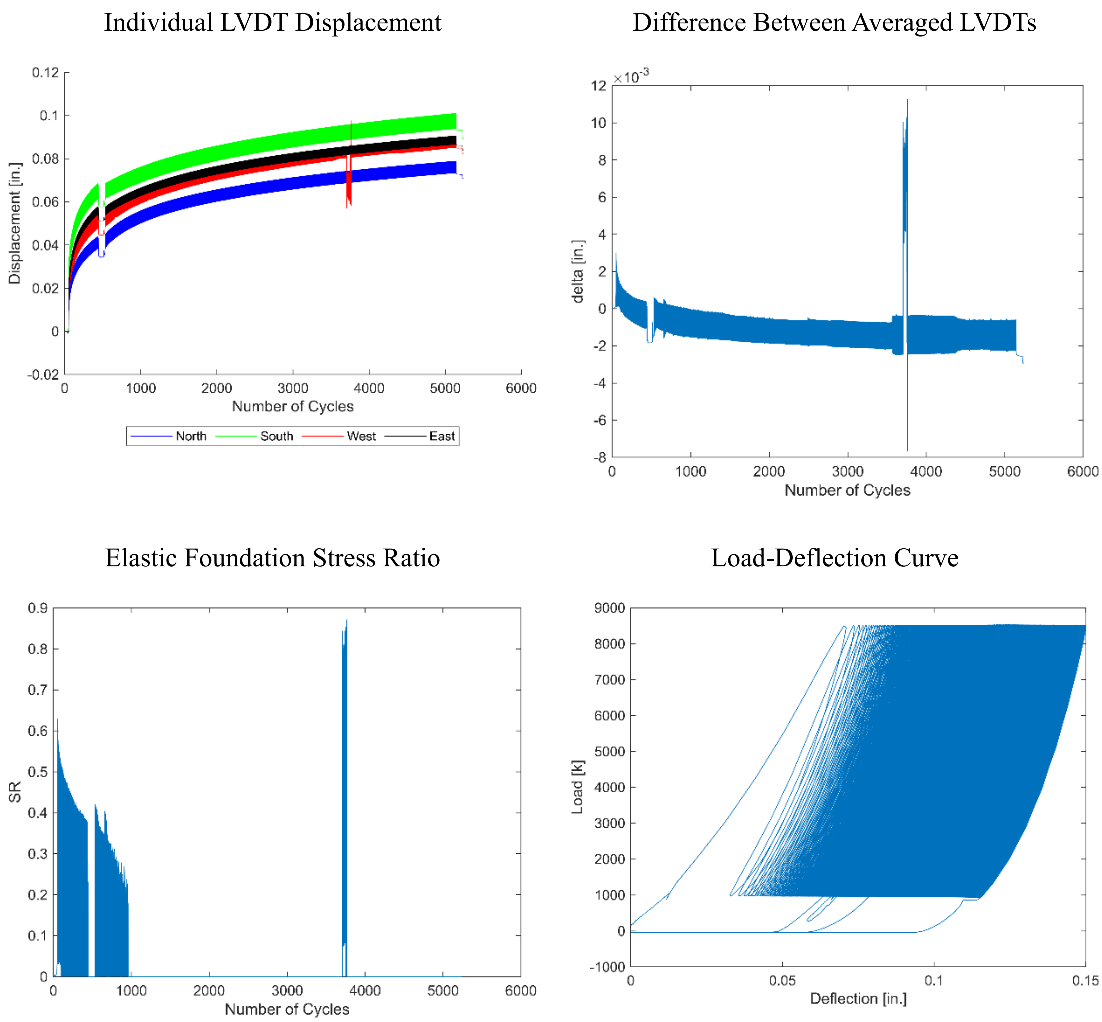

Figure 79: CSF2 Results - Step 1 (Elastic Foundation)

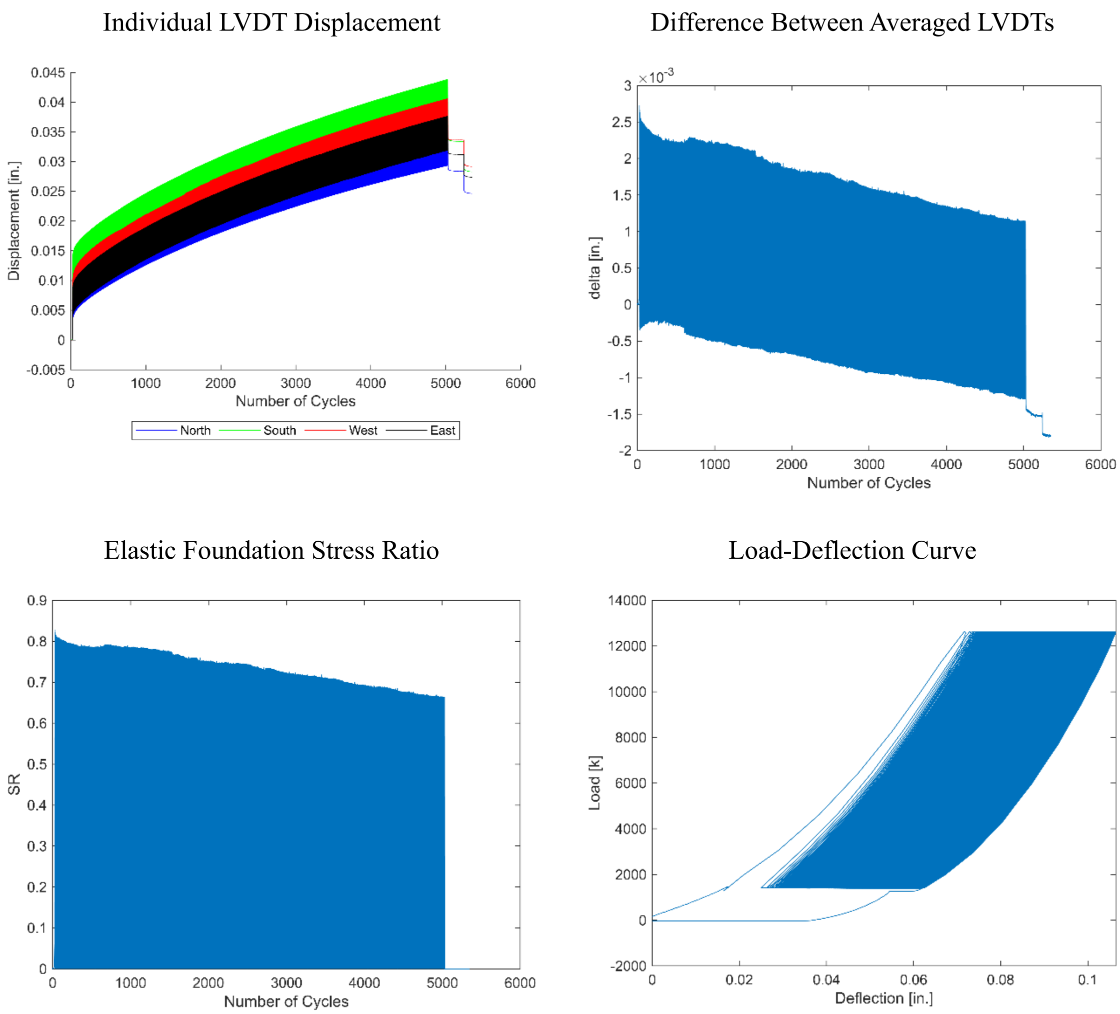

Figure 80: CSF2 Results - Step 2 (Elastic Foundation)

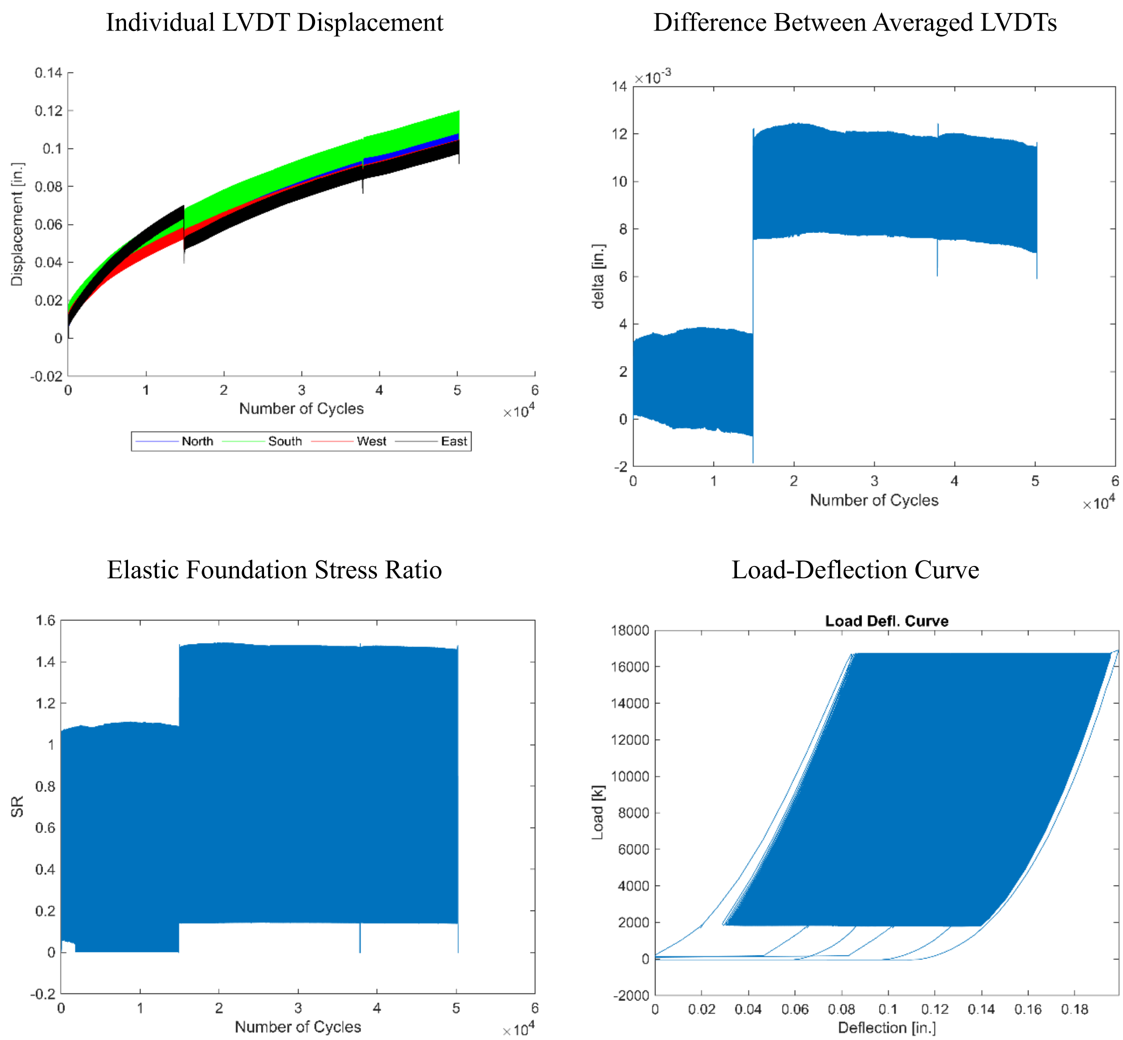

Figure 81: CSF2 Results - Step 3 (Elastic Foundation)

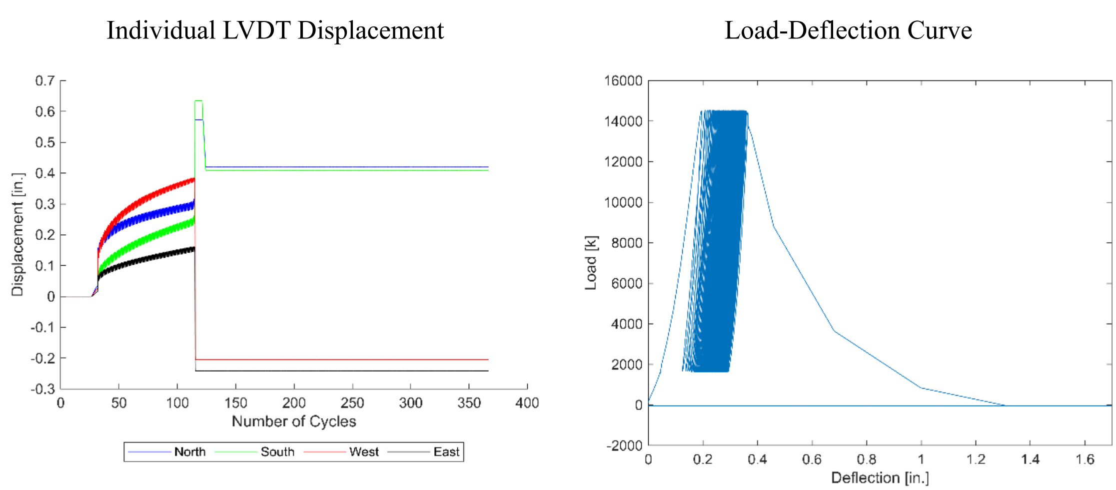

Figure 82: CSF2 Results - Step 4 (Simple Span)

Sudden temporary increased deflections occurred randomly during Step 2 of testing the CSF1 specimen as seen in load-deflection curve of Figure 76. As deflection returned to the previous magnitude rather quickly, the instability in the load-defection curve is more likely related to an equipment error than a signal of cracking. A similar instability was observed for Step 3 of the same specimen as it showed an increased deflection in the trend of the load-deflection curve, rather than returning to its previous deflection. This could be indicative of cracking development as increased deflection would be a result of decreased stiffness; however, no cracks were observed during this step of the loading protocol.

The average cycle at failure during Step 4 for the fiber-reinforced BCSA specimens was 120, both resulting in sudden failures. The stress ratio in Step 4 of CSF2 being over 1 further supports the notion that specimens are subjected to an actual flexural stress lower than the calculated stress due to difference between the idealized and actual deformed shape. All steps indicated global tilting and support settlement.

4.4.5 Continuously-Reinforced Expansive BCSA

Specimens CSCR1 and CSCR2 were subjected to the loading detailed in Table 11. Figures 83 through 90 plot testing results.

Table 11: CSCR1 & CSCR2 Loading Protocol

Step	Load (k)	Cycles	Configuration
1	8	5000	Elastic Foundation
2	12	5000	Elastic Foundation
3	15.5	50000	Elastic Foundation
4	12.7	Until Failure	Simple Span

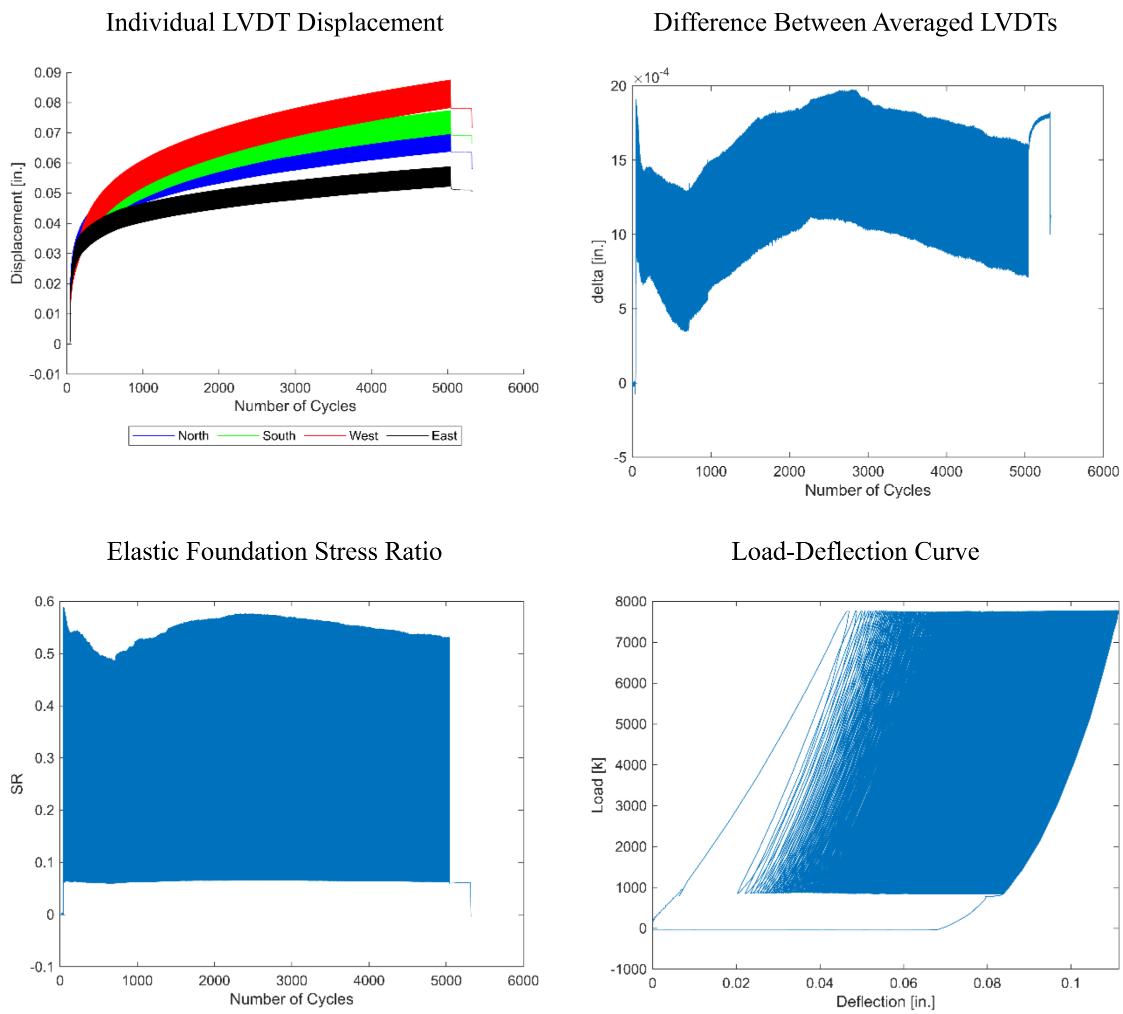

Figure 83: CSCR1 Results - Step 1 (Elastic Foundation)

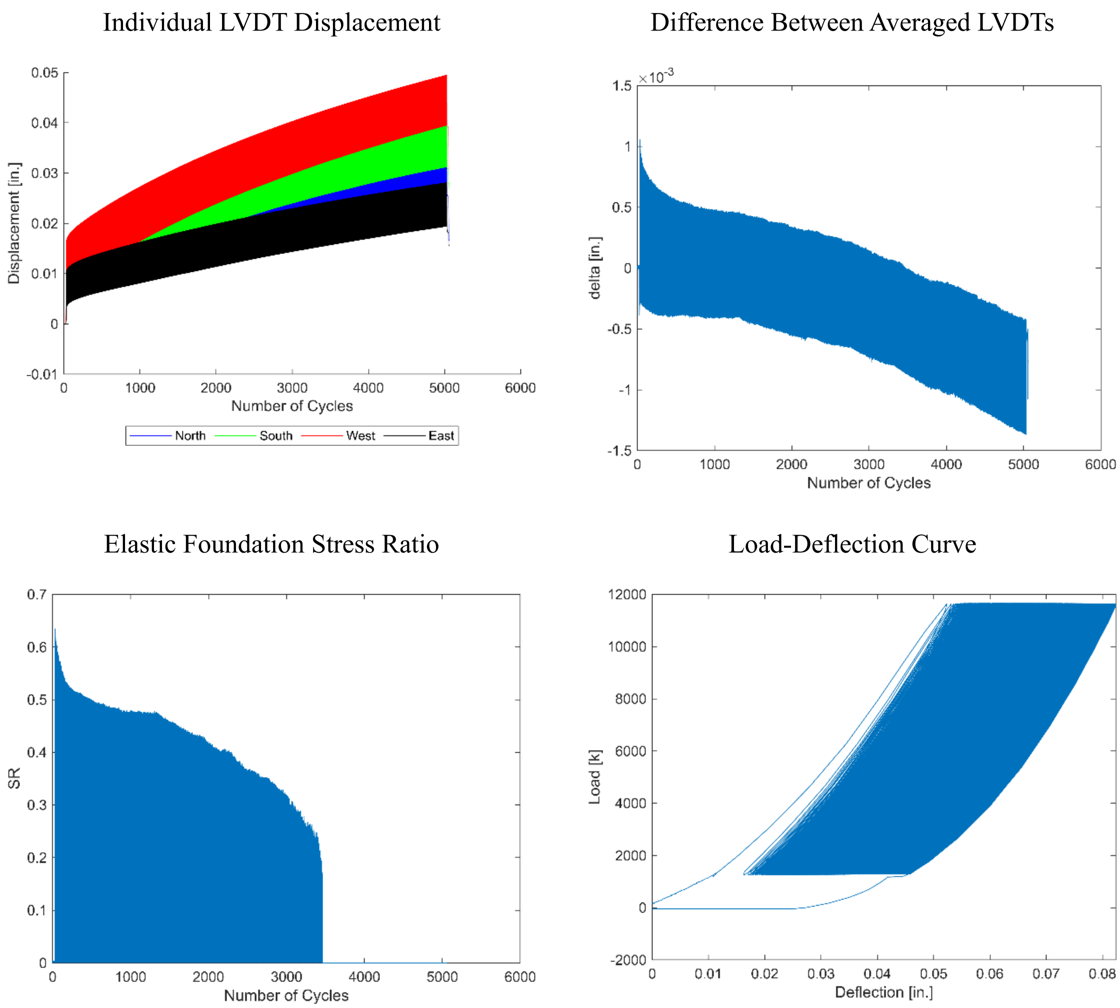

Figure 84: CSCR1 Results - Step 2 (Elastic Foundation)

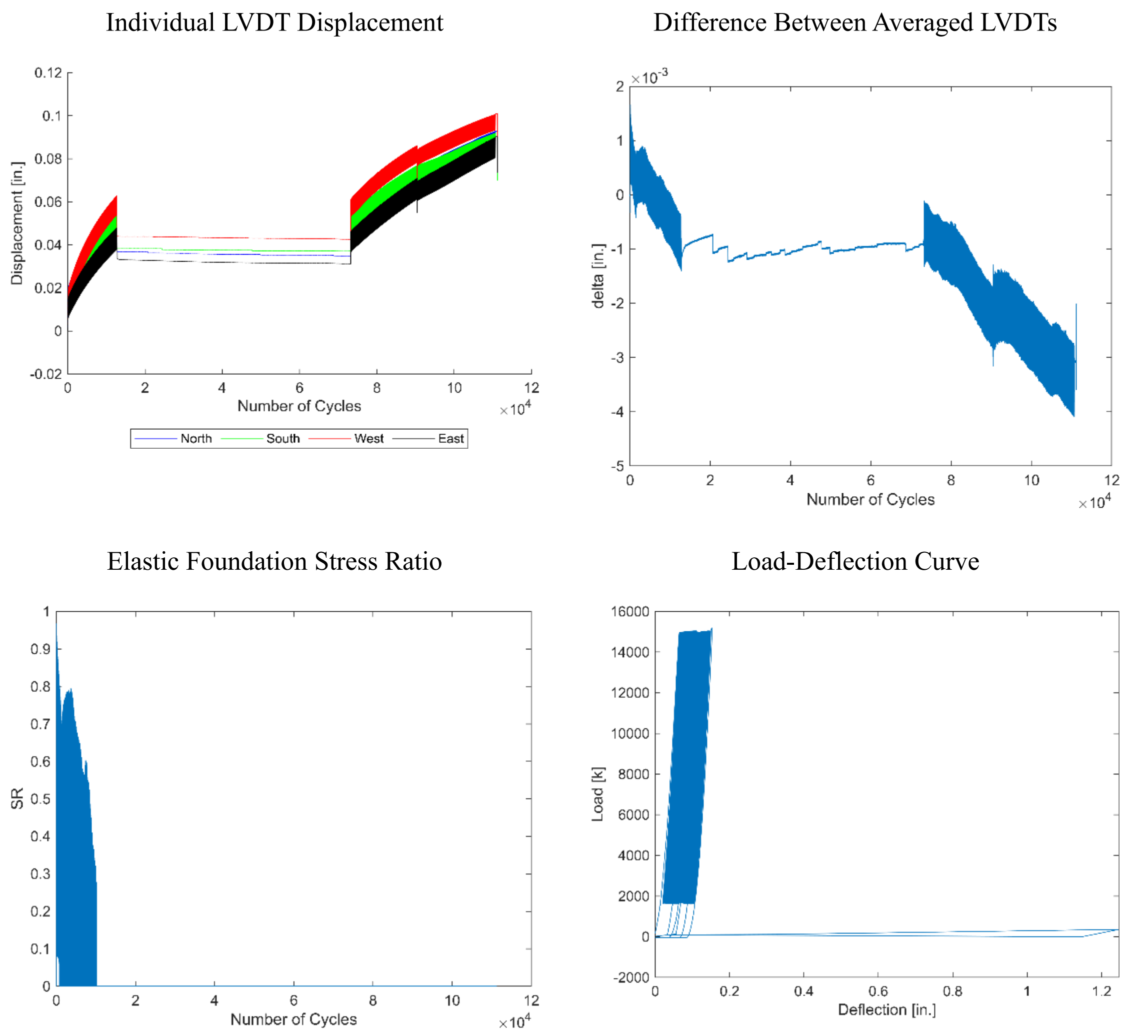

Figure 85: CSCR1 Results - Step 3 (Elastic Foundation)

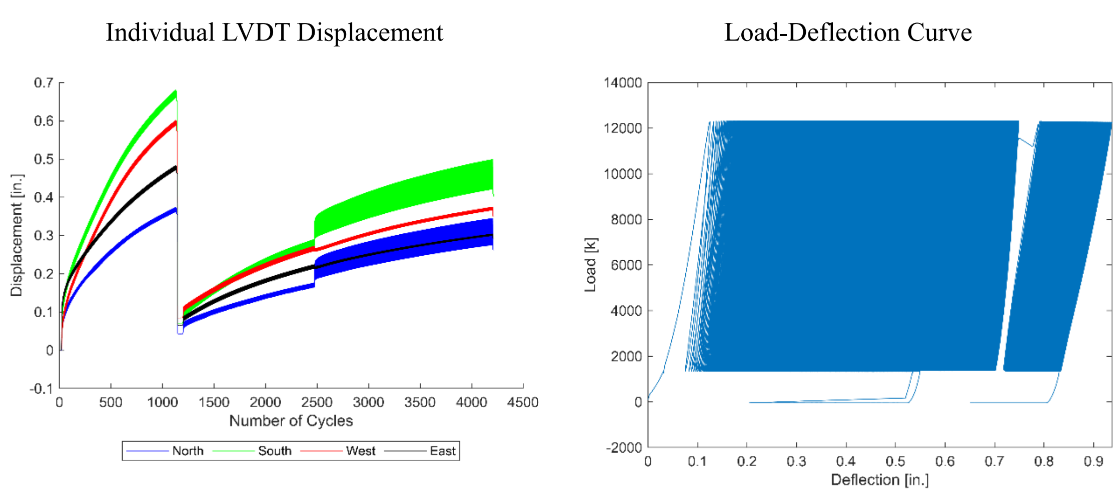

Figure 86: CSCR1 Results - Step 4 (Simple Span)

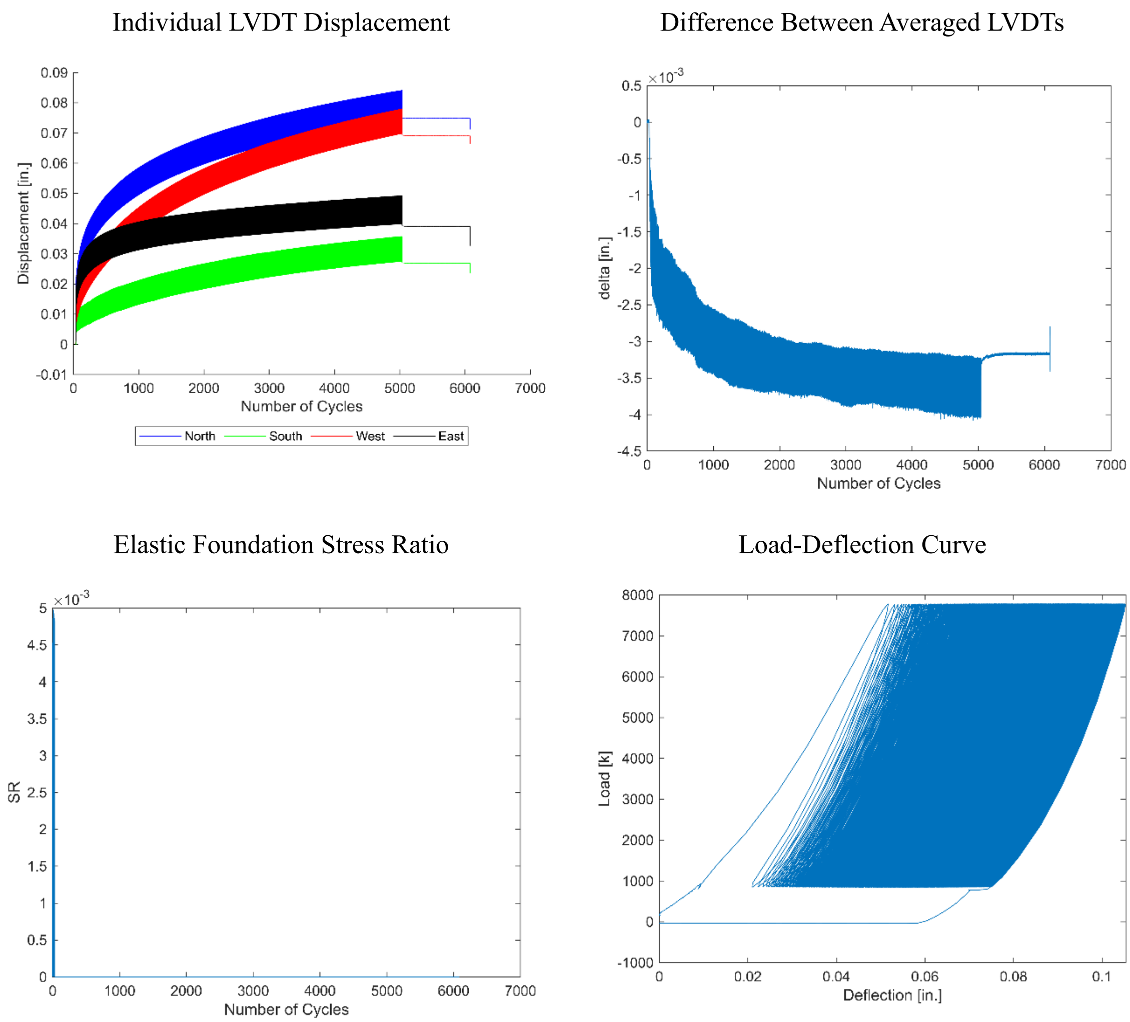

Figure 87: CSCR2 Results - Step 1 (Elastic Foundation)

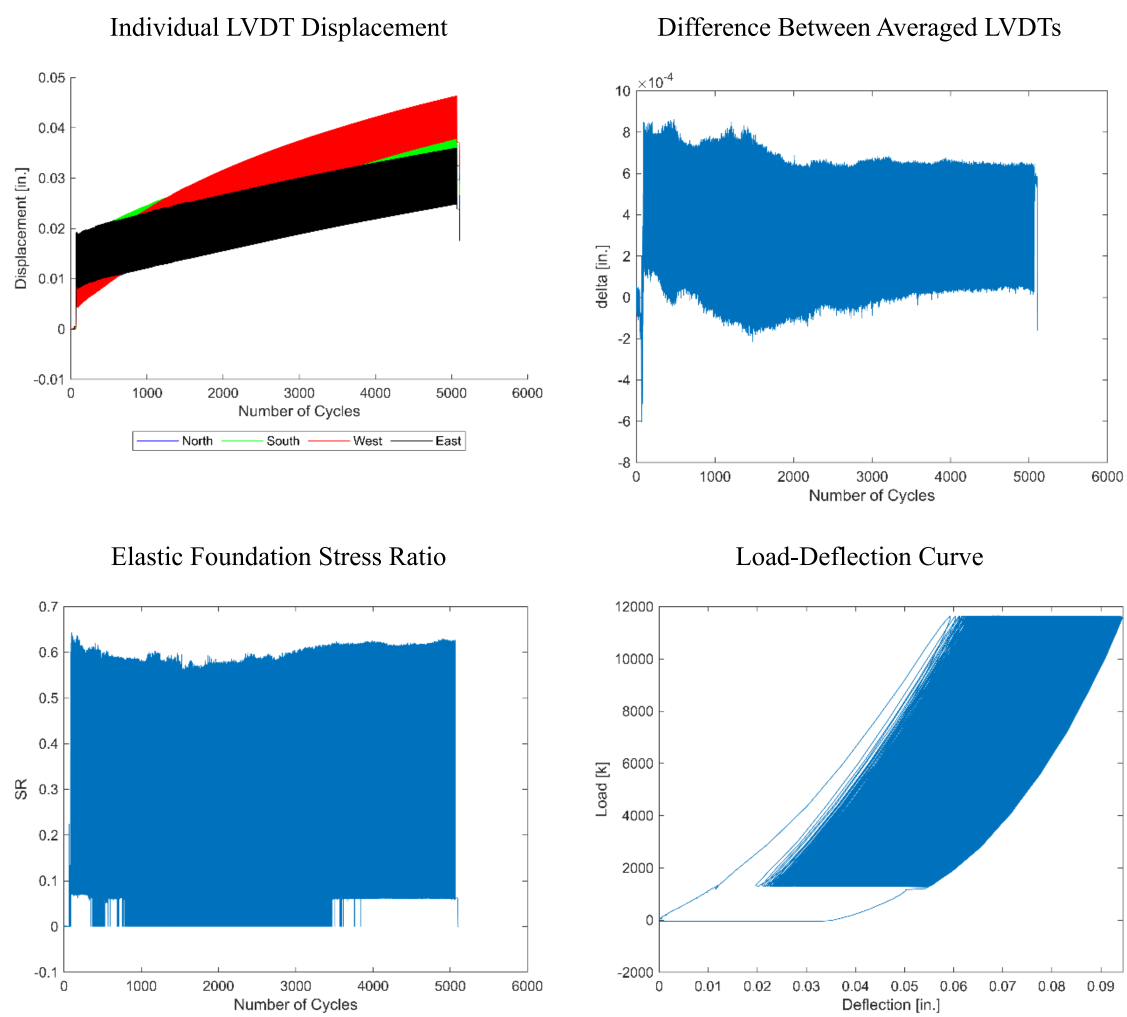

Figure 88: CSCR2 Results - Step 2 (Elastic Foundation)

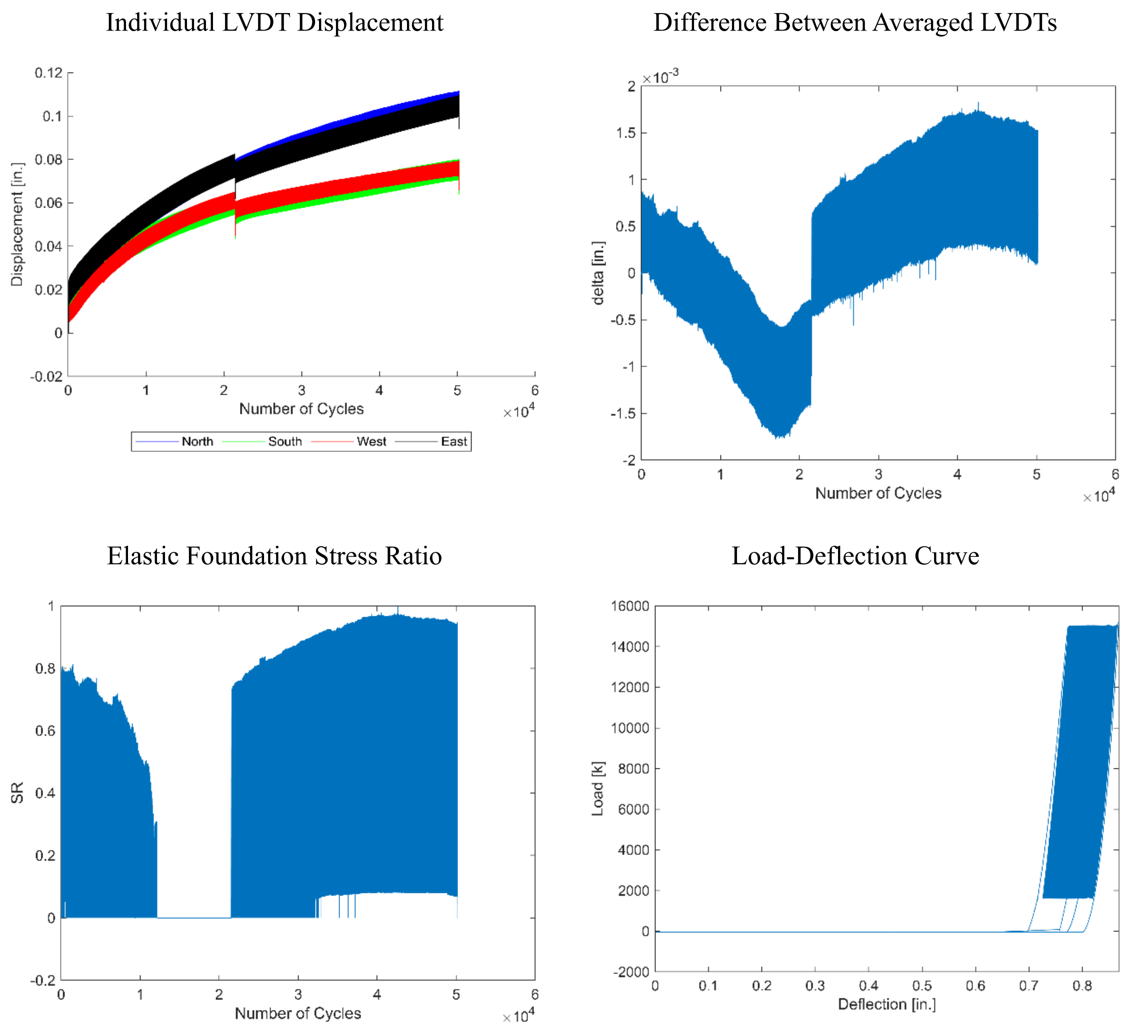

Figure 89: CSCR2 Results - Step 3 (Elastic Foundation)

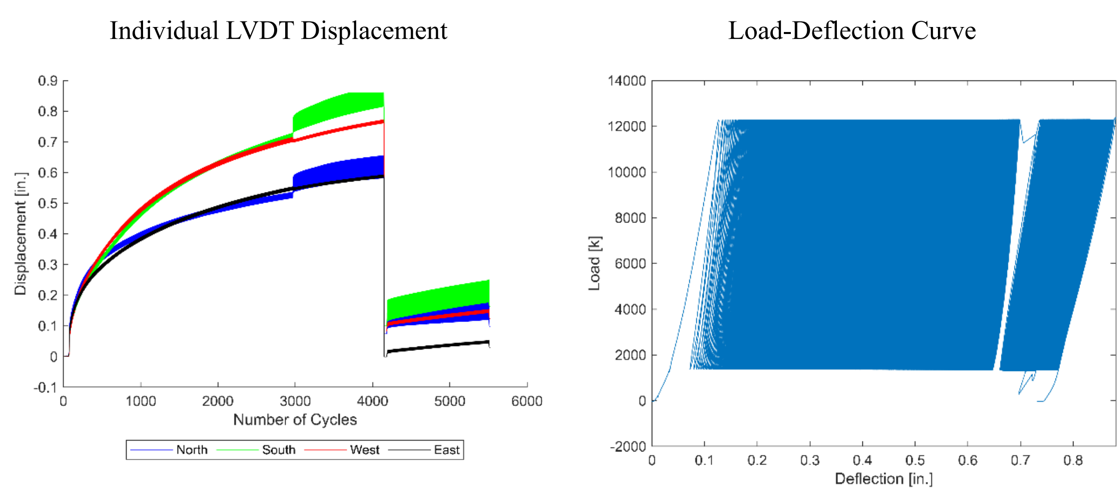

Figure 90: CSCR2 Results - Step 4 (Simple Span)

The average cycle at failure on Step 4 for the continuously-reinforced BCSA specimens was 4823. However, this number should be viewed more heuristically as the number of load cycles at the point of initial cracking was not definitively identified. A straight-forward failure criteria creates some difficulty as unlike previous specimens, the first crack did not result in a sudden failure. In fact, the specimens were able to sustain the cyclic loading after substantial cracks were formed as seen in Figure 9. The lack of a clear failure on the load-deflection curve contributes to this difficulty. However, effort was made to notice cracking as soon as possible.

Figure 91: Cracked CSCR Specimen

The sudden offsets in Step 4 for both specimens are a result of starting and ending the cyclic loading due to excessive displacement in the overall system (bearing pad, specimen and elastic foundation) exceeding the displacement limits set when defining the loading parameters.

4.4.6 Summary of Expansive BCSA Specimens

Table 12 provides a summary of results for Step 4 of all Expansive BCSA specimens. Cycle of failure by designation is plotted in Figure 92.

Table 12: Summary of Loading for Simply Supported Expansive BCSA Specimens

Designation	Load (k)	Failure Cycle
CSP1	12.5	270
CSF1	12.5	157
CSF2	15	83
CSCR1	12.7	4206
CSCR2	12.7	5440

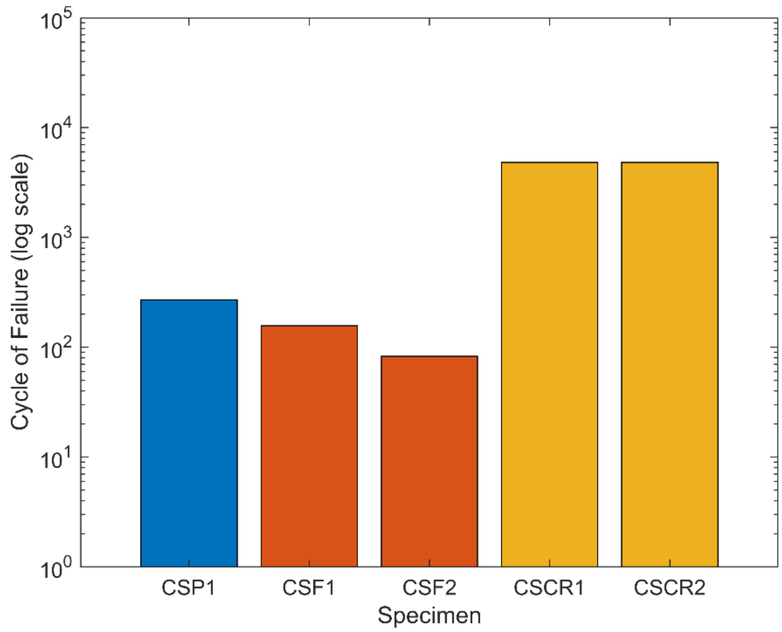

Figure 92: Cycle of Failure for Simply Supported Expansive BCSA Specimens

As seen in Figure 92, there is an expected increase in the cycle of failure between the plain specimen and the continuously-reinforced specimens. The cycle of failure recorded for the continuously-reinforced specimens may be overestimated due to the cycle not necessarily representing the cycle that induced cracking. However, the gains in its performance such as its prevention of a global collapse after its initial crack is not reflected in Figure 92. Unexpectedly, there was a slight decrease in cycle of failure when introducing fiber reinforcement.

Figure 93 plots the elastic stress ratios calculated for the first three steps of the loading protocol for each Expansive BCSA specimen. While efforts were made to give each specimen a similar induced stress ratio through the loading protocol, the variable nature of the elastic foundation did not allow for fine control and the determined stress ratios may have been influenced by the unexpected deformed shapes. As seen in Figure 93, the fiber-reinforced Expansive BCSA specimen typically experienced a larger calculated stress ratio, especially for CSF2, which could explain the lower performance from these specimens compared to the plain specimen.

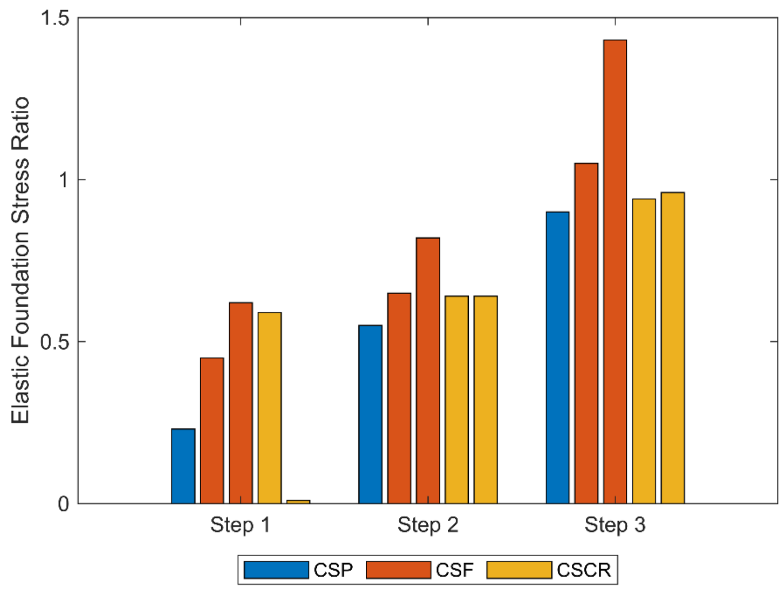

Figure 93: Elastic Stress Ratio of Expansive BCSA Specimens by Step

Further insights can be found when utilizing an S-N equation (4) being developed using fatigue data for the Expansive BCSA cement concrete used in the concurrent research project mentioned in Chapter 3. S in this equation refers to the flexural stress ratio induced by cyclical loading with N referring to the number of cycles to induce failure.

$$S = -0.028\ln(N) + 1.0268 \quad (4)$$

Table 13 is an expanded summary of Expansive BCSA results for step 4 of the loading protocol with the inclusion of Equation 4. By dividing the load for each specimen by its calculated S, a max load that would induce failure with 1 cycle can be estimated and is also included in Table 13. Figure 94 plots the average load at S = 1 for each reinforcement type. Compressive strengths for each reinforcement design are shown in Figure 95.

Table 13: Expanded Summary of Simply Supported Expansive BCSA Specimens

Designation	**Load (k)**	**Failure Cycle**	**S (Eq. 4)**	**Load at S = 1 (k)**
CSP1	12.5	270	0.87	14.12
CSF1	12.5	157	0.89	16.61
CSF2	15	83	0.90	14.37
CSCR1	12.7	4206	0.79	16.16
CSCR2	12.7	5440	0.79	16.01

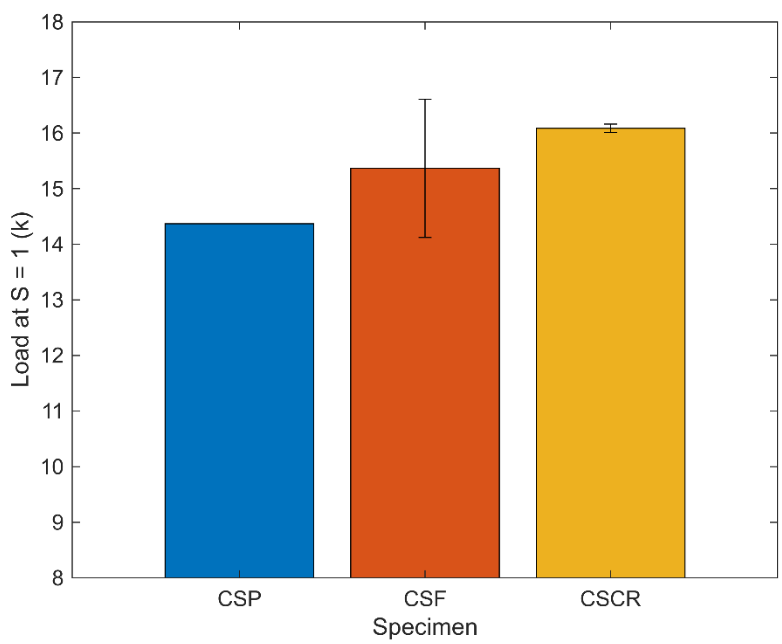

Figure 94: Average Load at S = 1 for Expansive BCSA Pavement Designs

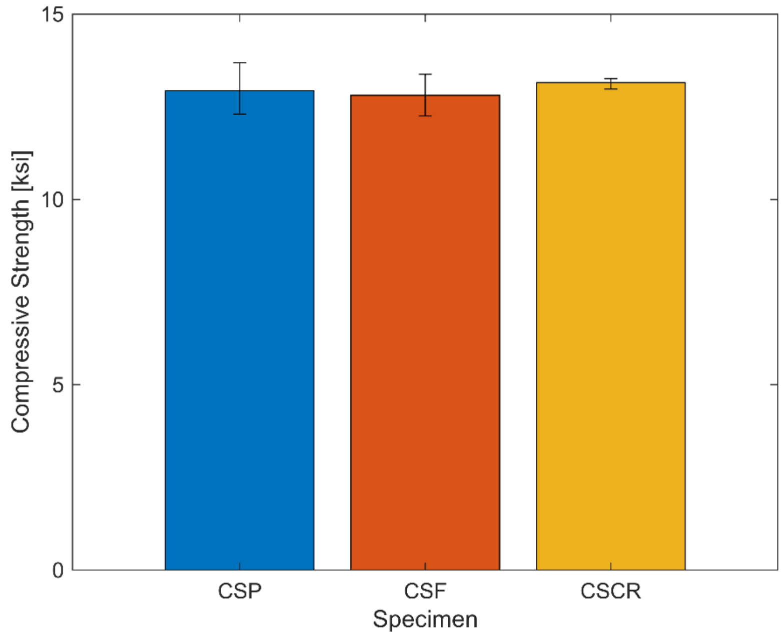

Figure 95: 28-Day Compressive Strengths of Large-Scale Expansive BCSA Specimens

When considering each specimen's actual applied load along with a calculated S from the empirical equation in development, it is found that fiber-reinforcement enhanced performance with a further increase for the continuously-reinforced pavement design. It is expected for the continuously-reinforcement to provide significant gains due to the increased confinement to the expansion of Expansive BCSA cement concrete due to compressive prestress offsetting the tensile stress induced by the cyclic loading. The fiber-reinforced specimens falling between plain and the continuous-reinforced pavement in Figure 94 indicates that the steel fibers were able to contribute to performance in a similar manner for a significantly smaller overall volume of steel in the specimen.

4.4.7 Plain OPC

Specimens OPC1 and OPC2 were subjected to the loading detailed in Table 14. Figures 96 through 103 plot testing results.

Table 14: OPC1 & OPC2 Loading Protocol

Step	Load (k)	Cycles	Configuration
1	8	5000	Elastic Foundation
2	12	5000	Elastic Foundation
3	15.5	50000	Elastic Foundation
4	12.5	Until Failure	Simple Span

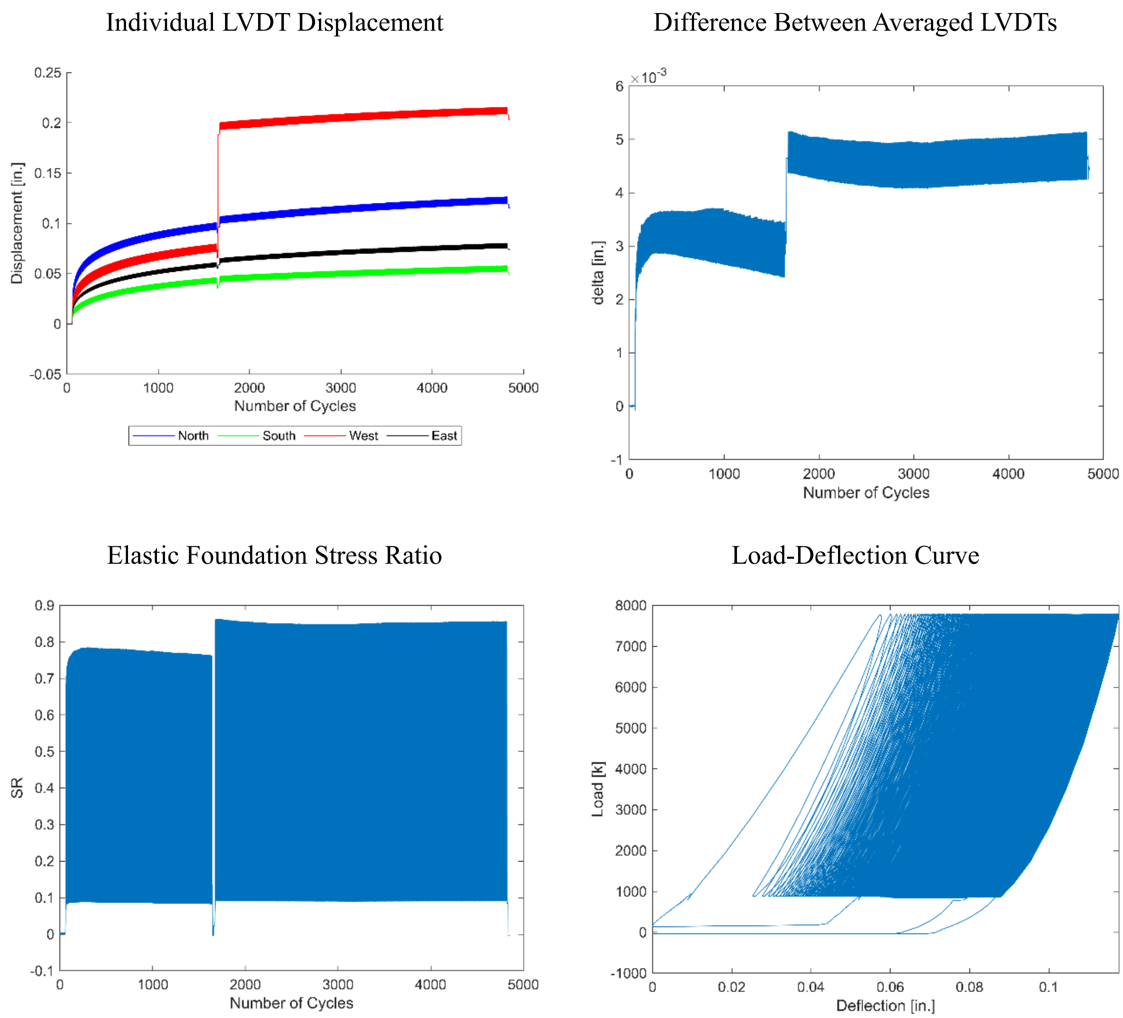

Figure 96: OPC1 Results - Step 1 (Elastic Foundation)

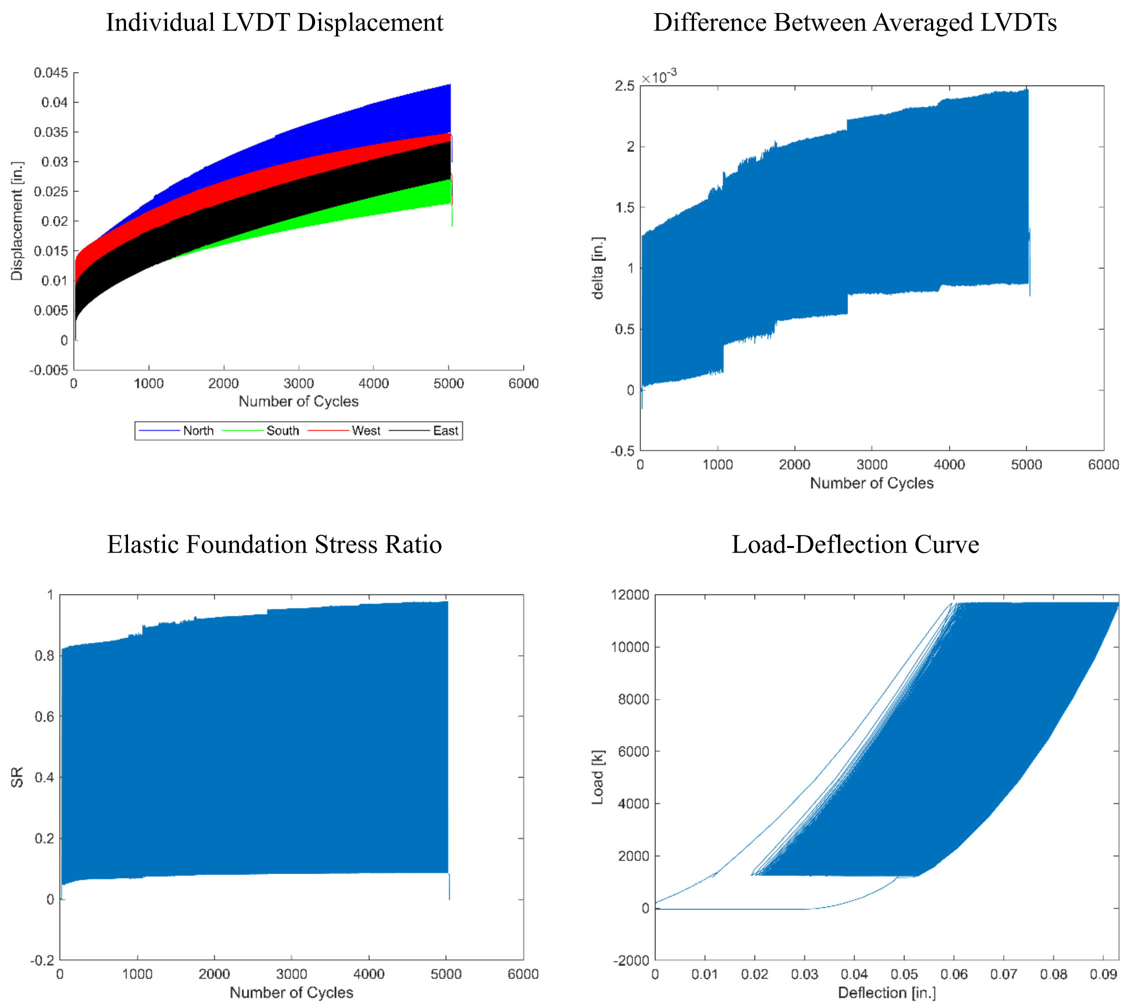

Figure 97: OPC1 Results - Step 2 (Elastic Foundation)

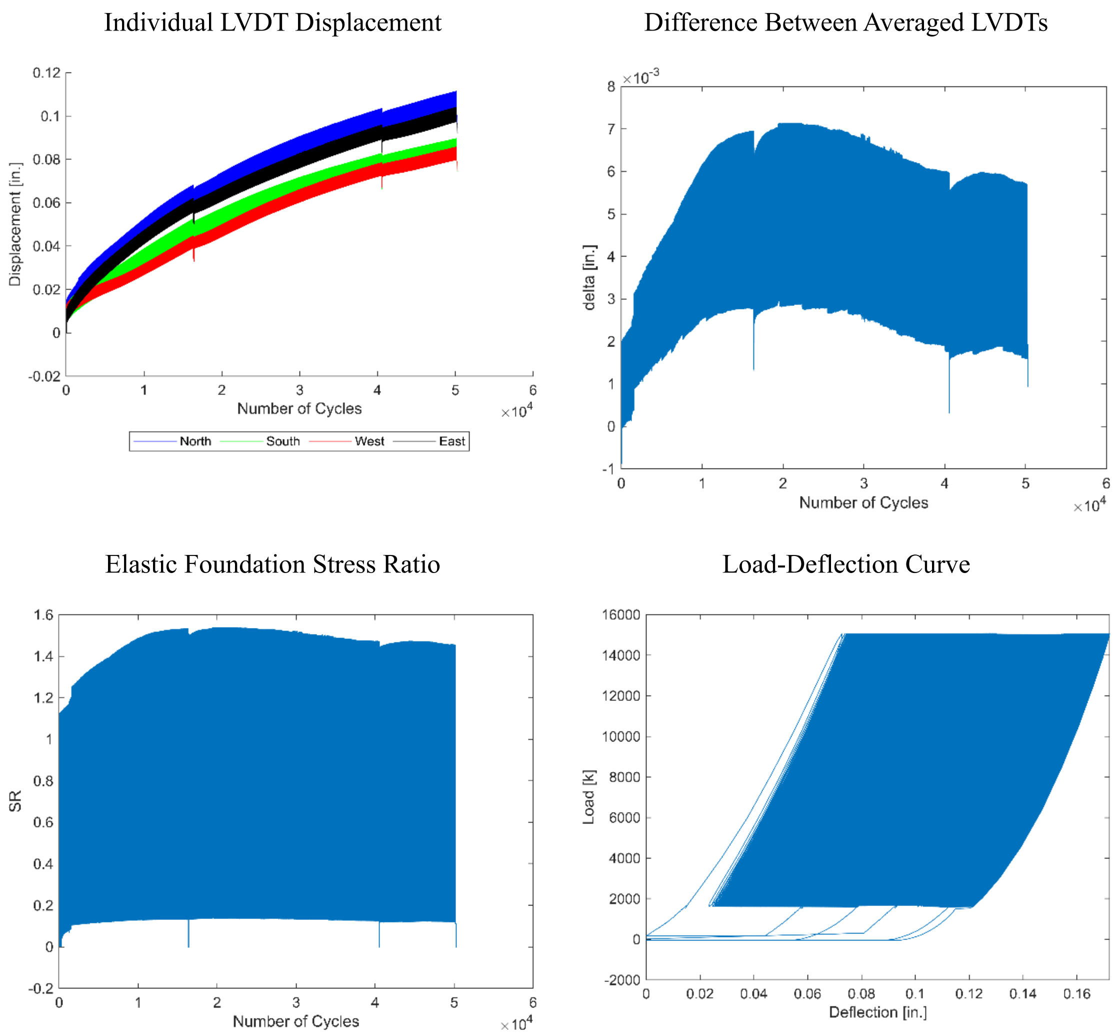

Figure 98: OPC1 Results - Step 3 (Elastic Foundation)

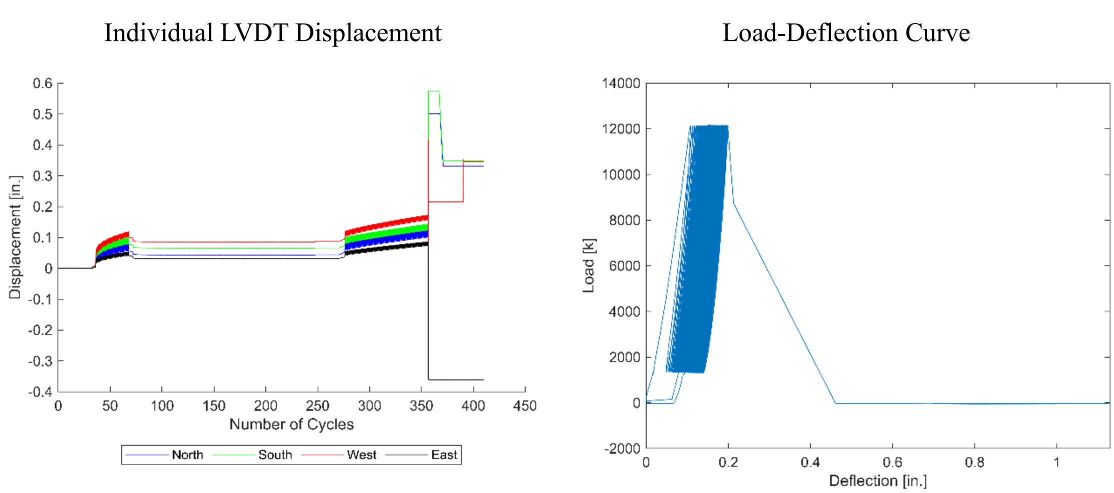

Figure 99: OPC1 Results - Step 4 (Simple Span)

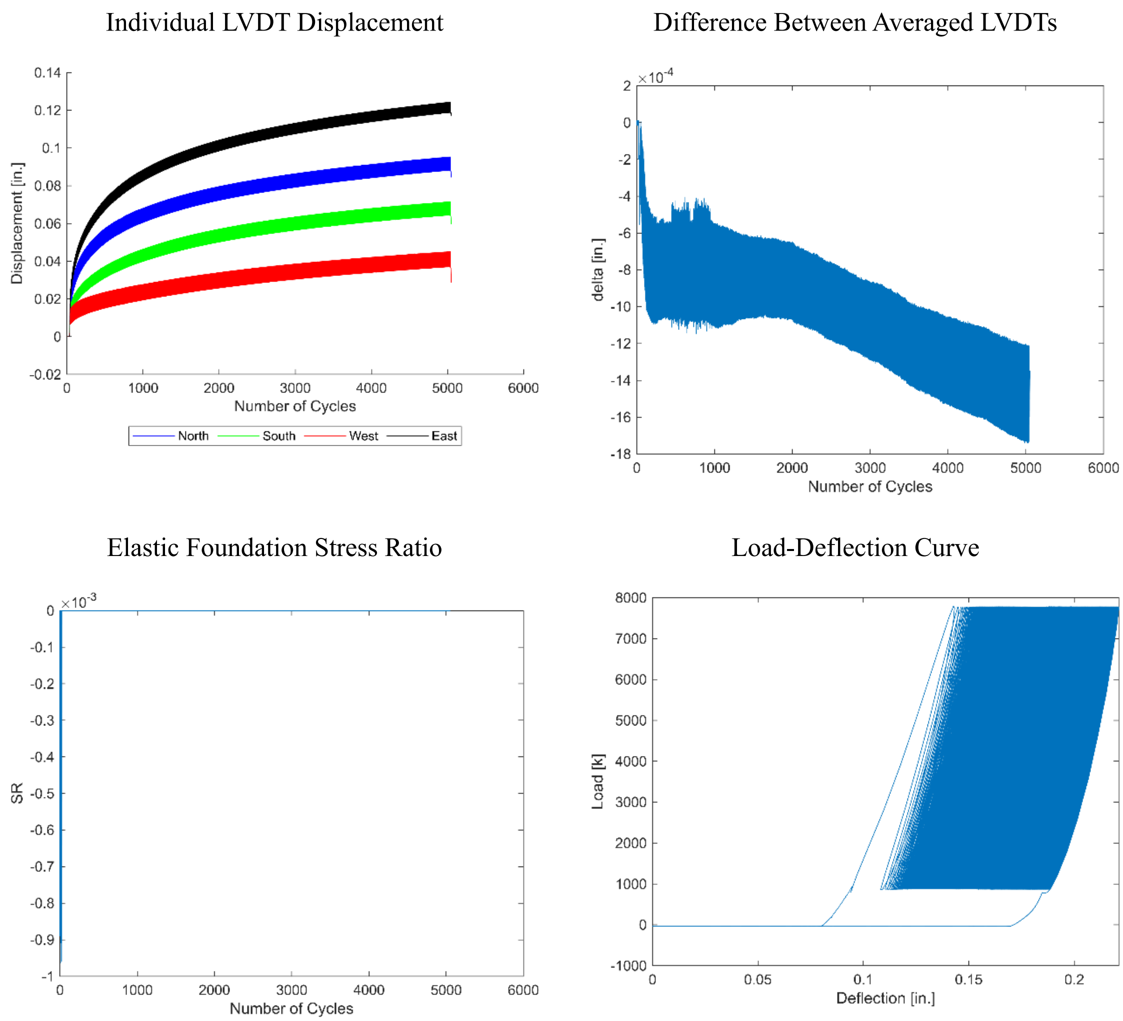

Figure 100: OPC2 Results - Step 1 (Elastic Foundation)

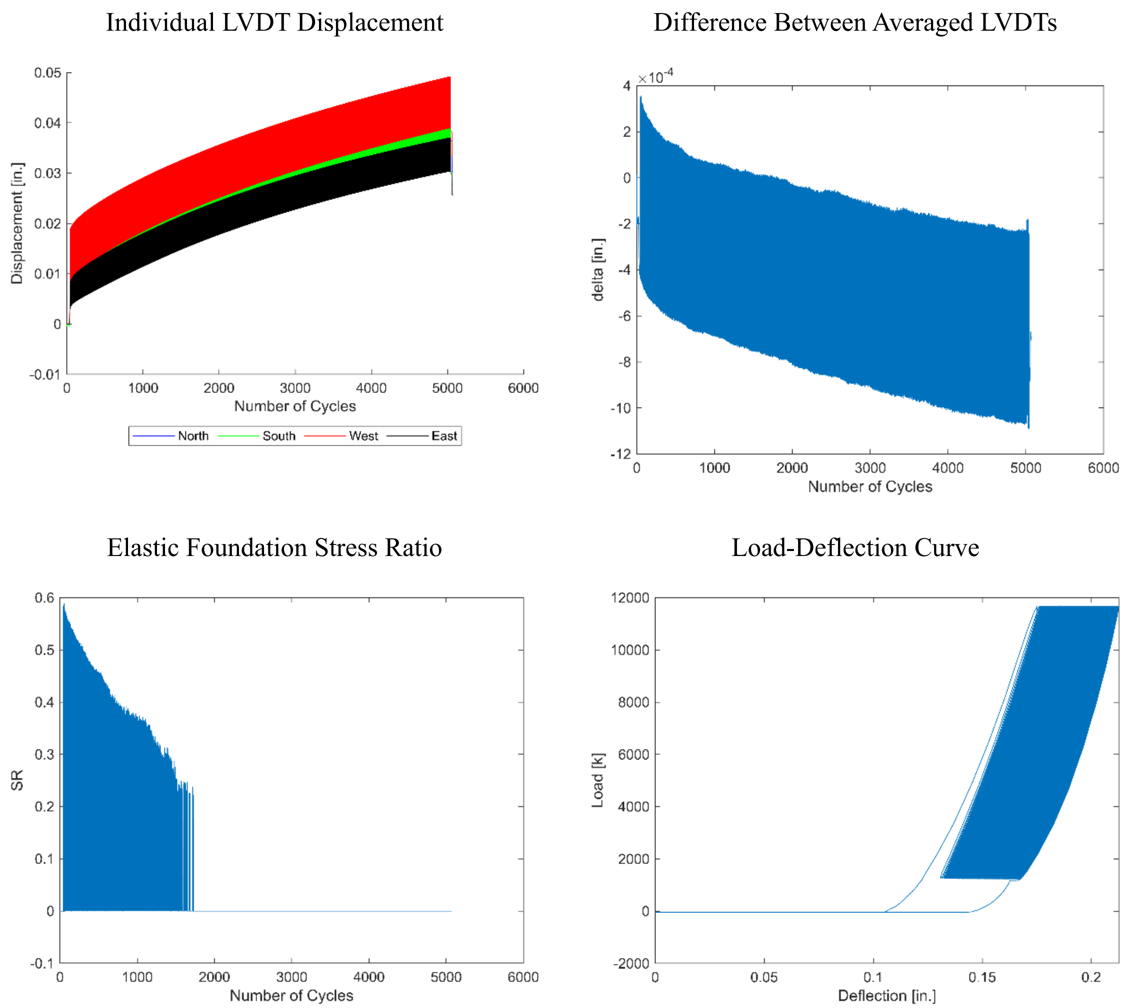

Figure 101: OPC2 Results - Step 2 (Elastic Foundation)

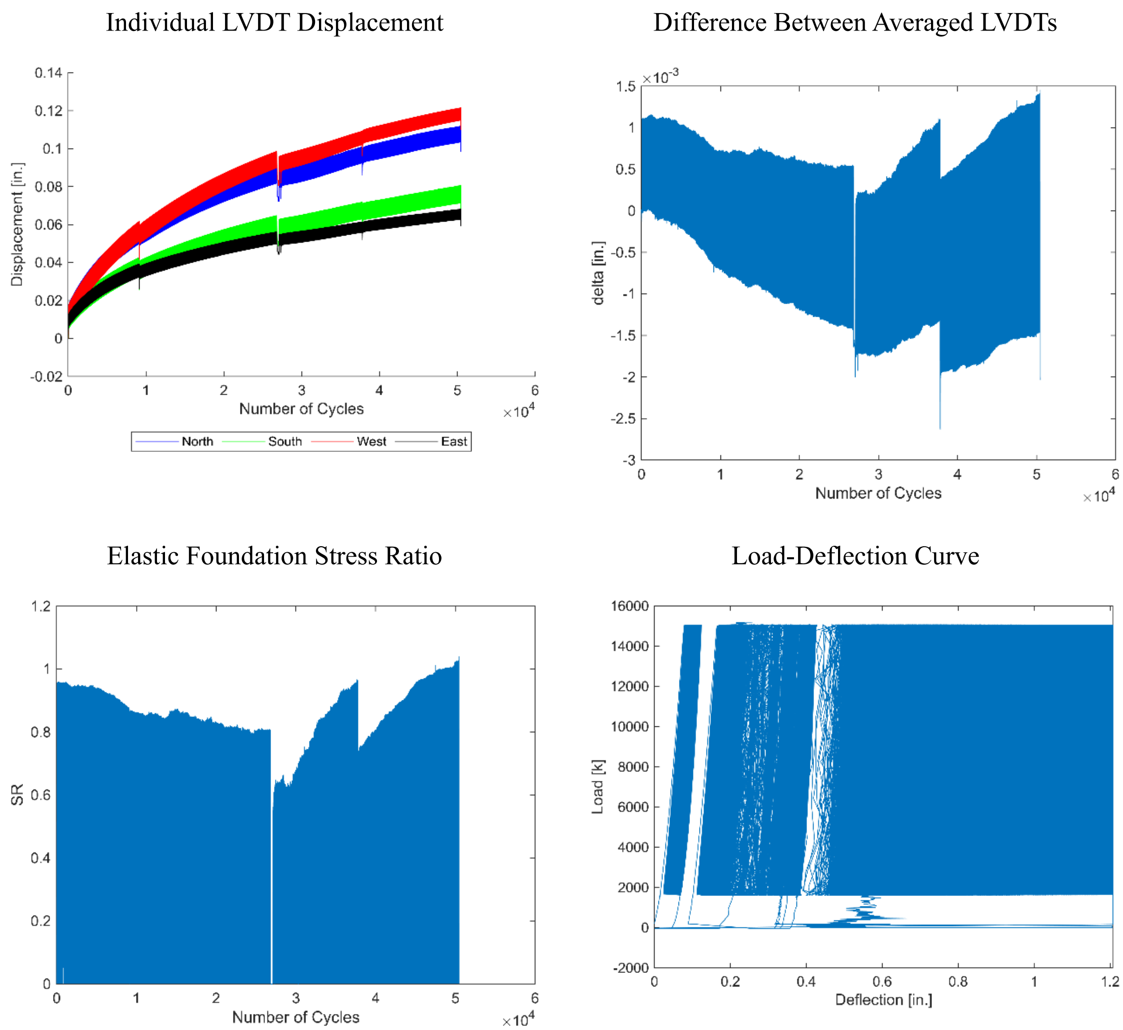

Figure 102: OPC2 Results - Step 3 (Elastic Foundation)

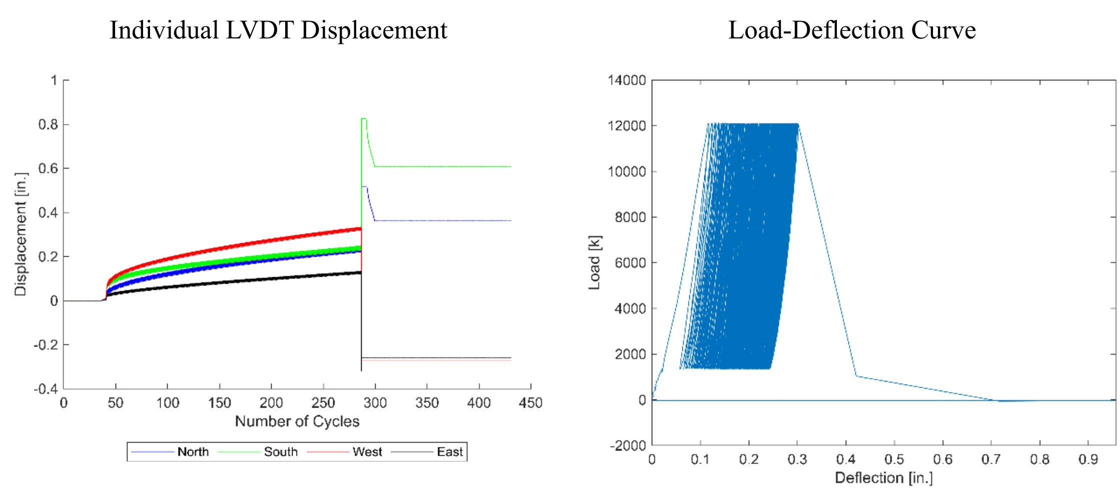

Figure 103: OPC2 Results - Step 4 (Simple Span)

The west LVDT data for specimen OPC1 experienced a sudden offset during loading Step 1. It is believed that the offset was the result of a disruption in the power supply to the data acquisition equipment. While the data acquisition equipment was supported by a dedicated power circuit designed to keep consistent voltage, no other explanation could be identified. By using a point before the offset, the data was adjusted by adding a constant to produce Figures 104. Further analysis and other plots developed for Step 1 uses the adjusted values.

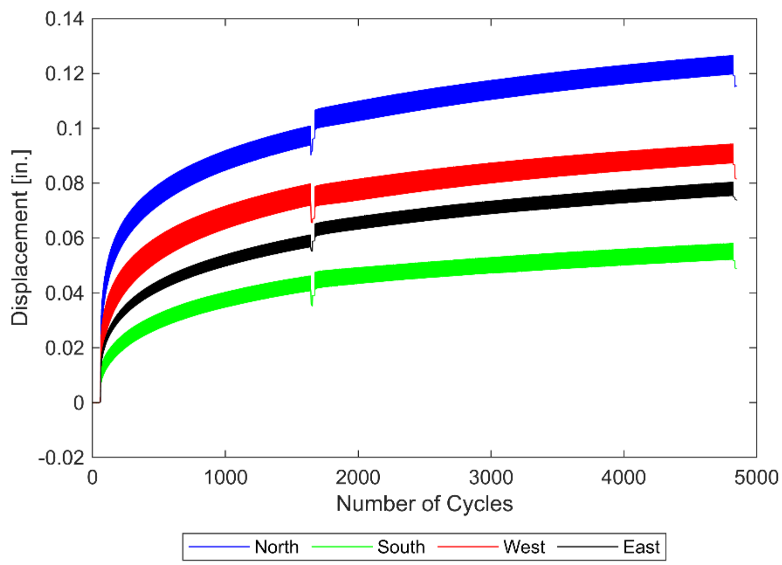

Figure 104: Adjusted OPC1 Individual LDVT Displacement - Step 1 (Elastic Foundation)

The average cycle of failure for OPC1 and OPC2 was 177, lower than the plain Expansive BCSA counterpart. This is expected based on the difference between material properties of the two cement concretes, particularly compressive strength and modulus of elasticity. The calculated stress ratios were typically higher for the plain OPC specimens over the plain Expansive BCSA specimens indicating OPC specimens had less stiffness than the Expansive BCSA specimens.

4.4.8 Fiber-Reinforced OPC

OPCF1 and OPCF2 were subjected to the loading detailed in Table 15. Figures 105 through 112 plot testing results.

Table 15: OPCF1 & OPCF2 Loading Protocol

Step	Load (k)	Cycles	Configuration
1	8	5000	Elastic Foundation
2	12	5000	Elastic Foundation
3	15.5	50000	Elastic Foundation
4	12.5	Until Failure	Simple Span

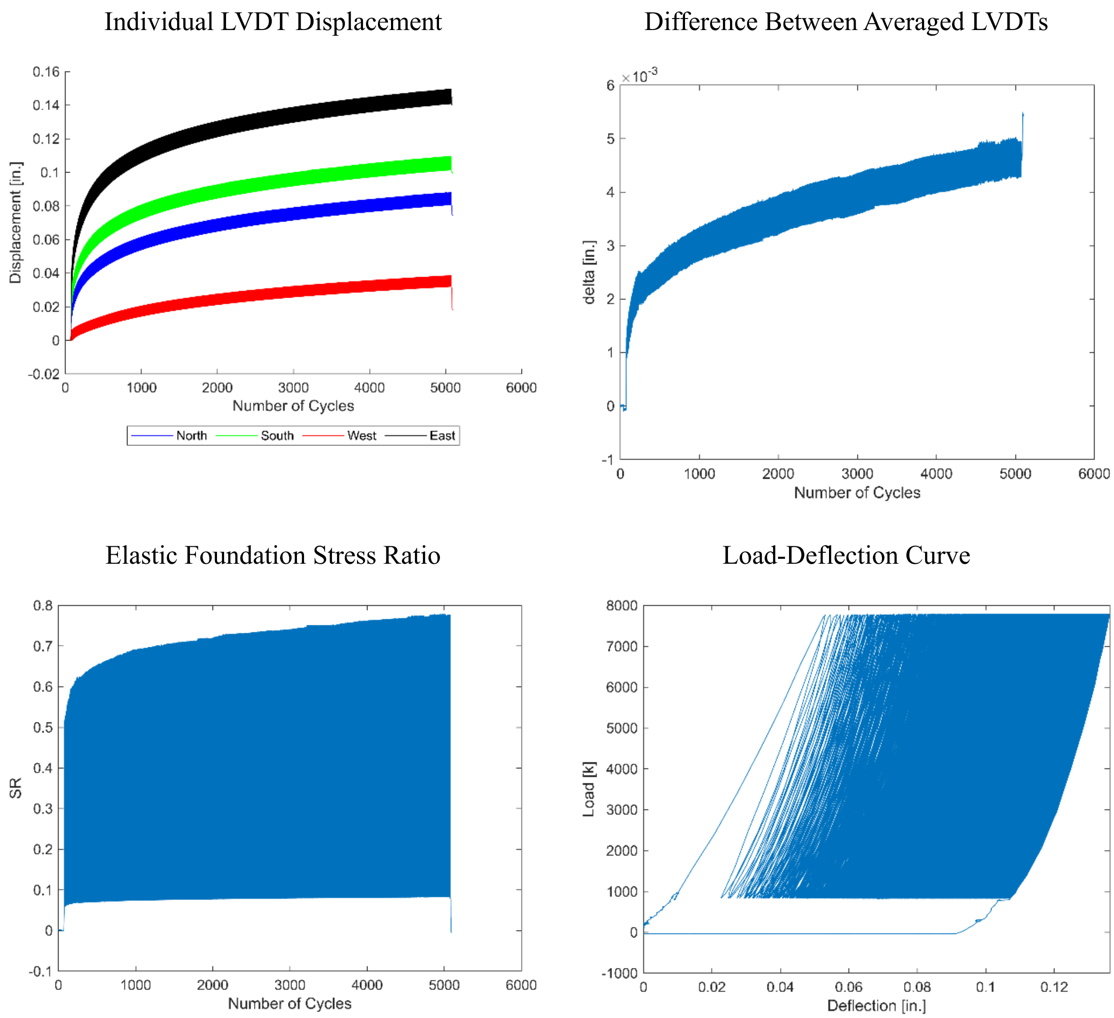

Figure 105: OPCF1 Results - Step 1 (Elastic Foundation)

Individual LVDT Displacement

Difference Between Averaged LVDTs

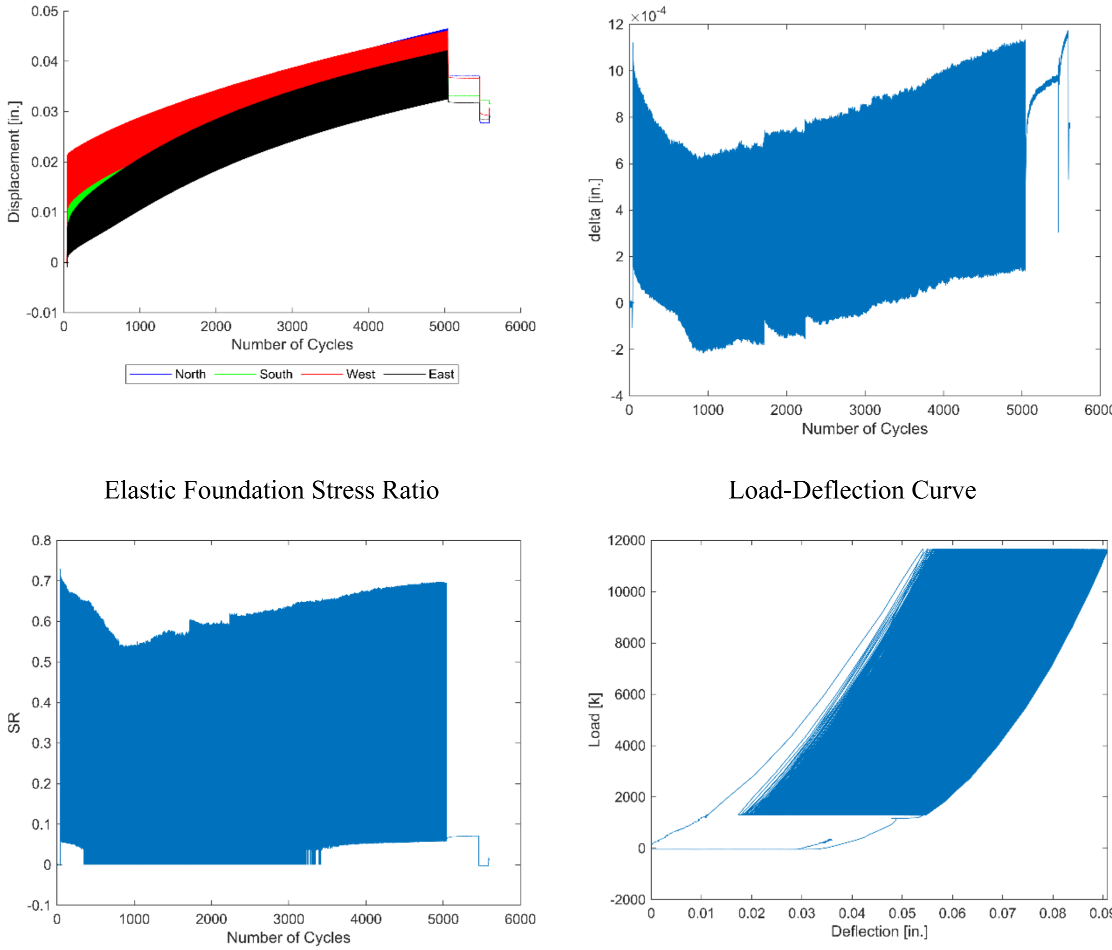

Figure 106: OPCF1 Results – Step 2 (Elastic Foundation)

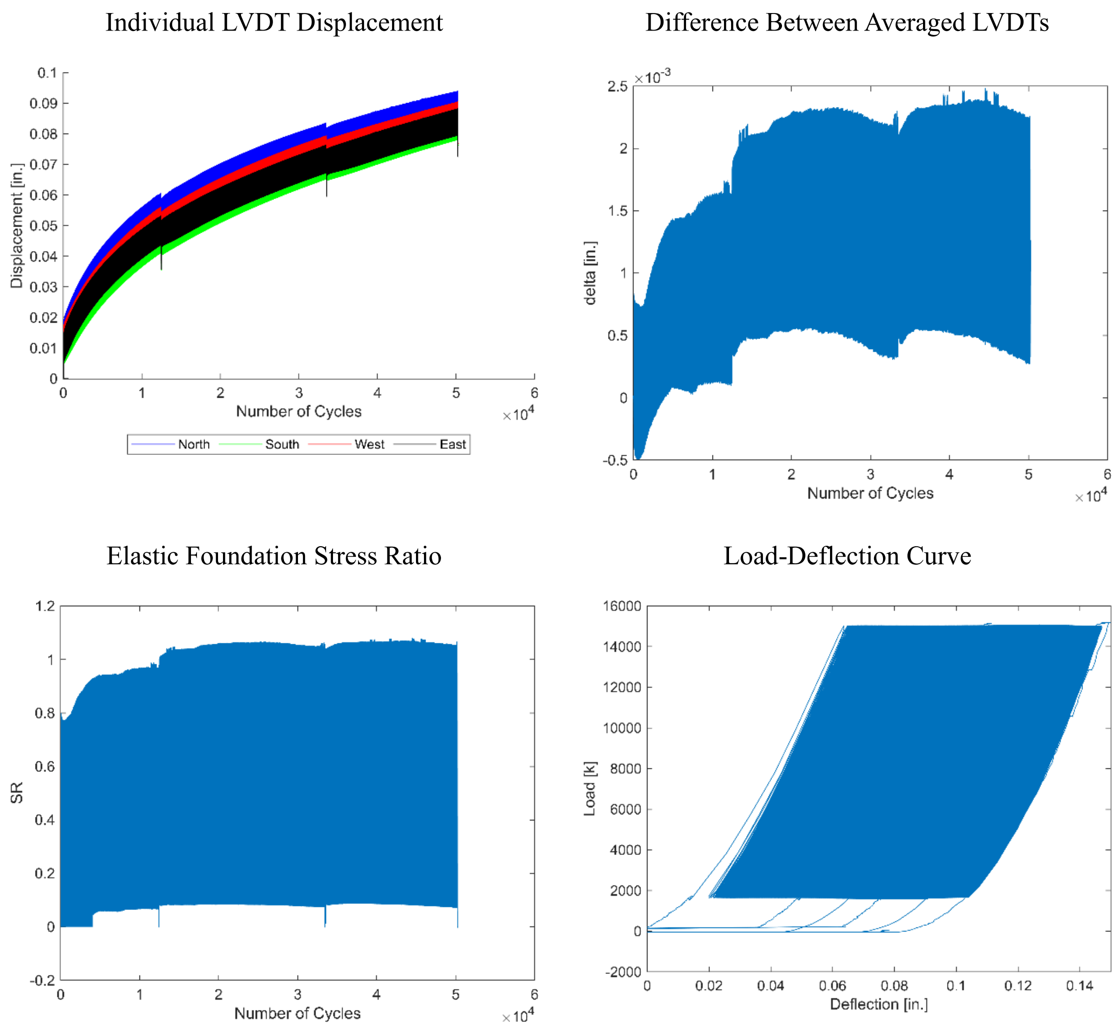

Figure 107: OPCF1 Results - Step 3 (Elastic Foundation)

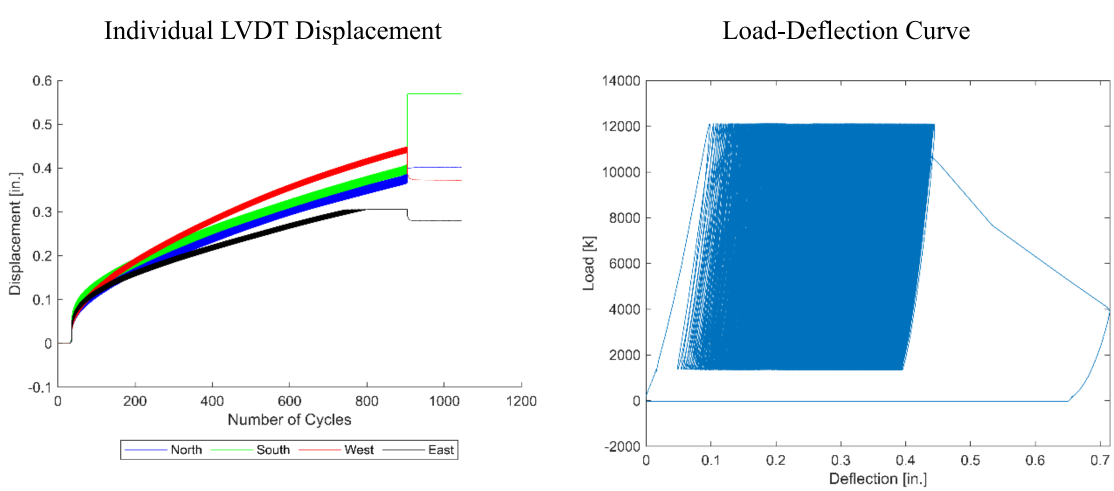

Figure 108: OPCF1 Results - Step 4 (Simple Span)

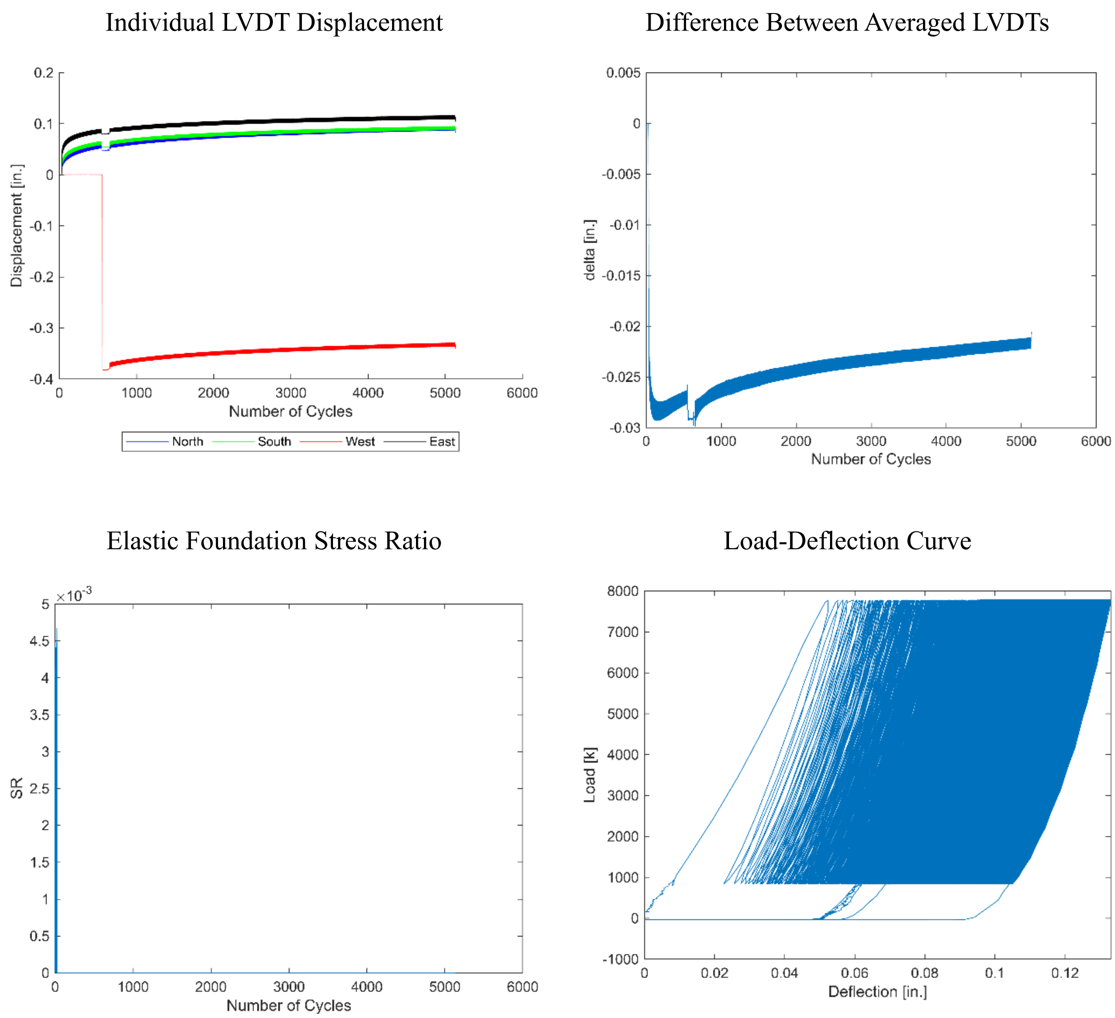

Figure 109: OPCF2 Results - Step 1 (Elastic Foundation)

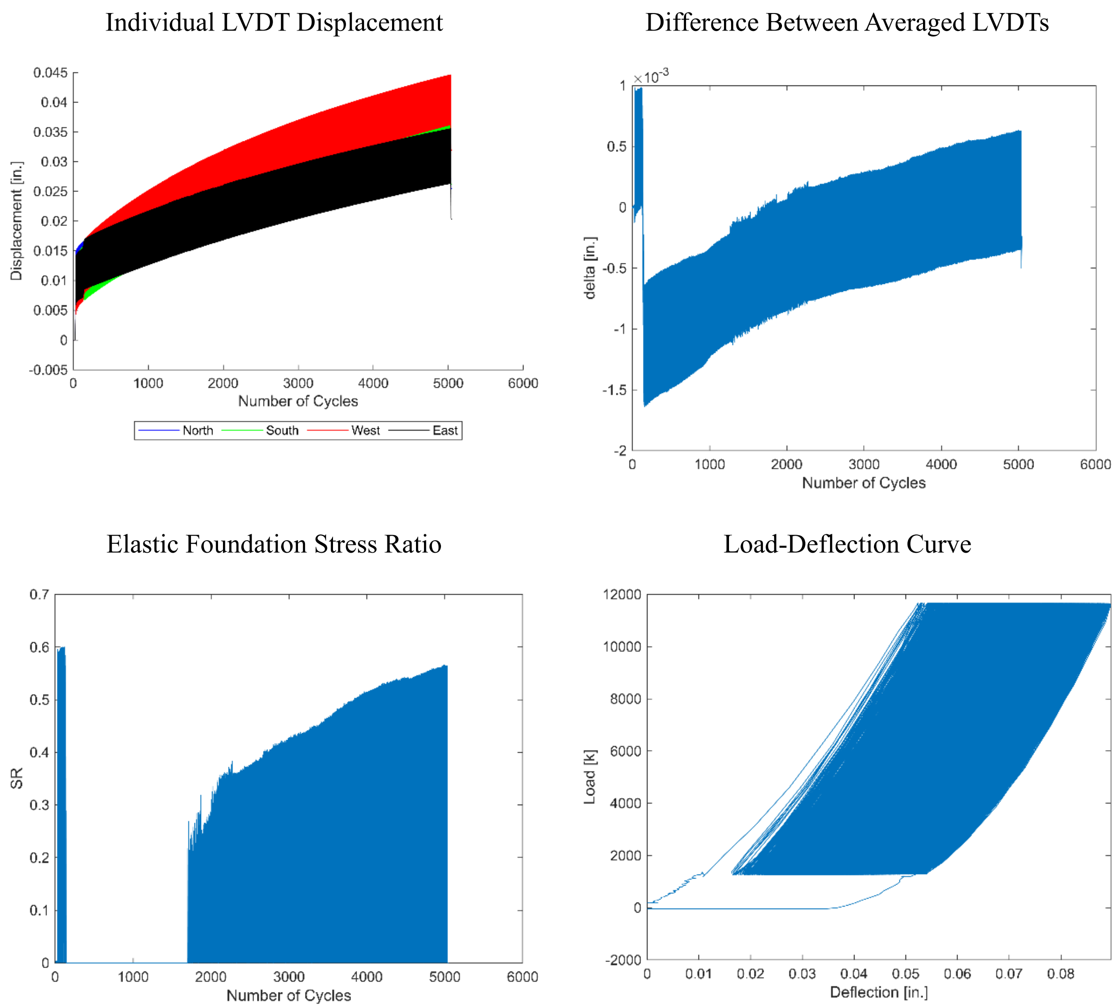

Figure 110: OPCF2 Results - Test 2 (Elastic Foundation)

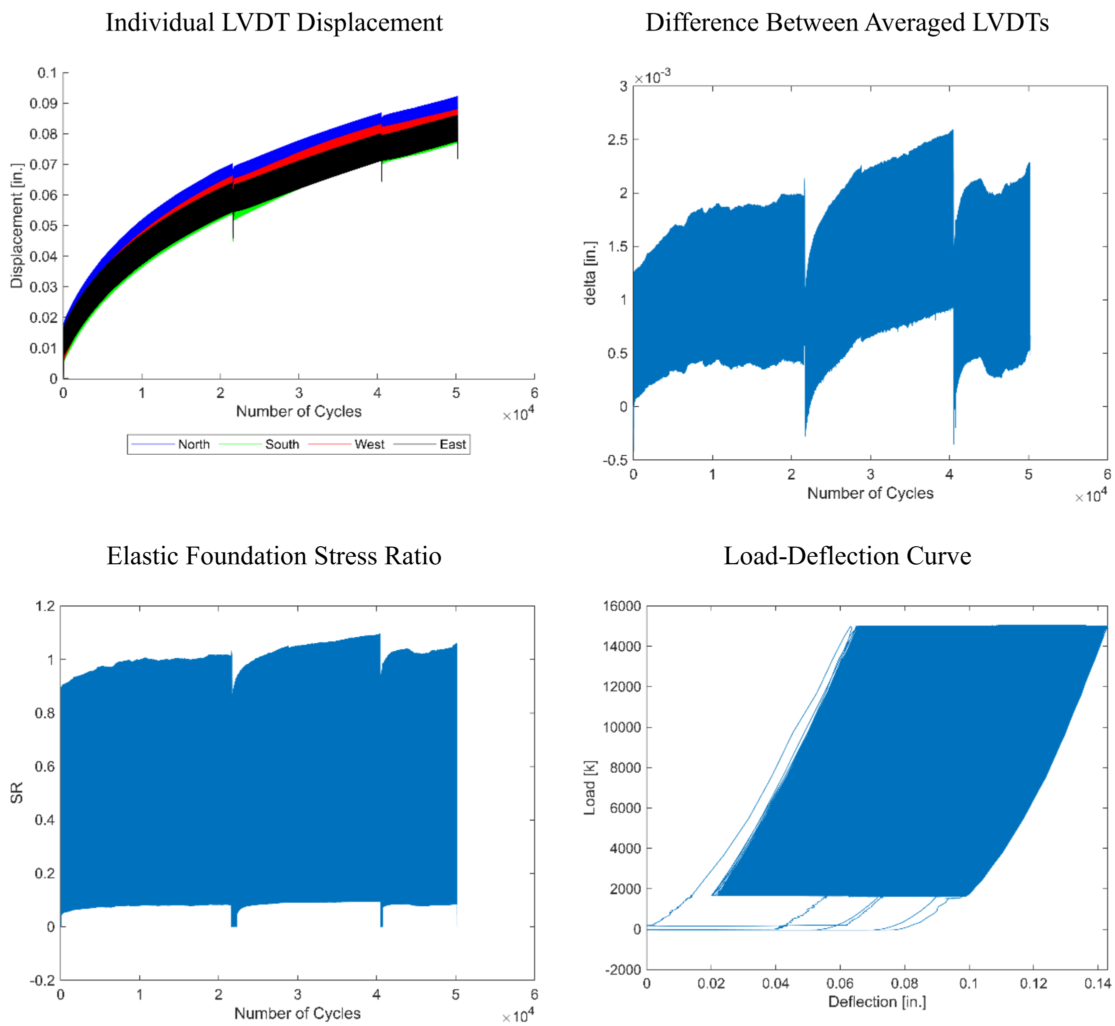

Figure 111: OPCF2 Results - Step 3 (Elastic Foundation)

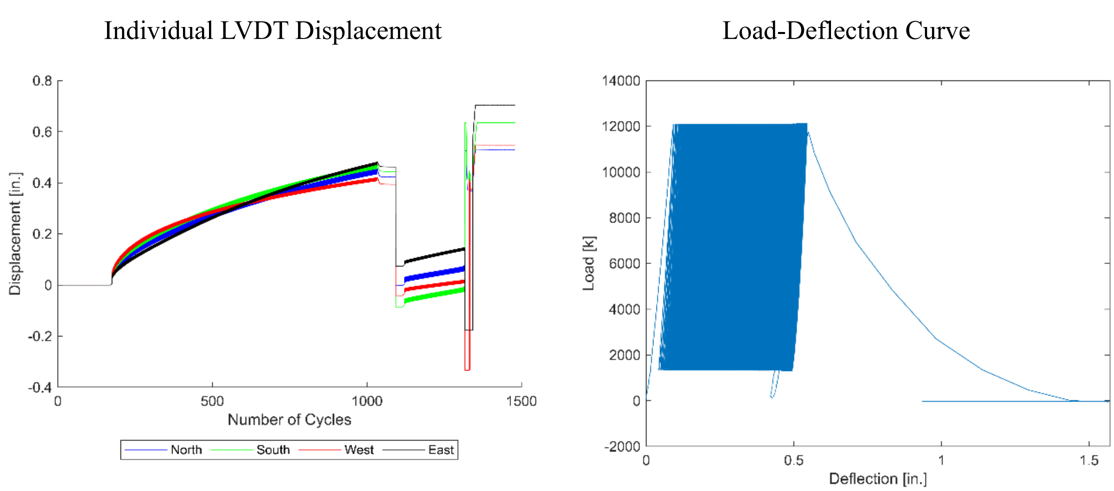

Figure 112: OPCF2 Results - Step 4 (Simple Span)

The West LVDT experienced a failure from the beginning of Step 1 for specimen OPCF2, and although it did start giving an output curve that followed the same shape as the other LVDTs, the lack of a baseline to adjust for the offset made the data from this LVDT not useful for analysis of deformed shape and was disregarded for analysis and the generation of the other figures for Step 1.

The average cycle of failure for OPC1 and OPC2 was 859. This is a higher number of cycles compared to the fiber reinforced Expansive BCSA specimens. However, the maximum back-calculated stress ratio tended to be less than for the CSF specimens. While similar loads were applied to the fiber-reinforced specimens for both CS and OPC concretes, the flexural stress heavily depends on the deformed shape.

4.4.9 Continuously-Reinforced OPC

Specimens OPCCR1 and OPCCR2 were subjected to the loading detailed in Table 16. Figures 113 through 120 plot testing results.

Table 16: OPCCR1 & OPCCR 2 Loading Protocol

Step	**Load (k)**	**Cycles**	**Configuration**
1	8	5000	Elastic Foundation
2	12	5000	Elastic Foundation
3	15.5	50000	Elastic Foundation
4	10.6	Until Failure	Simple Span

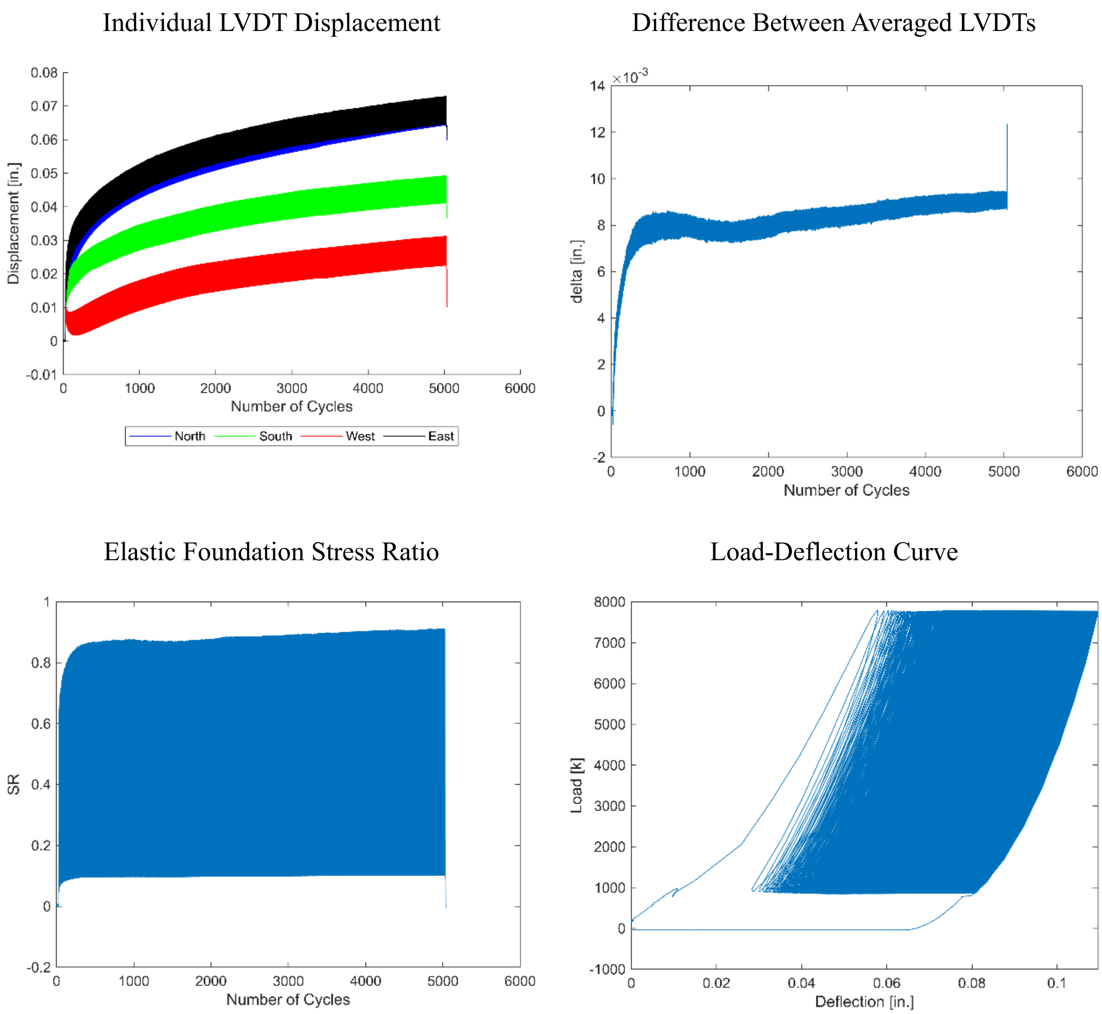

Figure 113: OPCCR1 Results - Step 1 (Elastic Foundation)

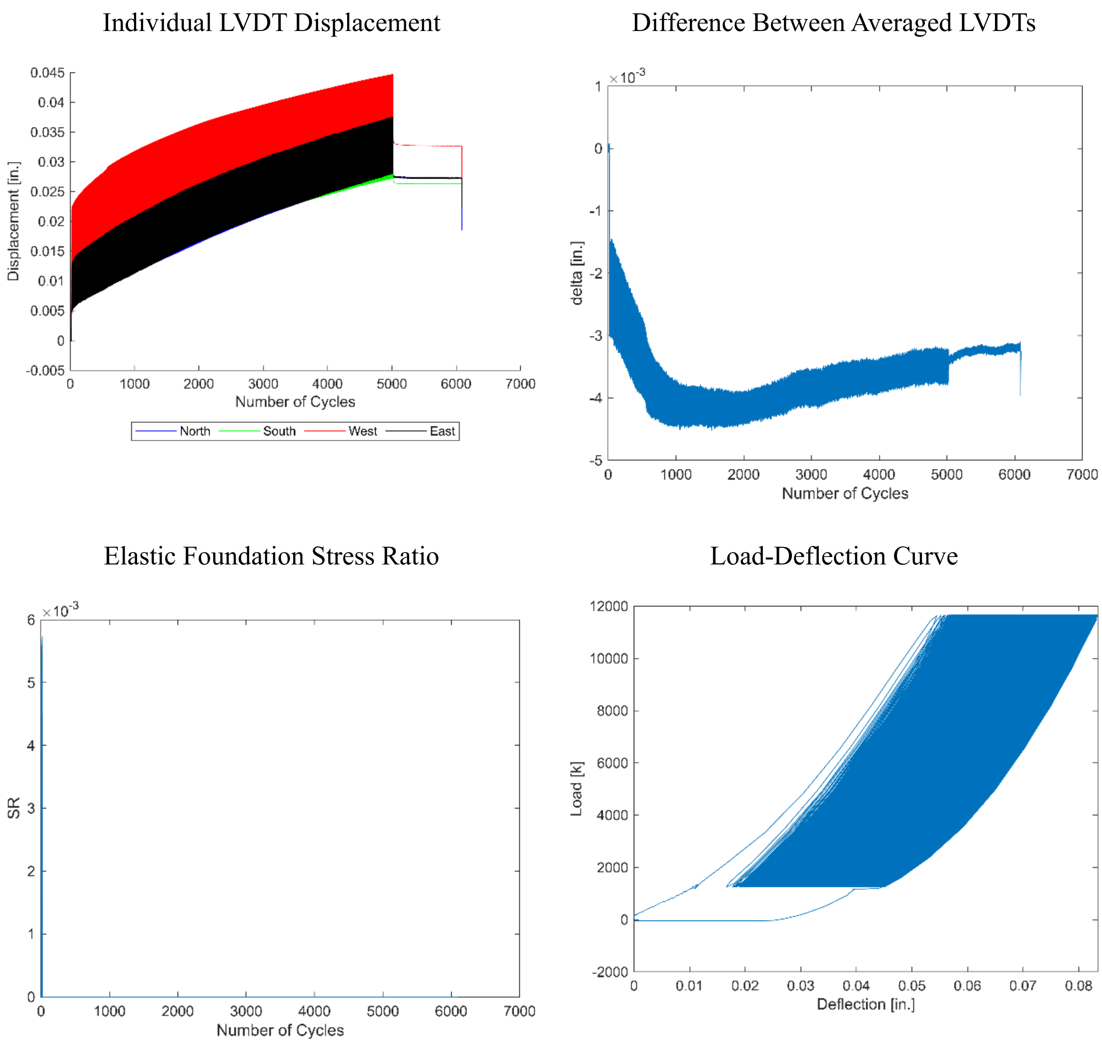

Figure 114: OPCCR1 Results - Step 2 (Elastic Foundation)

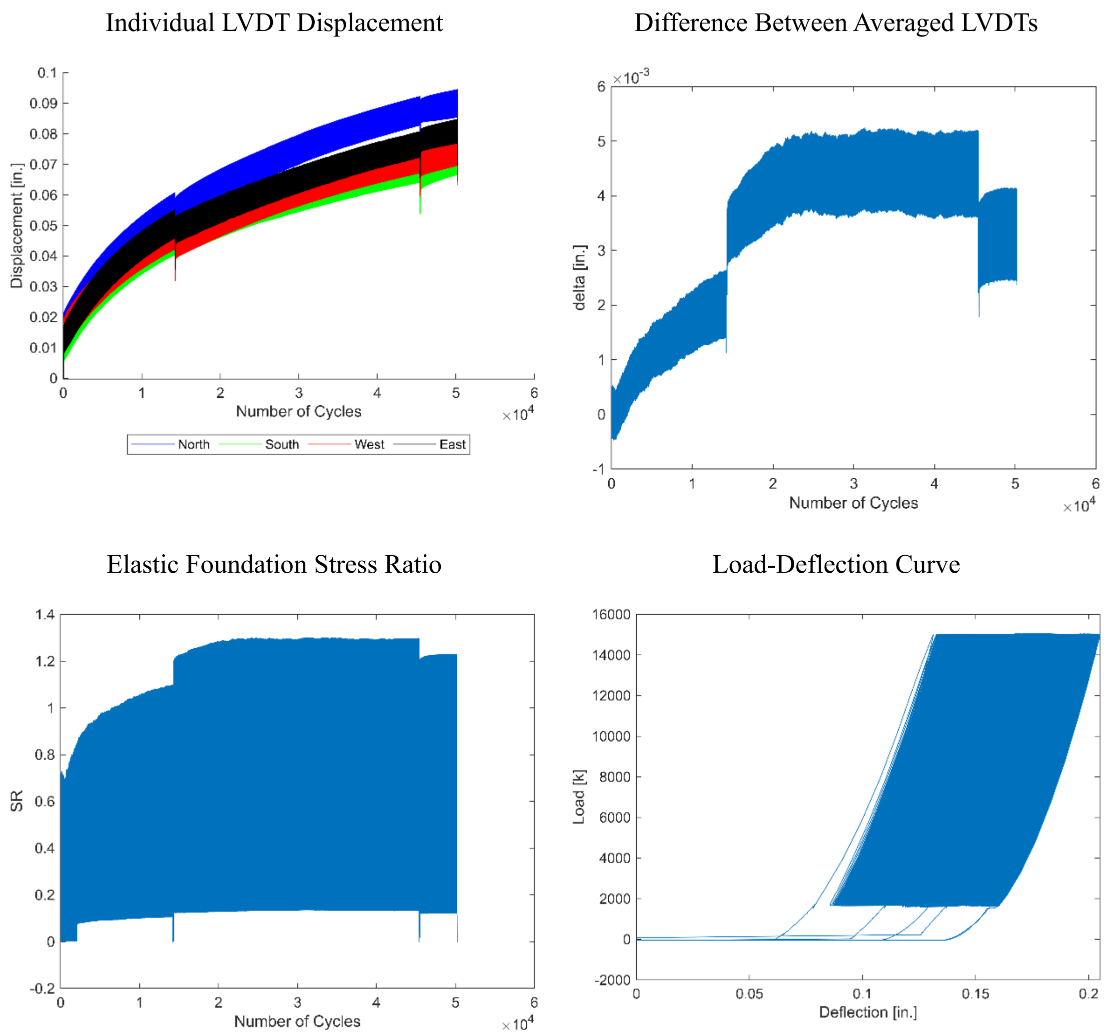

Figure 115: OPCCR1 Results - Step 3 (Elastic Foundation)

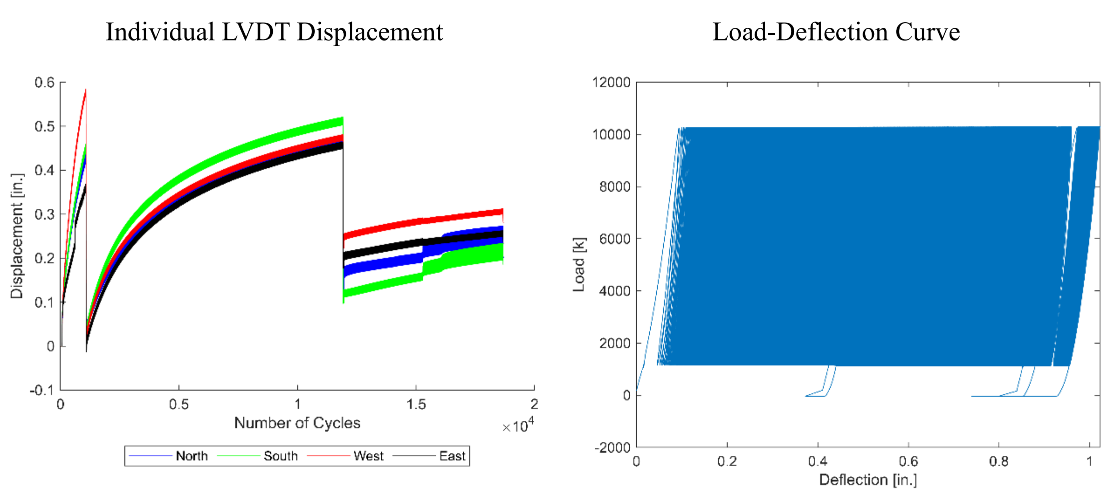

Figure 116: OPCCR1 Results - Step 4 (Simple Span)

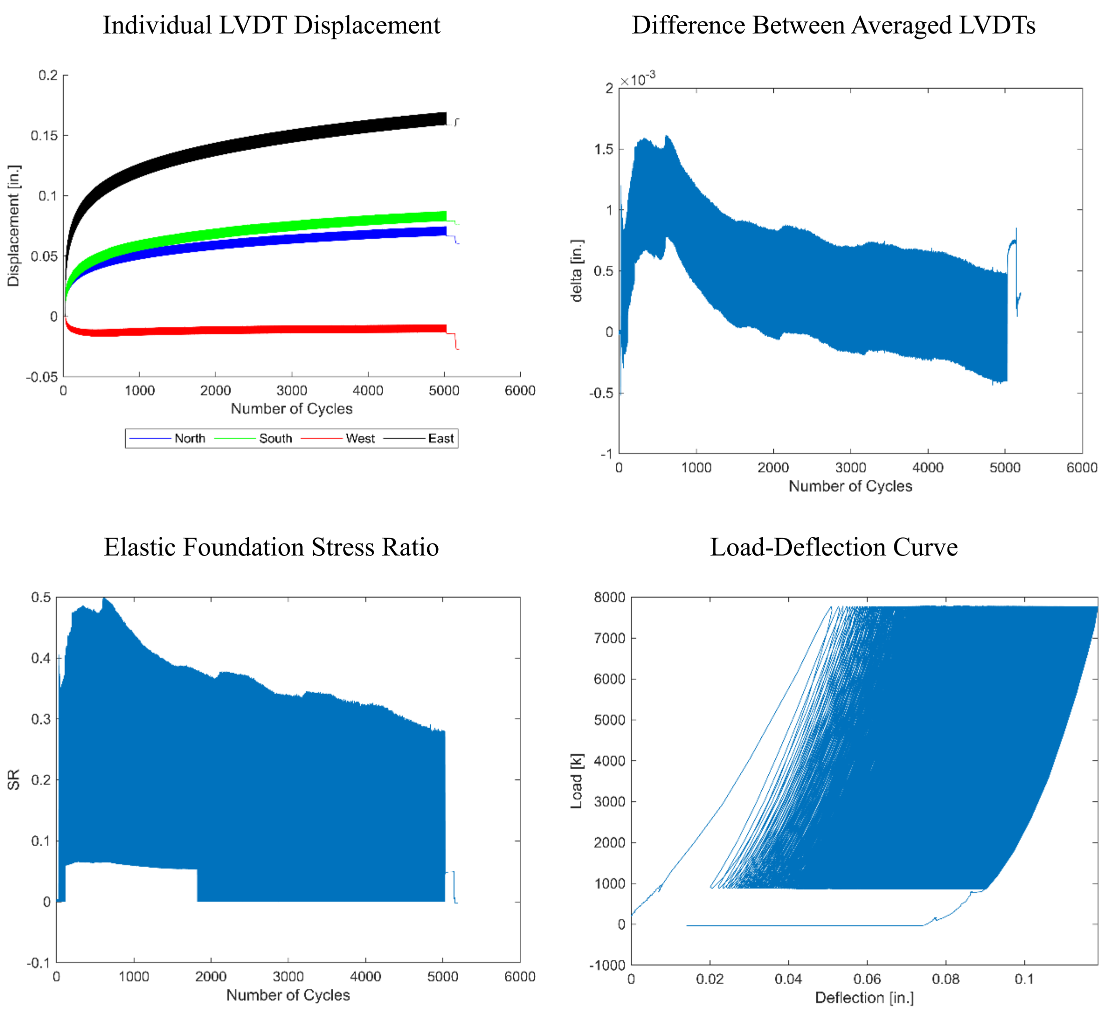

Figure 117: OPCCR2 Results - Step 1 (Elastic Foundation)

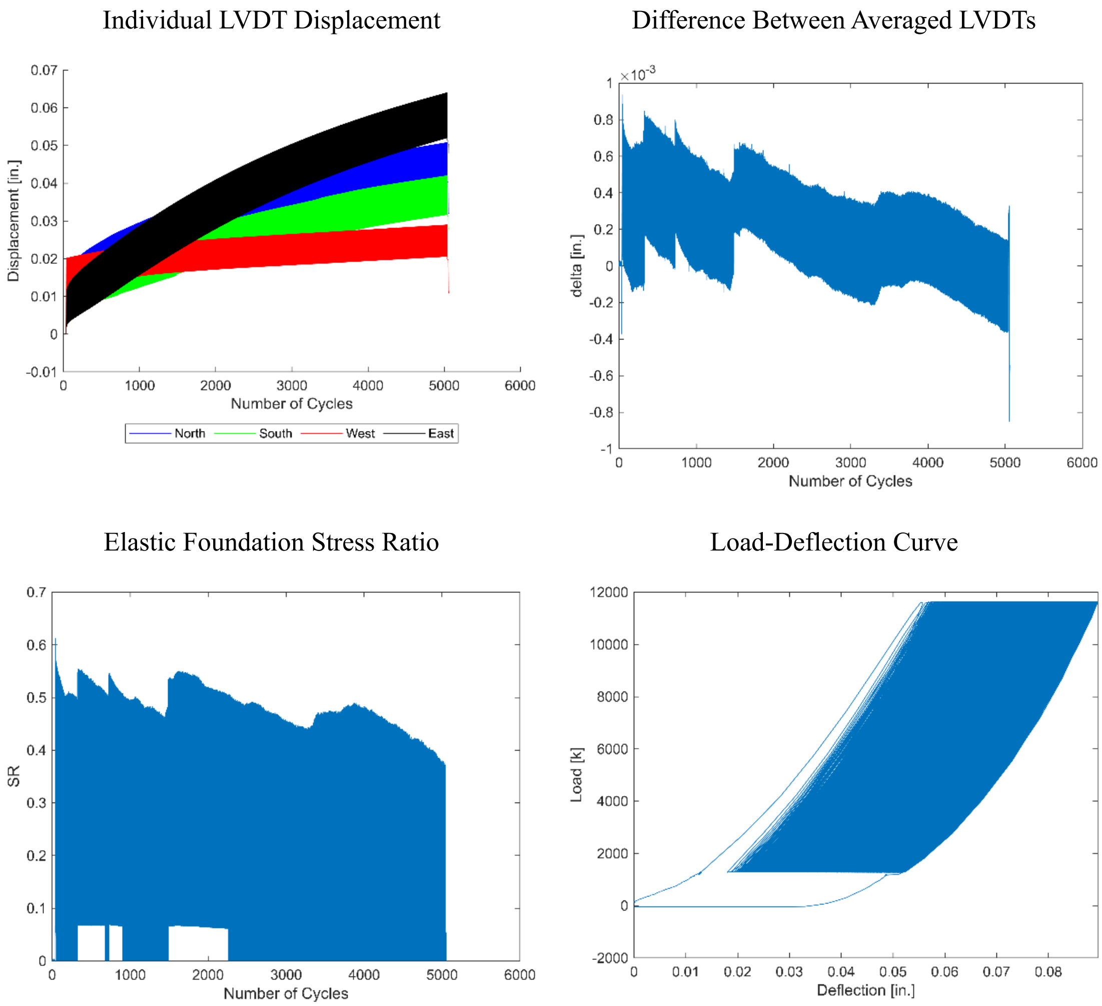

Figure 118: OPCCR2 Results - Step 2 (Elastic Foundation)

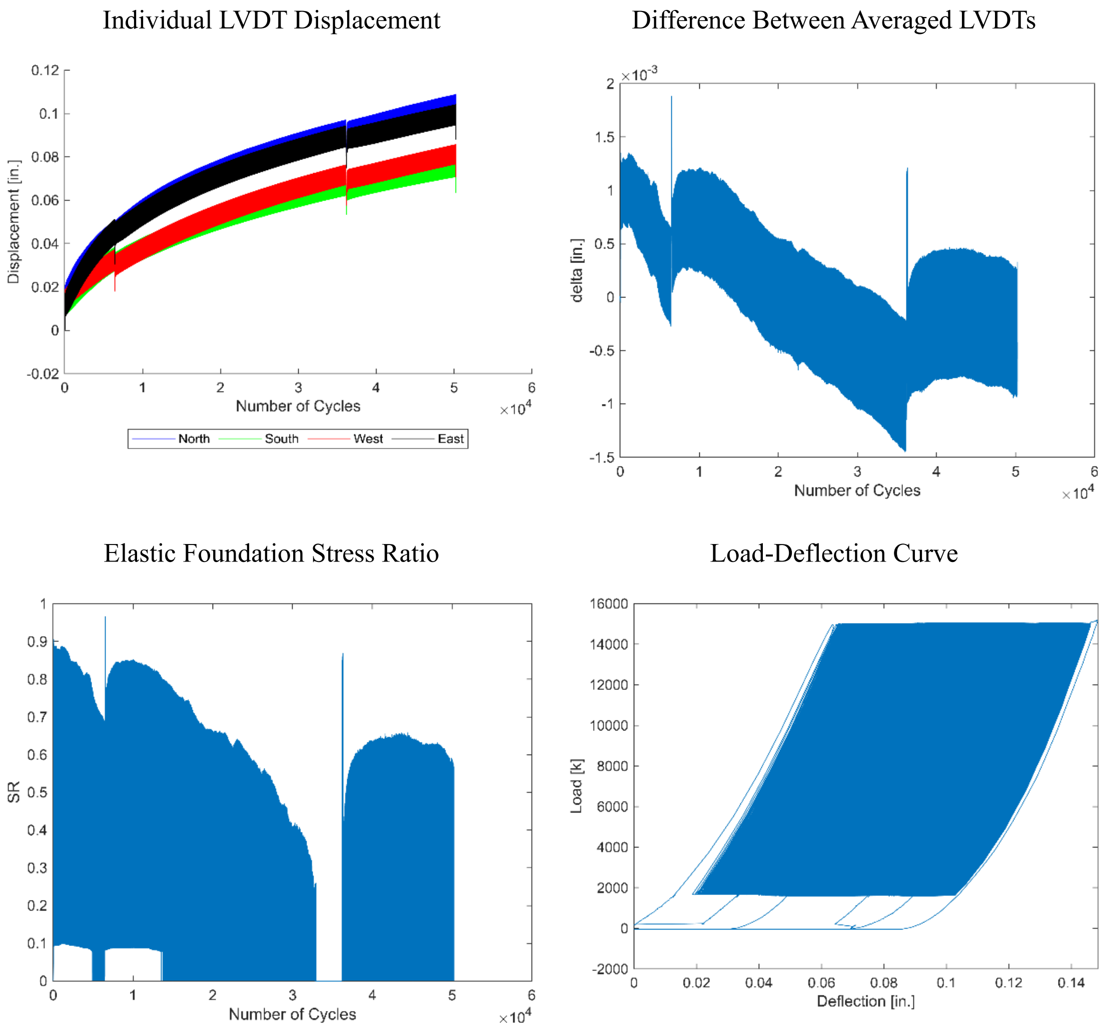

Figure 119: OPCCR2 Results - Step 3 (Elastic Foundation)

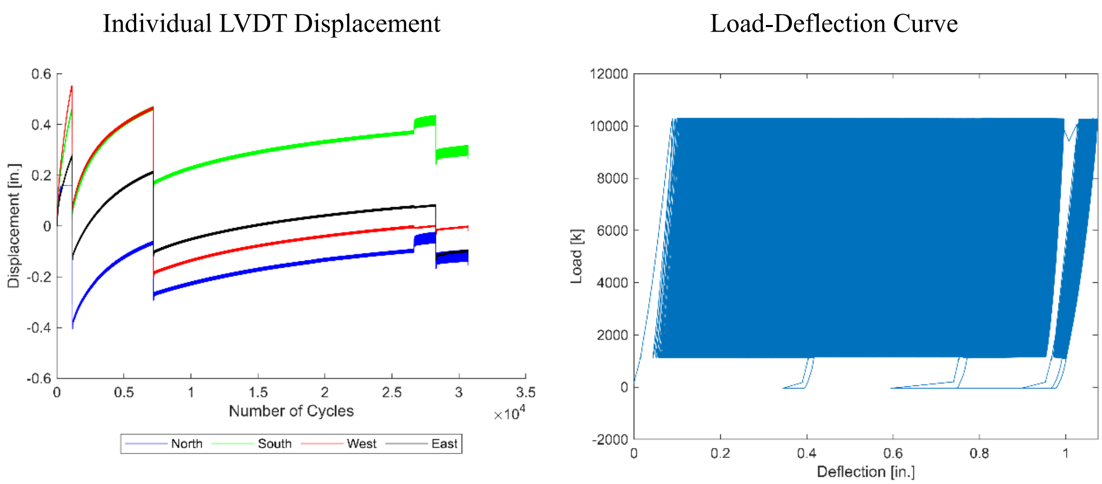

Figure 120: OPCCR Results - Step 4 (Simple Span)

The difficulty in a clear failure criterion was also present for the continuously-reinforced OPC specimens. Load-deflection curves display a similar behavior to the continuously-reinforced Expansive BCSA specimens as the reinforcement was able to resist sudden deflections once cracking occurred. The average failure cycle for the OPCCR specimens was 24692, however the load in Step 4 was noticeably lower than previous specimens as these specimens were loaded at its original intended load for Step 4.

4.4.10 Summary of OPC Specimens

Table 17 provides a summary of results for Step 4 for all OPC specimens for reference. Cycle of failure by specimen designation is plotted in Figure 121. Compressive strengths for each reinforcement design are shown in Figure 122.

Table 17: Summary of Loading for Simply Supported OPC Specimens

Designation	Load (k)	Failure Cycle
OPC1	12.5	108
OPC2	12.5	245
OPCF1	12.5	862
OPCF2	12.5	855
OPCCR1	10.6	18679
OPCCR2	10.6	30706

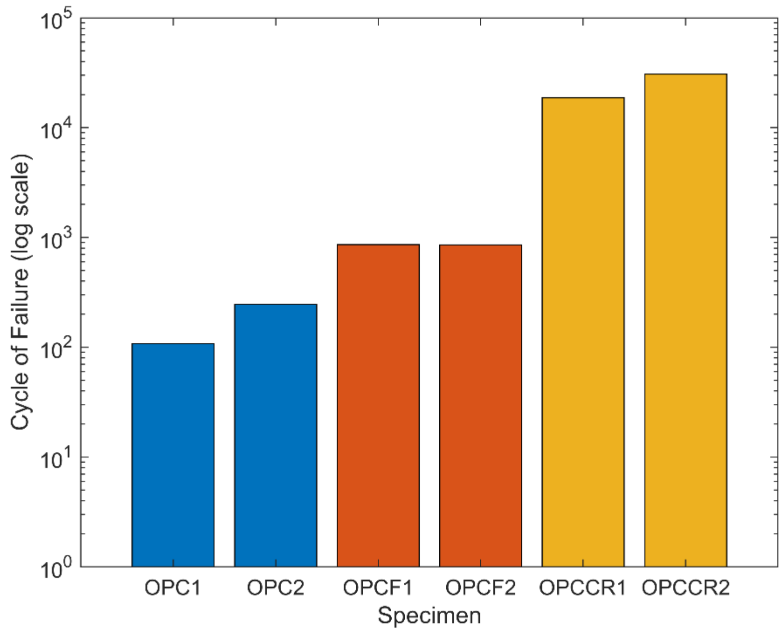

Figure 121: Cycle of Failure for Simply Supported OPC Specimens

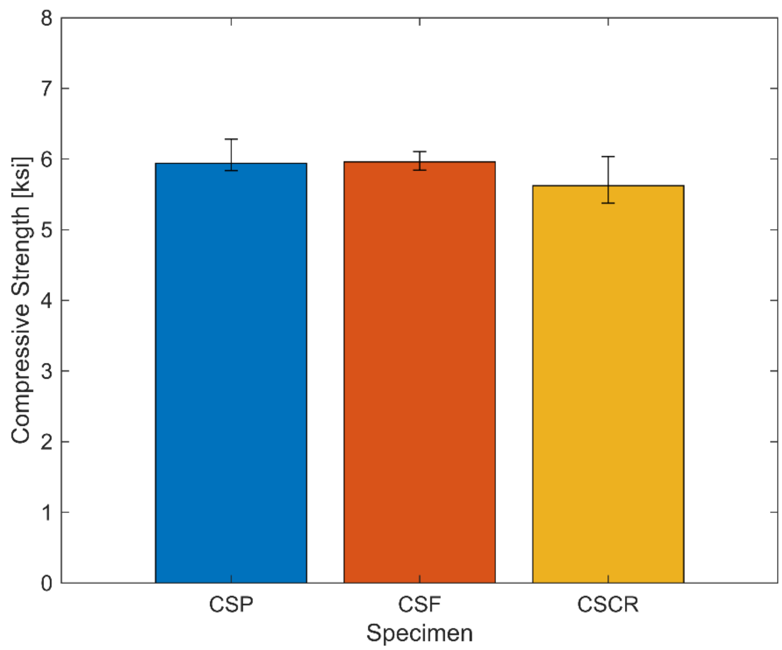

Figure 122: 28-Day Compressive Strengths of Large-Scale OPC Specimens

The OPC specimens had a similar pattern to the Expansive BCSA specimens with a larger failure cycle for increased reinforcement in the specimen (Figure 121). Since identification of first cracking was difficult for the continuously-reinforced specimens, the cycle of failure may be overestimated. However, the prevention of collapse at initial cracking, which isn't reflected in the cycle of failure, is its more significant contribution to overall performance. Additionally, the peak load for the continuously-reinforced specimen is lower than for the other reinforcement design specimens due to differences in concrete compressive strength.

Figure 123 plots the elastic stress ratios calculated for the first three steps of the loading protocol for each OPC specimen. The OPC specimens tended to have more variability in the induced stress ratio than the Expansive BCSA specimens between steps within its own loading protocol and compared to the other specimens. As the stress ratio is calculated by the difference between the average end and midspan LDVT displacements, the flexural stress is considered 0 if that difference becomes negative.

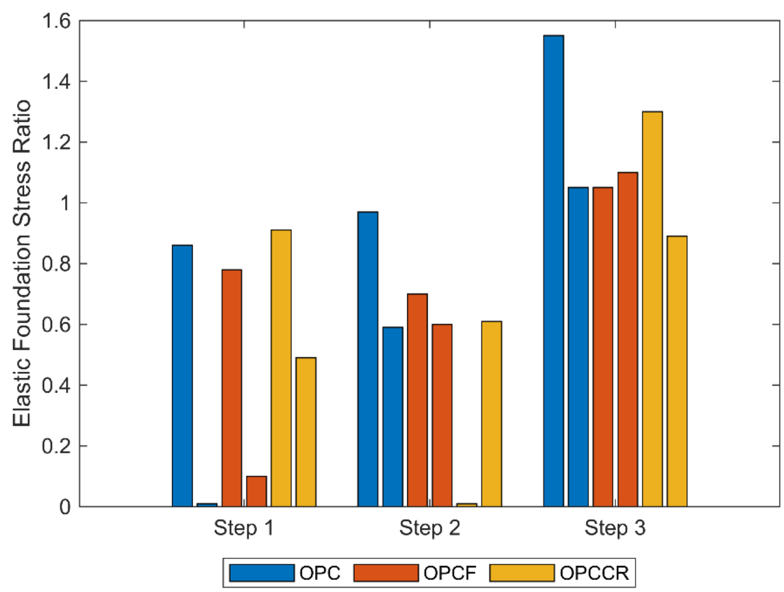

Figure 123: Elastic Stress Ratio of Expansive BCSA Specimens by Step

The S-N equation (5) developed by the concurrent research project for OPC specimens is used to expand the tabular summary of results for all OPC specimens.

$$S = -0.026 \ln(N) + 0.9732 \quad (5)$$

In a similar manner to the Expansive BCSA specimens, the load to produce a stress ratio of 1 was determined based on the calculated S (Eq. 5) which is plotted in Figure 124 for each reinforcement type. This method allows for a better comparison for the continuously-reinforced specimens than the failure cycles as it controls for the variability in applied load.

Table 18: Expanded Summary of Simply Supported OPC Specimens

Designation	Load (k)	Failure Cycle	S (Eq. 5)	Load at S = 1 (k)
OPC1	12.5	108	0.85	14.68
OPC2	12.5	245	0.83	15.06
OPCF1	12.5	862	0.8	15.67
OPCF2	12.5	855	0.8	15.67
OPCCR1	10.6	18679	0.72	14.77
OPCCR2	10.6	30706	0.70	15.04

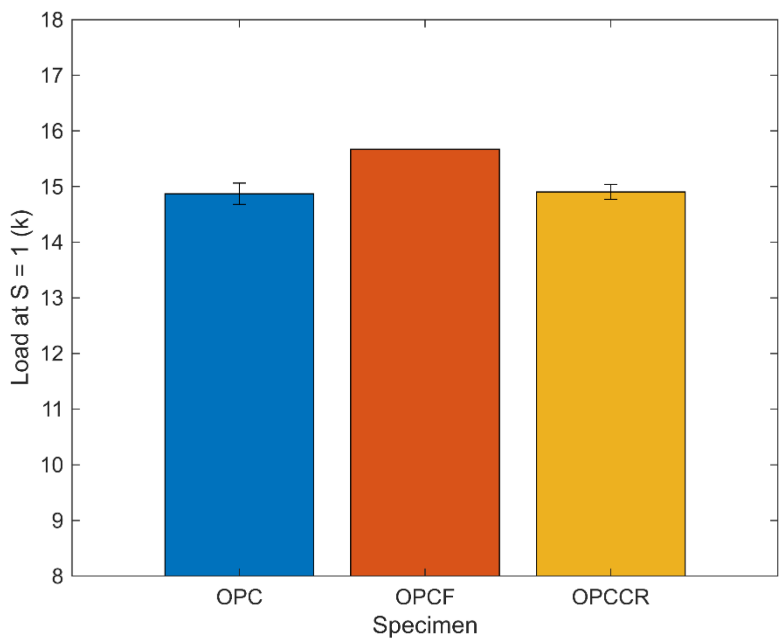

Figure 124: Average Load at S = 1 for OPC Pavement Designs

The OPC specimens had less variability in the load at S =1 (with OPCF sharing the same calculated load) than the Expansive BCSA which could be related to the Expansive BCSA cement being more sensitive to curing conditions as complications with providing a consistent wet-cure period is detrimental to the expansive behavior of the cement. While the load at S = 1 increased with more reinforcement for the Expansive BCSA specimens, the continuously-reinforced specimens appear nearly identical to the plain specimens. As the Expansive BCSA specimens benefited from increased confinement, confining concretes made with cement without an expansive property induces the reverse effect as resisting the shrinkage of the specimen will induce tensile stresses rather than a compressive prestress, therefore reducing the applied stress required to crack the specimen. The increase in load at S =1 for the fiber-reinforced OPC specimens indicates that the confinement from the fibers did not induce any significant tensile stress. However, this does not necessarily suggest that fiber-reinforced OPC pavements would have an overall performance better than continuously-reinforced OPC pavements as the comparison used in this research project relies on initial cracking rather than lifetime performance. As many structural concrete members are designed to be cracked to utilize the reinforcing steel, the load to induce cracking is often less than the design load. For members that are designed to not be cracked in-service, using fiber-reinforcement may be a viable solution to improving overall performance. While the S = 1 load only increased by 0.8 kips between plain and fiber-reinforced OPC specimens, the mix design for the fiber-reinforced specimens only contained 0.75% fibers by volume. The inclusion of more fibers could result in more gains in this regard before providing enough confinement to induce tensile stresses from restrained shrinkage.

Chapter 5: Conclusions & Recommendations

5.1 Conclusions

The scope of this project was to investigate the applicability of the novel rapid setting Expansive BCSA for pavement applications, with a general understanding that the expansive behavior and rapid-setting nature of CSA cements can make the Expansive BCSA especially useful for applications requiring accelerated construction and mitigation of shrinkage-related cracking. Additionally, traditional benefits from fiber-reinforcement such as post-cracking tensile strength could be expanded upon by an expansive cement concrete as the confinement from the fibers could induce a state of chemical prestress to improve performance against flexural loading with less manual labor than traditional reinforcement.

The investigation of the Expansive BCSA used a similar expansive CSA cement made with 25% Komponent® for comparison. The study involved evaluating compressive strength, modulus of elasticity, modulus of rupture, expansive properties, creep, shrinkage, and fatigue performance for fiber-reinforced concrete mix designs with the two cements and comparing to data already collected for plain concrete mix designs in Starks (2023).

5.1.1 Hardened Strength Properties

- Fiber-reinforced Expansive BCSA and 25% Komponent® concrete specimens had a 28-day compressive strength less than their plain concrete counterparts. This may indicate that the fiber-reinforcement induced compressive prestressing, lowering the required applied load to fail in concrete in compression.
- Expansive BCSA and 25% Komponent® concrete specimens gained approximately 70% of their 28 day compressive strength by the end of their wet-cure period, regardless of presence of fiber-reinforcement.
- Fiber-reinforcement resulted in 30% gains in the modulus of elasticity for both Expansive and 25% Komponent® concrete specimens and was better correlated with the square root of compressive strength rather than unaltered compressive strengths as found for plain specimens.

- While the ACI 318-19 equation overpredicts the modulus of elasticity for both CSA cement concretes, fiber-reinforced concrete specimens were closer to the predicted value at all testing ages.
- The modulus of rupture was slightly improved by the addition of fiber-reinforcement for the Expansive BCSA concrete specimens.
- Load-deflection curves indicate that post-cracking tensile strength of fiber-reinforced Expansive BCSA concrete and 25% Komponent® concrete is 74% and 85.5% of the strength at failure, respectively.
- The ACI 318-19 equation is not recommended for prediction of the modulus of rupture as it lacks consideration of the effects of wet-curing, particularly the development of tensile stresses as the specimen dries.

5.1.2 Expansive Properties

- Fiber-reinforced and plain Expansive BCSA concrete specimens maintained similar expansion, indicating no significant prestressing through confinement. Specimens made with double the fiber-dosage for the standard fiber-reinforced mix design only saw a reduction in expansion when indefinitely wet-cured.
- For a wet-cure period of seven days, the expansion displayed by Expansive BCSA concrete specimens was larger than the shrinkage later observed resulting in a net expansion.
- For indefinite wet-cure specimens, continued expansion was observed for Expansive BCSA concrete when compared to the seven-day wet-cured specimens which was not observed for the 25% Komponent® concrete.

- The Expansive BCSA concrete has expansive potential beyond the current recommended practice for wet-curing expansive cement concretes.

5.1.3 Creep and Shrinkage Behavior

- Fiber-reinforced Expansive BCSA concrete specimens showed less immediate creep compared to their plain concrete counterparts, but both concretes developed approximately 90% of their ultimate creep strain during the wet-cure period and were able to mitigate a third of the true creep due the expansive behavior.
- Unfortunately, all VWSGs in the three 25% Komponent® concrete creep specimens failed at the beginning of testing and collected no usable data.

5.1.4 Fatigue Behavior

- When evaluated by the estimated strength determined using an empirical S-N equation developed using small-scale test specimens, Expansive BCSA concrete slab specimens saw increased gains for increasing reinforcement as more confinement generates more compressive prestressing to offset the tensile stresses from flexure.
- OPC concrete specimens saw no benefit from continuous reinforcement when evaluated by initial cracking as confinement generates tensile stresses for concretes without expansive behavior.
- OPC concrete specimens did benefit from fiber-reinforcement, indicating the level of reinforcement did not induce unwanted tensile stresses from restraining the shrinkage of the concrete.

5.2 Recommendations

5.2.1 Application

The criteria for the applicability of the Expansive BCSA was set as a comparison of fatigue performance and expansive behavior to a similar industry-standard expansive CSA cement (Komponent®) with the intent to consider effects of fiber-reinforcement. While this research project was unfortunately altered to not include fatigue testing of 25% Komponent® concrete, the novel Expansive BCSA cement concrete can still be evaluated with these considerations.

While having a minimal effect on the expansive behavior of Expansive BCSA concrete specimens, fiber-reinforced specimens showed gains in the modulus of elasticity and fatigue performance. While continuously-reinforced Expansive BCSA concrete specimens did have a better fatigue performance, within the evaluation methods defined in this project, the fiber-reinforced concrete could make an apt candidate for pavements without substantial sacrifices in performance with considerably less manual labor than traditional reinforcing methods.

The development of specific pavement design practices with fiber-reinforced Expansive BCSA is outside the scope of this project. However, the investigation of standard design parameters used in pavement design such as compressive strengths and the modulus of rupture is useful to incorporate the material into existing design methods for applications where the rapid-setting and expansive behavior of this concrete would be beneficial. Specifically, these behaviors not seen in OPC concretes are especially desirable to applications that require accelerated construction or mitigation of shrinkage-related cracking. The findings from this project can contribute to guidelines for the use of the Expansive BCSA including:

- Use a seven-day wet-cure period to benefit from the expansive behavior. Longer wet-cure periods can be used for more expansion if needed.
- Fiber-reinforced mix designs using 0.75% fibers by volume may not realize significant differences in expansive behavior, but show gains in modulus of elasticity and fatigue performance along with a reduction in manual labor. Using a mix design with more fibers may prove beneficial for chemical prestressing pending further investigations.

5.2.2 Further Research

Recommendations for further research is listed in the following:

- Conduct similar large-scale fatigue testing methods for concrete specimens made using ordinary portland cement with a 25% Komponent® replacement.
- Investigate more consistent internal and external instruments to collect strain data for the concrete slab specimens.
- Investigate fatigue performance of concrete specimens with alternative subgrade and subbase soil types along with methods for compaction in the soil containment box.
- Collect more fatigue data for further development of S-N equations for Expansive BCSA including the effect of cross-sectional dimensions.
- Conduct comprehensive pavement studies on Expansive BCSA and Komponent® mixes using an accelerated loading facility (ALF) machine to simulate years of service for evaluation of pavement performance.
- Investigate Expansive BCSA and OPC concrete made with an array of fiber-reinforcement to further understand effect on chemical prestressing (both compressive and tensile prestresses) for fatigue loading with induced flexural stresses.

- Investigate compressive strength development of Expansive BCSA in regard to the restraint offered by fiber-reinforcement, particularly with consideration of development during wet-curing and post-wet-curing.
- Explore the bond between Expansive BCSA concrete and fibers with varying size, shapes, and materials and subsequent effects on expansive behavior. Suggested alternative shapes include hooked and T-shaped fibers.

References

AASHTO Guide for Design of Pavement Structures (AASHTO, 1993)

Acarturk, B. C., & Burris, L. E. (2023). Investigations of the optimal requirements for curing of calcium sulfoaluminate cement systems. *CEMENT*, *12*, 100072. doi:10.1016/j.cement.2023.100072

“ACI 223, Standard Practice for the Use of Shrinkage-Compensating Concrete, “American Concrete Institute, Farmington Hills, MI.

“ASTM Standard C39 Standard Test Method for Compressive Strength of Cylindrical Concrete Specimens,” ASTM International, West Conshohocken, PA.

“ASTM Standard C78 Standard Test Method for Flexural Strength of Concrete (Using Simple Beam with Third-Point Loading,” ASTM International, West Conshohocken, PA.

“ASTM Standard C157 Standard Test Method for Length Change of Hardened Hydraulic-Cement Mortar and Concrete,” ASTM International, West Conshohocken, PA.

“ASTM Standard C469 Standard Test Method for Static Modulus of Elasticity and Poisson's Ratio of Concrete in Compression,” ASTM International, West Conshohocken, PA.

“ASTM Standard C512 Standard Test Method for Creep of Concrete in Compression,” ASTM International, West Conshohocken, PA.

“ASTM Standard C878 Standard Test Method for Restrained Expansion of Shrinkage Compensating Concrete,” ASTM International, West Conshohocken, PA.

“ASTM Standard C1609 Standard Test Method for Flexural Performance of Fiber-Reinforced Concrete (Using Beam With Third-Point Loading),” ASTM International, West Conshohocken, PA.

“ASTM Standard D1557 Standard Test Methods for Laboratory Compaction Characteristics of Soil Using Modified Effort,” ASTM International, West Conshohocken, PA.

Battaglia, I. K. (2012). *Experimental use of type K cement concrete in Wisconsin Highway Bridge decks*. TRID. https://trid.trb.org/view/1471533

Bescher, E., Stremfel, J., Ramseyer, C., Rice, E. K. (2012). *The Role of Calcium Sulfoaluminate In Concrete Sustainability*.

Bowser, Troy & Murray, Cameron & Floyd, Royce. (2020). Bond Behavior of 0.6 in.

Prestressing Strand in BSCA Cement Concrete. ACI Structural Journal. 117. 10.14359/51720196.

Dillard, R. J., Murray, C. D., & Deschenes, R. A. (2022). Belitic calcium sulfoaluminate cement subjected to sulfate attack and sulfuric acid. *Construction and Building Materials*, *343*, 128089. doi:10.1016/j.conbuildmat.2022.128089

Gennings, D. (2018). *Investigation of Chemically Prestressed Concrete* [Master's thesis, University of Oklahoma]. SHAREOK. https://hdl.handle.net/11244/299692

Ideker, J. H., Deboodt, T., & Fu, T. (2013). *Internal curing of high-performance concrete for bridge decks*. Retrieved from https://rosap.ntl.bts.gov/view/dot/25824

Kevern, J. T., Rupnow, T. D., Mulheron, M., Collier, Z., & Icenogle, P. (2016). *Evaluation of the fatigue and toughness of fiber reinforced concrete for use as a new highway pavement design*. Retrieved from https://rosap.ntl.bts.gov/view/dot/30759

McNerney, M. T., Kim, J., Paniagua, F., Paniagua, J., Chung, D., Morgan, M., Bescher, E. P. (2021, June 4). Drying behavior of a quadruple-sized belitic calcium sulfoaluminate airfield concrete slab. *Airfield and Highway Pavements 2021*. Presented at the International Airfield and Highway Pavements Conference 2021, Virtual Conference. doi:10.1061/9780784483527.005

Murray, C. D., Floyd, R.W., and Ramseyer, C.E. (2019). Using Belitic Calcium Sulfoaluminate Cement for Precast, Prestressed Concrete Beams. *PCI Journal*. Vol. 64, No. 2, 55-67

Ramseyer, C. C., & Myers, D. S. (2009). *Creation of an ODOT specification for patching or overlay of bridge decks*. Retrieved from https://rosap.ntl.bts.gov/view/dot/23091

Roesler, J.R., Hiller, J.E., & Brand, A.S. (2016). *Continuously Reinforced Concrete Pavement Manual, Guidelines for Design, Construction, Maintenance, and Rehabilitation*.

Sorensen, A., Thomas, R., Maguire, M., & Quezada, I. (2018). Calcium Sulfoaluminate (CSA) Cement: Benefits and Applications. *Concrete International*, *40*, 65–69.

Starks, J. (2023). *Mechanical performance of post-tensioned residential foundation slabs using expansive BCSA cements* [Master's thesis, University of Oklahoma]. SHAREOK. https://hdl.handle.net/11244/337589

Appendix

Expansive BCSA Concrete
Fiber-Reinforced, Creep & Shrinkage Cylinders

Mix Information

Mix Date	6/2/2023	
Slump	8.5	in.

Mix Design

	1 yd	2.5 cf		Notes
Portland Cement	0.00	0.00	lb	
ChemStress Cement	559.74	51.83	lb	
Komponent	0.00	0.00	lb	
Fly Ash	0.00	0.00	lb	
Coarse Aggregate, #67	1413.07	130.84	lb	
Fine Aggregate, Dover Sand	1703.19	157.70	lb	
Water	278.59	25.80	lb	w/cm = 0.5
Citric Acid Retarder	2.24	0.21	lb	0.40%
ADVA, (MRWR)	62.00	169.75	ml	
Fibers	100.00	9.26	lb	0.75%

Compressive Strength (psi)

	Specimen			
Age	1	2	3	Avg.
6h	3636	3624	3632	3631
1d	4989	4948	4930	4956
7d	9354	8876	8875	9035
28d	11122	10926	12341	11463

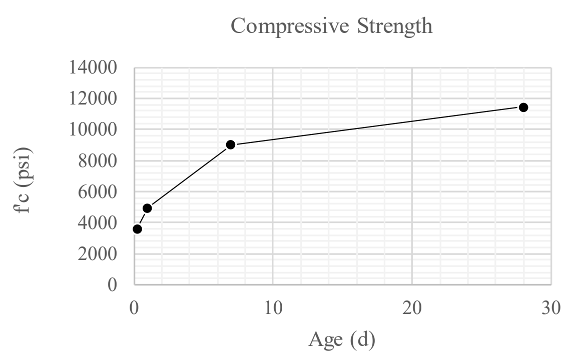

Expansive BCSA Concrete

Fiber-Reinforced, Modulus of Rupture

Mix Information

Mix Date	8/9/2023	
Slump	8.5	in.

Mix Design

	1 yd	5 cf		Notes
Portland Cement	0.00	0.00	lb	
ChemStress Cement	559.74	103.65	lb	
Komponent	0.00	0.00	lb	
Fly Ash	0.00	0.00	lb	
Coarse Aggregate, #67	1413.07	260.39	lb	
Fine Aggregate, Dover Sand	1703.19	312.86	lb	
Water	278.59	55.44	lb	w/cm = 0.5
Citric Acid Retarder	2.24	0.41	lb	0.40%
ADVA, (MRWR)	62.00	197.13	ml	
Fibers	100.00	18.52	lb	0.75%

Compressive Strength (psi)

	Specimen			
Age	1	2	3	Avg.
6h	2992	3011	3112	3038
1d	4094	4079	4096	4090
7d	7164	7351	8524	7680
28d	11662	12187	11443	11764

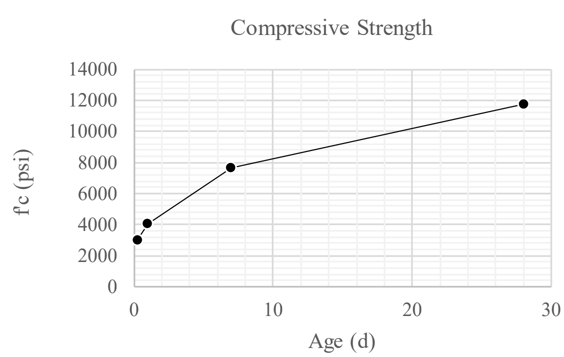

Expansive BCSA Concrete

Fiber-Reinforced, Expansion

Mix Information

Mix Date	9/14/2023	
Slump	7	in.

Mix Design

	1 yd	1.58 cf		Notes
Portland Cement	0.00	0.00	lb	
ChemStress Cement	559.74	32.75	lb	
Komponent	0.00	0.00	lb	
Fly Ash	0.00	0.00	lb	
Coarse Aggregate, #67	1413.07	82.40	lb	
Fine Aggregate, Dover Sand	1703.19	99.25	lb	
Water	278.59	17.02	lb	w/cm = 0.5
Citric Acid Retarder	2.24	0.13	lb	0.40%
ADVA, (MRWR)	62.00	62.29	ml	
Fibers	100.00	5.85	lb	0.75%

Compressive Strength (psi)

	Specimen			
Age	1	2	3	Avg.
6h	3003	3007	2951	2987
1d	4279	4540	4361	4393
7d	8888	8765	8575	8743
28d	11194	11601	11029	11275

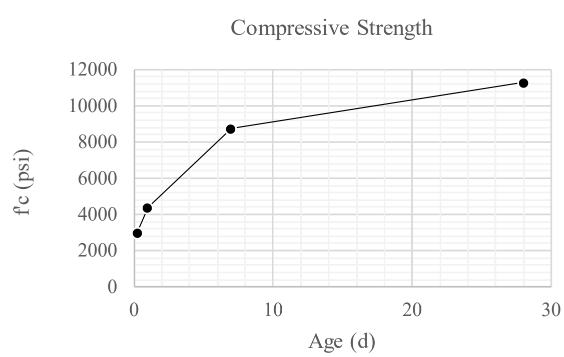

Expansive BCSA Concrete

Fiber-Reinforced, Modulus of Elasticity

Mix Information

Mix Date	9/25/2023	
Slump	7.5	in.

Mix Design

	1 yd	1.75 cf		Notes
Portland Cement	0.00	0.00	lb	
ChemStress Cement	559.74	36.28	lb	
Komponent	0.00	0.00	lb	
Fly Ash	0.00	0.00	lb	
Coarse Aggregate, #67	1413.07	91.36	lb	
Fine Aggregate, Dover Sand	1703.19	109.93	lb	
Water	278.59	18.75	lb	w/cm = 0.5
Citric Acid Retarder	2.24	0.15	lb	0.40%
ADVA, (MRWR)	62.00	86.25	ml	
Fibers	100.00	6.48	lb	0.75%

Compressive Strength (psi)

	Specimen			
Age	1	2	3	Avg.
6h	2992	3011	3112	3038
1d	4094	4079	4096	4090
7d	7164	7351	8524	7680
28d	11662	12187	11443	11764

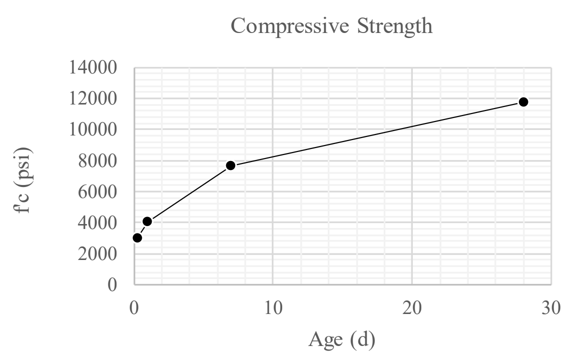

Expansive BCSA Concrete
Plain Slab

Mix Information

Mix Date	2/22/2024	
Slump	6.5	in.

Mix Design

	1 yd	19 cf		Notes
Portland Cement	0.00	0.00	lb	
ChemStress Cement	564.00	396.89	lb	
Komponent	0.00	0.00	lb	
Fly Ash	0.00	0.00	lb	
Coarse Aggregate, #67	1422.15	1000.77	lb	
Fine Aggregate, Dover Sand	1739.13	1223.83	lb	
Water	256.66	180.61	lb	w/cm = 0.5
Citric Acid Retarder	2.82	1.98	lb	0.40%
ADVA, (MRWR)	96.00	1997.62	ml	
Fibers	0.00	0.00	lb	0.75%

Compressive Strength (psi)

	Specimen			
Age	1	2	3	Avg.
6h	963	-	-	963
8h	3779	-	-	3779
7d	5408	4843	4752	5001
28d	13686	12812	12305	12934

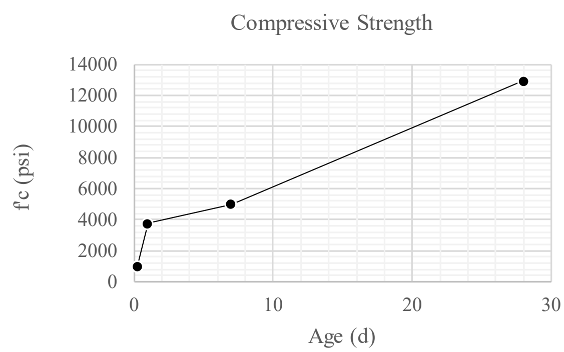

Expansive BCSA Concrete
Fiber-Reinforced Slab

Mix Information

Mix Date	3/14/2024	
Slump	8.5	in.

Mix Design

	1 yd	18 cf		Notes
Portland Cement	0.00	0.00	lb	
ChemStress Cement	559.74	373.16	lb	
Komponent	0.00	0.00	lb	
Fly Ash	0.00	0.00	lb	
Coarse Aggregate, #67	1413.07	937.34	lb	
Fine Aggregate, Dover Sand	1703.19	1153.05	lb	
Water	278.59	172.32	lb	w/cm = 0.5
Citric Acid Retarder	2.24	1.49	lb	0.40%
ADVA, (MRWR)	62.00	1261.65	ml	
Fibers	100.00	66.67	lb	0.75%

Compressive Strength (psi)

	Specimen			
Age	1	2	3	Avg.
6h	3694	3731	3588	3671
1d	5717	5827	5808	5784
7d	9550	9345	6928	9448
28d	12801	13376	12253	12810

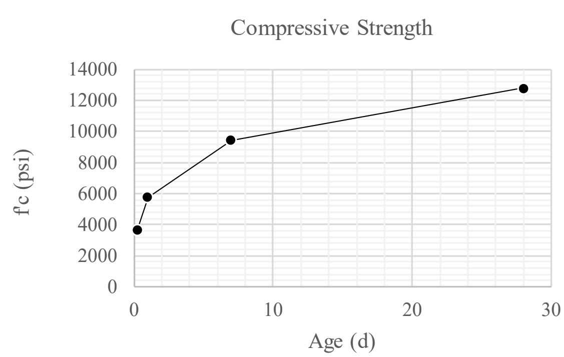

Expansive BCSA Concrete

Continuously-Reinforced Slab

Mix Information

Mix Date	4/1/2024	
Slump	8.75	in.

Mix Design

	1 yd	18 cf		Notes
Portland Cement	0.00	0.00	lb	
ChemStress Cement	564.00	376.00	lb	
Komponent	0.00	0.00	lb	
Fly Ash	0.00	0.00	lb	
Coarse Aggregate, #67	1423.33	948.89	lb	
Fine Aggregate, Dover Sand	1748.40	1165.60	lb	
Water	245.77	163.85	lb	w/cm = 0.5
Citric Acid Retarder	2.26	1.50	lb	0.40%
ADVA, (MRWR)	64.00	1261.65	ml	
Fibers	0.00	0.00	lb	0.75%

Compressive Strength (psi)

	Specimen			
Age	1	2	3	Avg.
6h	3797	3783	3806	3795
1d	5710	5740	5860	5770
7d	9572	9329	9916	9606
28d	13215	12976	13258	13150

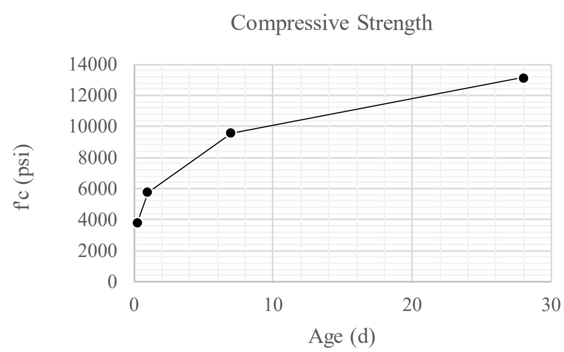

Expansive BCSA Concrete

Double Fiber-Reinforced, Expansion

Mix Information

Mix Date	2/29/2024	
Slump	2.5	in.

Mix Design

	1 yd	1.25 cf		Notes
Portland Cement	0.00	0.00	lb	
ChemStress Cement	555.47	25.72	lb	
Komponent	0.00	0.00	lb	
Fly Ash	0.00	0.00	lb	
Coarse Aggregate, #67	1395.13	64.59	lb	
Fine Aggregate, Dover Sand	1717.11	79.50	lb	
Water	258.09	11.95	lb	w/cm = 0.5
Citric Acid Retarder	2.22	0.10	lb	0.40%
ADVA, (MRWR)	67.00	91.72	ml	
Fibers	200.00	9.26	lb	0.75%

Compressive Strength (psi)

	Specimen			
Age	1	2	3	Avg.
6h	3699	3684	3790	3724
1d	5890	5413	5994	5766
7d	10397	10083	10542	10341
28d	14403	12933	12624	13320

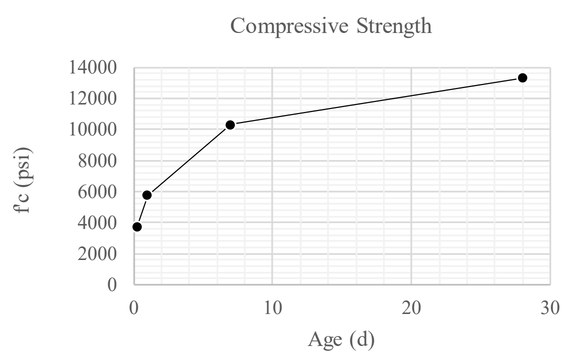

25% Komponent® Concrete

Fiber-Reinforced, Creep & Shrinkage Cylinders

Mix Information

Mix Date	5/30/2023	
Slump	8.5	in.

Mix Design

	1 yd	2.5 cf		Notes
Portland Cement	421.56	39.03	lb	
ChemStress Cement	0.00	0.00	lb	
Komponent	139.93	12.96	lb	
Fly Ash	0.00	0.00	lb	
Coarse Aggregate, #67	1428.24	132.24	lb	
Fine Aggregate, Dover Sand	1721.46	159.39	lb	
Water	278.55	25.79	lb	w/cm = 0.5
Citric Acid Retarder	1.68	0.16	lb	0.30%
ADVA, (MRWR)	54.00	147.85	ml	
Fibers	100.00	9.26	lb	0.75%

Compressive Strength (psi)

	Specimen			
Age	1	2	3	Avg.
3d	1419	1559	1545	1508
10d	4662	4455	4383	4500
28d	6746	6858	6356	6653

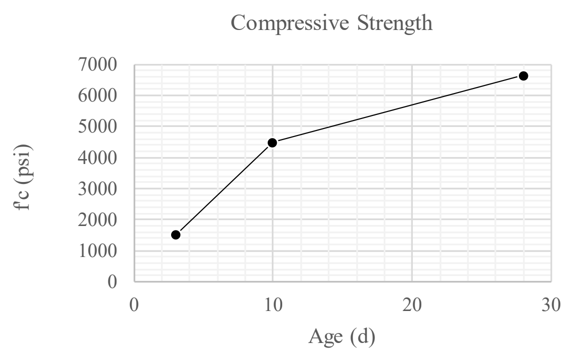

25% Komponent® Concrete

Fiber-Reinforced, Modulus of Rupture

Mix Information

Mix Date	8/15/2023	
Slump	7.75	in.

Mix Design

	1 yd	5 cf		Notes
Portland Cement	421.56	78.07	lb	
ChemStress Cement	0.00	0.00	lb	
Komponent	139.93	25.91	lb	
Fly Ash	0.00	0.00	lb	
Coarse Aggregate, #67	1428.24	263.65	lb	
Fine Aggregate, Dover Sand	1721.46	321.19	lb	
Water	278.55	49.98	lb	w/cm = 0.5
Citric Acid Retarder	1.68	0.16	lb	0.15%
ADVA, (MRWR)	54.00	191.66	ml	
Fibers	100.00	18.52	lb	0.75%

Compressive Strength (psi)

	Specimen			
Age	1	2	3	Avg.
3d	4020	3774	3862	3885
7d	4555	4555	4742	4617
10d	5817	5886	5949	5884
28d	6514	6653	6620	6596

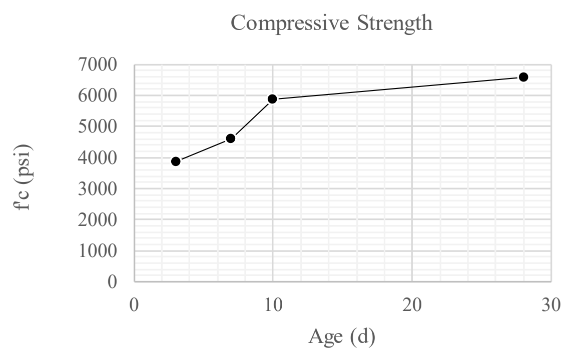

25% Komponent® Concrete

Fiber-Reinforced, Expansion

Mix Information

Mix Date	10/3/2023	
Slump	7.5	in.

Mix Design

	1 yd	1.58 cf		Notes
Portland Cement	421.56	24.67	lb	
ChemStress Cement	0.00	0.00	lb	
Komponent	139.93	8.19	lb	
Fly Ash	0.00	0.00	lb	
Coarse Aggregate, #67	1428.24	83.26	lb	
Fine Aggregate, Dover Sand	1721.46	101.28	lb	
Water	278.55	16.08	lb	w/cm = 0.5
Citric Acid Retarder	1.68	0.05	lb	0.15%
ADVA, (MRWR)	54.00	77.87	ml	
Fibers	100.00	5.85	lb	0.75%

Compressive Strength (psi)

	Specimen			
Age	1	2	3	Avg.
3d	3983	3737	3945	3888
7d	4683	4648	4650	4660
10d	6460	6511	6623	6531
28d	7366	6760	7452	7193

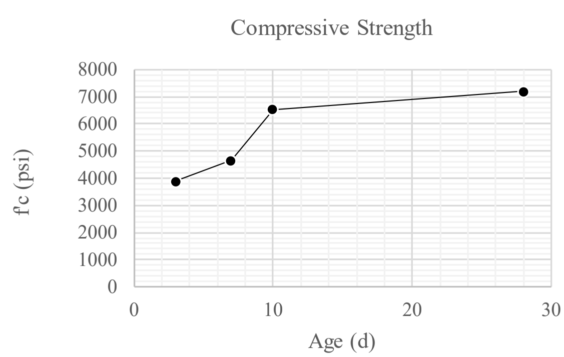

25% Komponent® Concrete

Fiber-Reinforced, Modulus of Elasticity

Mix Information

Mix Date	10/13/2023	
Slump	9	in.

Mix Design

	1 yd	1.75 cf		Notes
Portland Cement	421.56	27.32	lb	
ChemStress Cement	0.00	0.00	lb	
Komponent	139.93	9.07	lb	
Fly Ash	0.00	0.00	lb	
Coarse Aggregate, #67	1428.24	91.99	lb	
Fine Aggregate, Dover Sand	1721.46	111.13	lb	
Water	278.55	19.08	lb	w/cm = 0.5
Citric Acid Retarder	1.68	0.05	lb	0.15%
ADVA, (MRWR)	54.00	124.58	ml	
Fibers	100.00	6.48	lb	0.75%

Compressive Strength (psi)

	Specimen			
Age	1	2	3	Avg.
3d	2449	2280	2323	2351
14d	5257	5083	5121	5154
28d	5641	6289	6064	5998

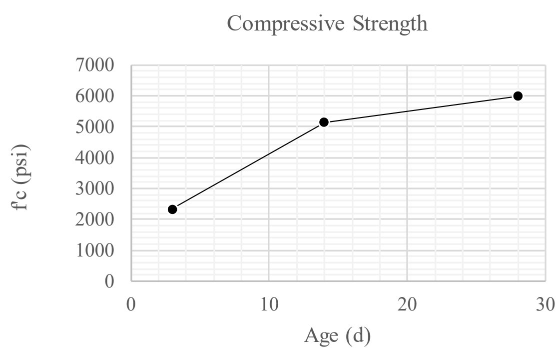

Ordinary Portland Cement Concrete
Plain Slab

Mix Information

Mix Date	2/8/2024	
Slump	6	in.

Mix Design

	1 yd	17 cf		Notes
Cement	682.00	429.41	lb	
Fly Ash	0.00	0.00	lb	
BFS	0.00	0.00	lb	
Silica Fume	0.00	0.00	lb	
Rock	1718.19	1081.82	lb	
LWA	0.00	0.00	lb	
Sand	1246.06	784.56	lb	
Water	307.32	193.50	ml	w/cm = 0.48
HRWR	201.67	126.98	lb	
C.A.	0.00	0.00	ml	
Air Ent.	0.00	0.00	ml	
Fibers	0.00	0.00	lb	

Compressive Strength (psi)

	Specimen			
Age	1	2	3	Avg.
6h	4798	4940	5074	4937
1d	6152	6282	5387	5940

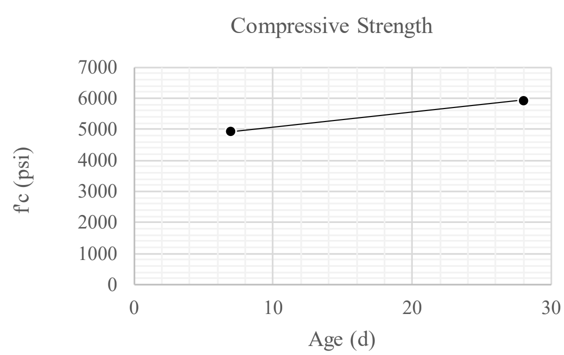

Ordinary Portland Cement Concrete

Fiber-Reinforced Slab

Mix Information

Mix Date	4/9/2024	
Slump	7	in.

Mix Design

	1 yd	17 cf		Notes
Cement	682.00	429.41	lb	
Fly Ash	0.00	0.00	lb	
BFS	0.00	0.00	lb	
Silica Fume	0.00	0.00	lb	
Rock	1718.02	1081.72	lb	
LWA	0.00	0.00	lb	
Sand	1219.00	767.52	lb	
Water	334.34	210.51	ml	w/cm = 0.48
HRWR	201.67	253.95	lb	
C.A.	0.00	0.00	ml	
Air Ent.	0.00	0.00	ml	
Fibers	100.00	62.96	lb	

Compressive Strength (psi)

	Specimen			
Age	1	2	3	Avg.
6h	4808	4880	5046	4911
1d	6104	5932	5842	5959

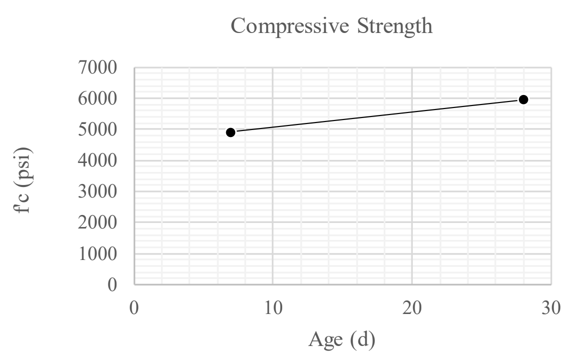

Ordinary Portland Cement Concrete

Continuously-Reinforced Slab

Mix Information

Mix Date	4/19/2024	
Slump	7.5	in.

Mix Design

	1 yd	17 cf		Notes
Cement	682.00	429.41	lb	
Fly Ash	0.00	0.00	lb	
BFS	0.00	0.00	lb	
Silica Fume	0.00	0.00	lb	
Rock	1718.19	1081.82	lb	
LWA	0.00	0.00	lb	
Sand	1244.72	783.71	lb	
Water	308.66	194.34	ml	w/cm = 0.48
HRWR	201.67	253.95	lb	
C.A.	0.00	0.00	ml	
Air Ent.	0.00	0.00	ml	
Fibers	0.00	0.00	lb	

Compressive Strength (psi)

	Specimen			
Age	1	2	3	Avg.
6h	5121	5219	4946	5095
1d	5623	5456	6035	5378